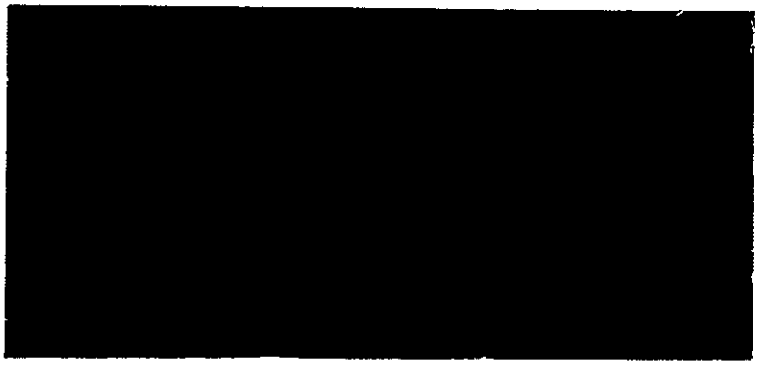

N76-14558

(E76-10075) DESIGN DATA COLLECTION WITH SKYLAB MICROWAVE RADIOMETER-SCATTEROMETER S-193, VOLUME 2 Final Report, 26 Mar. 1973 - 31 Dec. 1975 (Kansas Univ. Center for Research, Inc.) 119 p HC $5.50 CSCL 08B G3/43

Unclas 00075

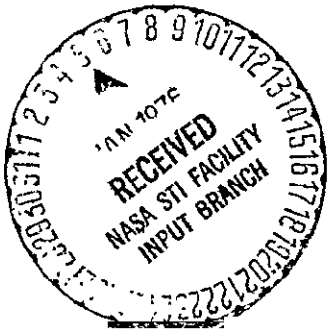

THE UNIVERSITY OF KANSAS / CENTER FOR RESEARCH, INC.

Irving Hill Rd.—West Campus Lawrence, Kansas 66044

THE UNIVERSITY OF KANSAS SPACE TECHNOLOGY CENTER
Raymond Nichols Hall

2291 Irving Hill Drive—Campus West Lawrence, Kansas 66045

Telephone:

Remote Sensing Laboratory
RSL Technical Report 243-12

DESIGN DATA COLLECTION WITH SKYLAB MICROWAVE RADIOMETER-SCATTEROMETER S-193

Final Report

NASA Contract NAS 9-13331

Volume 2

Prepared for:

Principal Investigations Management Office
Technical Monitor: Mr. Larry B. York
NASA Lyndon B. Johnson Space Center
Houston, Texas 77058

Prepared by:

Richard K. Moore, Principal Investigator
Fawwaz T. Ulaby, Co- Principal Investigator
Arun Sobti, Project Engineer
Saad T. Ulaby, Research Technician
Evan C. Davison, Research Technician
Samut Siriburi, Research Assistant
University of Kansas Center for Research, Inc.
Remote Sensing Laboratory
Lawrence, Kansas 66045

APPENDIX B

CLUSTER ANALYSIS OF SKYLAB

RADIOMETER AND SCATTEROMETER DATA

THE UNIVERSITY OF KANSAS SPACE TECHNOLOGY CENTER
Raymond Nichols Hall
2291 Irving Hill Drive—Campus West Lawrence, Kansas 66045
Telephone:

CLUSTER ANALYSIS OF SKYLAB RADIOMETER AND SCATTEROMETER DATA

Remote Sensing Laboratory
RSL Technical Report 243-5

Arun Sobti
Samut Siriburi
Richard K. Moore

August, 1975

Supported by:

NATIONAL AERONAUTICS AND SPACE ADMINISTRATION
Johnson Spacecraft Center
Houston, Texas 77058

Contract NAS9-13331

Organization Full Name:	The University of Kansas Center for Research, Inc. 2291 Irving Hill Drive - Campus West Lawrence, Kansas 66045
Title of Investigation:	Design Data Collection with SKYLAB/EREP Microwave Instrument S-193
Title of Report:	Cluster Analysis of Skylab Radscat Data
Period Covered:	3-26-73 through 12-31-75
NASA Contract:	NAS 9-13331
EREP Investigation:	549 M
Principal Investigator:	Professor Richard K. Moore
Date Written:	August 26, 1975
Monitor and Address:	Mr. Larry York Earth Observations Division Science and Applications Directorate NASA Manned Spacecraft Center Code TF 3 Houston, Texas 77058
Type of Report:	Advanced Report of Significant Results

APPENDIX B

CLUSTER ANALYSIS OF SKYLAB RADSCAT DATA

by A. Sobti, Samut Siriburi, and R. K. Moore

ABSTRACT

The Skylab S-193 radiometer/scatterometer produced terrain responses with various polarizations and observation angles for cells of 100 to 400 km^2 area. Classification of the observations into natural categories (for the sensor) was achieved by K-means and spatial clustering algorithms. The principal land use in each observation cell, or in representative sample cells, was determined by use of maps and Skylab S-190 photography. Little correlation was found between the clusters natural to the data and the land-use categories determined in this way, although water and land surfaces were usually separable and some gross trends could be inferred. Apparently natural clusters in microwave data are sufficiently affected by other factors to render such gross-resolution data ineffective for land use modelling.

INTRODUCTION

The Skylab radiometer/scatterometer operating at 13.9 GHz had a resolution cell ranging from approximately 100 sq. kms. at nadir incidence to approximately 400 sq. km. at 50° incidence. To determine if with such gross resolution the microwave response could be partitioned to identify or discriminate between major terrain features as discerned by maps and imagery, some clustering exercises were conducted. The Skylab radiometer/scatterometer provided backscattering coefficient and radiometric temperature at various angles of incidence and for various polarizations. The in-track modes provided multiple-angle observations of a target and the cross-track contiguous modes provided either a pair of radiometer or scatterometer measurements or one of each. The clustering exercises reported here are from data obtained with the in-track-contiguous and cross-track-contiguous pitch-offset 29° modes. The number of data points included in each clustering exercise varied and in one case exceeded 7000 points.

The principal procedure used was K-means clustering[1]. The computations were performed on a Honeywell 635 computer. Another clustering procedure, called spatial clustering[2] was attempted for one set of data. This latter procedure has been used quite effectively in the clustering of images from ERTS. The spatial clustering was performed on a PDP 15/20 computer. There was no significant difference in the ability to partition the data space into clusters corresponding to major terrain types.

---

[1] MacQueen, J., "Some Methods for Classification and Analysis of Multivariate Observations," 5th Berkeley Symposium on Probability and Statistics, 1972.

[2] Haralick, R. M. and I. Dinstein, "A Spatial Clustering Procedure for Multi-Image Data," IEEE Trans., v. CAS-22, May, 1975.

The Skylab Radiometer/Scatterometer Experiment

Skylab had on board a radiometer and scatterometer operating at 13.9 GHz which shared the same antenna and much of the rf hardware. The two sensors could be operated in near simultaneity; the sequence of observations and the various sensor configurations were predesigned into four possible modes which were selectable by the astronaut. The operation and characteristics of these sensors has already been described in numerous NASA publications, journals and technical reports, so only the portions germaine to this study will be reported.

Of the four modes possible, data from only two are reported in this study. The non-contiguous modes were used primarily over the ocean and data from these were not considering in the clustering exercises. The in-track-contiguous mode provided backscattering coefficient data at approximately 46°, 40°, 33°, 17°, and 3° off nadir. The targets with observations at all five angles of incidence were separated by approximately 25 kilometers and lay in the along-track direction. Radiometer measurements were made at angles from 46° to 3° where scatterometer measurements were not being made. These measurements were, however, not included in our data base. The cross-track-contiguous mode provided 12 measurements between $\pm 11^{\circ}$ of a scan initial point. The scan of the antenna was in the across-track direction and the scan could be initialized at 0°, 15°, 30°, or 40° in the pitch or roll direction. This cross-track-contiguous (CTC) mode could provide either a combination of a radiometer and a scatterometer measurement or two of either sensor with orthogonal polarizations. The pitch-off-set 30° submode of the CTC provided 12 measurement pairs with a very small change in incidence angles across the scan. This submode was the only one selected because the number of data points in the particular angle range (30°–33°) was largest for conducting the clustering exercises.

The targets viewed include areas in North America, South America and ocean surfaces. The South American targets were predominantly the tropical rain forest and savannah regions in Brazil. Maps and spacecraft imagery were used to determine the terrain composition of each cluster. Ideally a cluster based upon microwave responses should have been from only a singular terrain category for perfect discrimination or clustering.

Clustering Procedures

Two clustering procedures were attempted. The K-means clustering algorithm was used on all the data sets reported in this study. Spatial clustering was used as a comparison for one long ITC pass from Texas to Maine on day 253. The two methods of clustering are thoroughly described by references 1 for K-means and 2 for spatial clustering. The philosophies of the two clustering procedures are distinct and consequently the clusters formed are not the same.

K-Means Clustering

This procedure attempts to break up the data space into similarity groups. The procedure is not intended to find some unique, definitive grouping, but rather simply to aid the investigator in obtaining a qualitative and quantitative understanding of large amounts of N-dimensional data. The data base included for this study consisted of (1) all CTC pitch 29° data where the clustering was performed on the radiometer (reduced to emissivity) and scatterometer data for vertical polarization; (2) ITC data using all five angles for scatterometer measurements (3) ITC data using the middle three angles for scatterometer measurements, and (4) CTC pitch 29° data (scatterometer only).

The procedure involves two parameters: C for "coarsening" and R for "refinement". The data base is first converted so that all the data lie within a unit n dimensional sphere. This is a scaling procedure and the data can then be weighted by assigning weights to individual variables. The program starts with a user-specified value of K, and takes the first K points in the sample as the initial means. This selection can, however, be forced to select any particular points as the initial means (or seeds, as they are sometimes called). The clustering procedure is an iterative one where the nearest sample (in measurement space) based upon a distance criterion (usually square of the difference in magnitudes) is compared to the threshold values (C) selected; if the proximity is close enough, the sample is included in the group and a new mean computed. If the sample is greater than a distance R from each cluster, it is allowed to be another seed. In doing this, the group means are updated and each point iteratively assigned to groups or allowed to form its own cluster which can attract other samples. The final classification is performed with the means of the clusters obtained by the above iteration process. This classification is again based upon at least-distance criterion.

Figure B-1. The Non-Supervised Spatial Processing Approach

Non-Supervised Spatial Clustering

The spatial clustering algorithm differs from the usual clustering algorithms in that contextual information is used in the form of the spatial location of target cells. This algorithm was developed for analysis of image-like data where the partitioning of data into like regions must take into account the spatial distribution of each cell. The algorithm is carried out in two phases.

In the first phase, the spatial information of the image-like data base is used to determine regions of homogeneity. To create an image-like data base from data collected by the in-track modes of the S-193 sensors, the target cell was repeated in one direction (orthogonal to the track) so that there was a grid produced which had all columns equal. The clustering then only affected the rows. The regions of homogeneity are found by a boundary enhancement technique. This is shown in Figure B-1 as the gradient operator. The gradient image so produced is then processed through a threshold detector and the output image should then contain regions of homogeneity separated by boundaries where the gradient exceeded the threshold. The next step is labelling each homogeneous region.

The second phase of the algorithm consists of an iterative clustering procedure where each homogeneous region finds another homogeneous region that is closest (in measurement space) to it; if the two regions are close enough, they are merged to one cluster. This process of grouping homogeneous regions continues iteratively till there are only a few major clusters.

Determination of Composition of the Clusters

The composition by terrain categeries in the natural clusters produced by applying the clustering procedures to the microwave response was performed by a manual classification based upon maps and spacecraft imagery. The terrain categories chosen were quite gross and mixtures of two single categories (e.g. forest or agriculture) were combined to form composite categories (e.g. forest/agriculture where there was evidence of both and no predominance of either.

For some of the clustering exercises, the number of samples was very large and manually classifying each observation would have been prohibitively time-consuming. For such cases a random sample of up to 40 samples was manually classified for clusters which contained over 50 samples. For small-size samples, however, every point was classified manually.

The manual assignment of targets to terrain categories can often be in error because of two reasons: the maps were produced many years ago (5-20 years) and the land-use could have been somewhat altered; and examination of a gross-resolution map like, for example, the potential natural vegetation map calls for a subjective judgement on the part of the manual interpreter. Spacecraft imagery was used wherever available, but for the cross-track modes of operation only the inner angles in the cross-track scan were supported by imagery. Besides, large portions of the spacecraft imagery were rendered totally useless because of intervening clouds.

Results of Clustering

When considering only the land use and physiographic classifications as descriptors, the results of the clustering analysis were not encouraging. It would appear that factors other than those suggested by major biomes alone should be considered. The combinations of sensor responses that were considered in this study may not have been optimal for partitioning the terrain according to the physiographic features. Due to lack of time only a few clustering exercises were conducted. Future studies should consider clustering procedures with variables not considered here and should try to determine the casual relationship between some key parameters of the terrain and the microwave response. For example, one could introduce soil moisture variation as a terrain characteristic and assess if the clustered microwave measurements are keyed by the moisture variations of the surface. Such an analysis is more complicated than it would appear because soil moisture variations can often be masked by vegetation canopies. Clustering on some set of terrain descriptors and on some set of microwave response should provide similar clustered groups. This choice of terrain descriptors and set of microwave responses will be a culmination of many clustering attempts with various terrain descriptors and various sensor configuration responses.

The results reported here represent a first step in the exploratory process and suggest that more sophisitication in the definition of the terrain categories is required. These clustering analyses were conducted by considering the following combination of sensor configuration responses.

CROSS-TRACK CONTIGUOUS

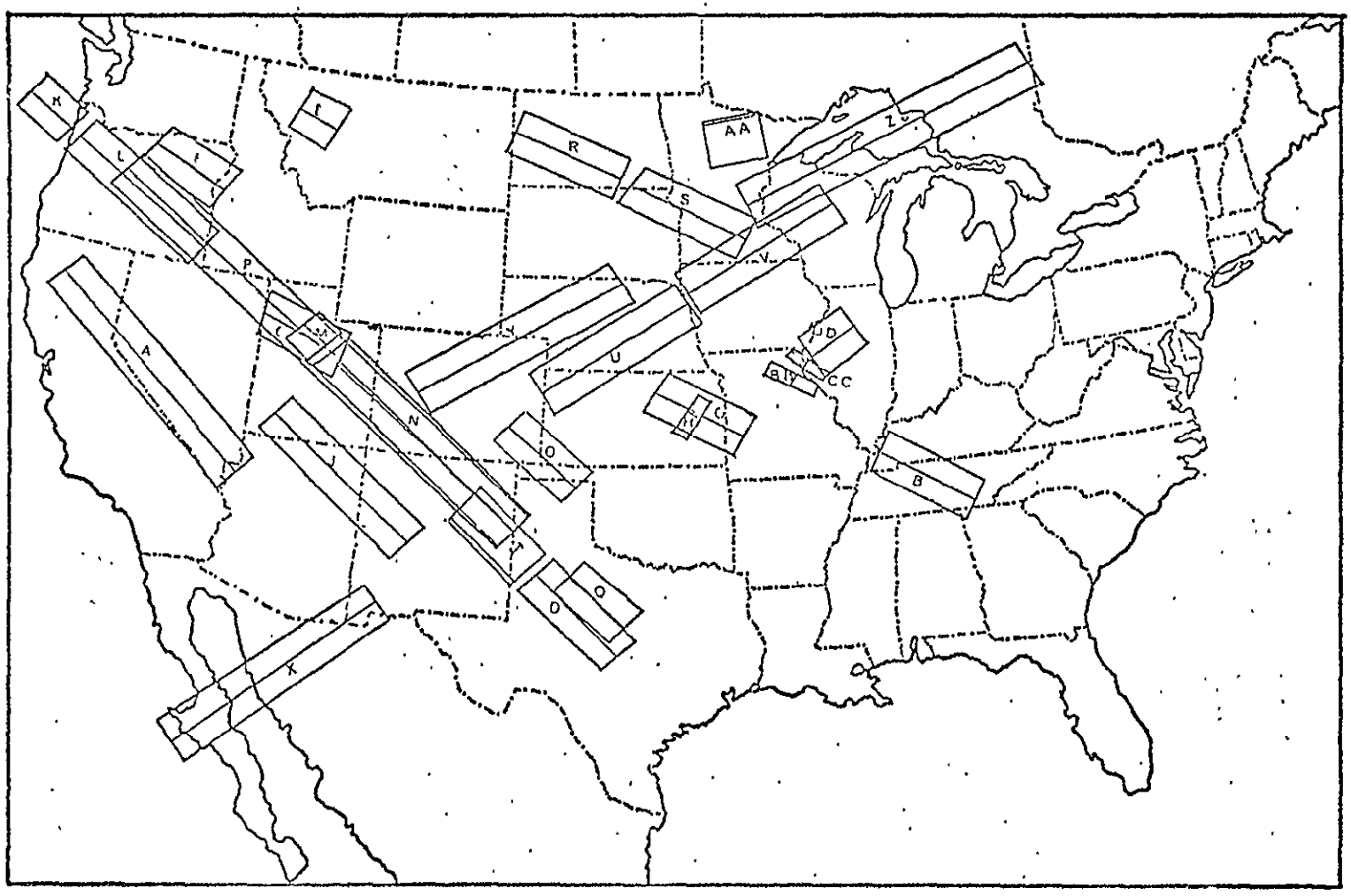

Figure B-2a. Cross-track contiguous data takes over U.S.A. during SL2 and SL3 missions considered in designing data catalogue.

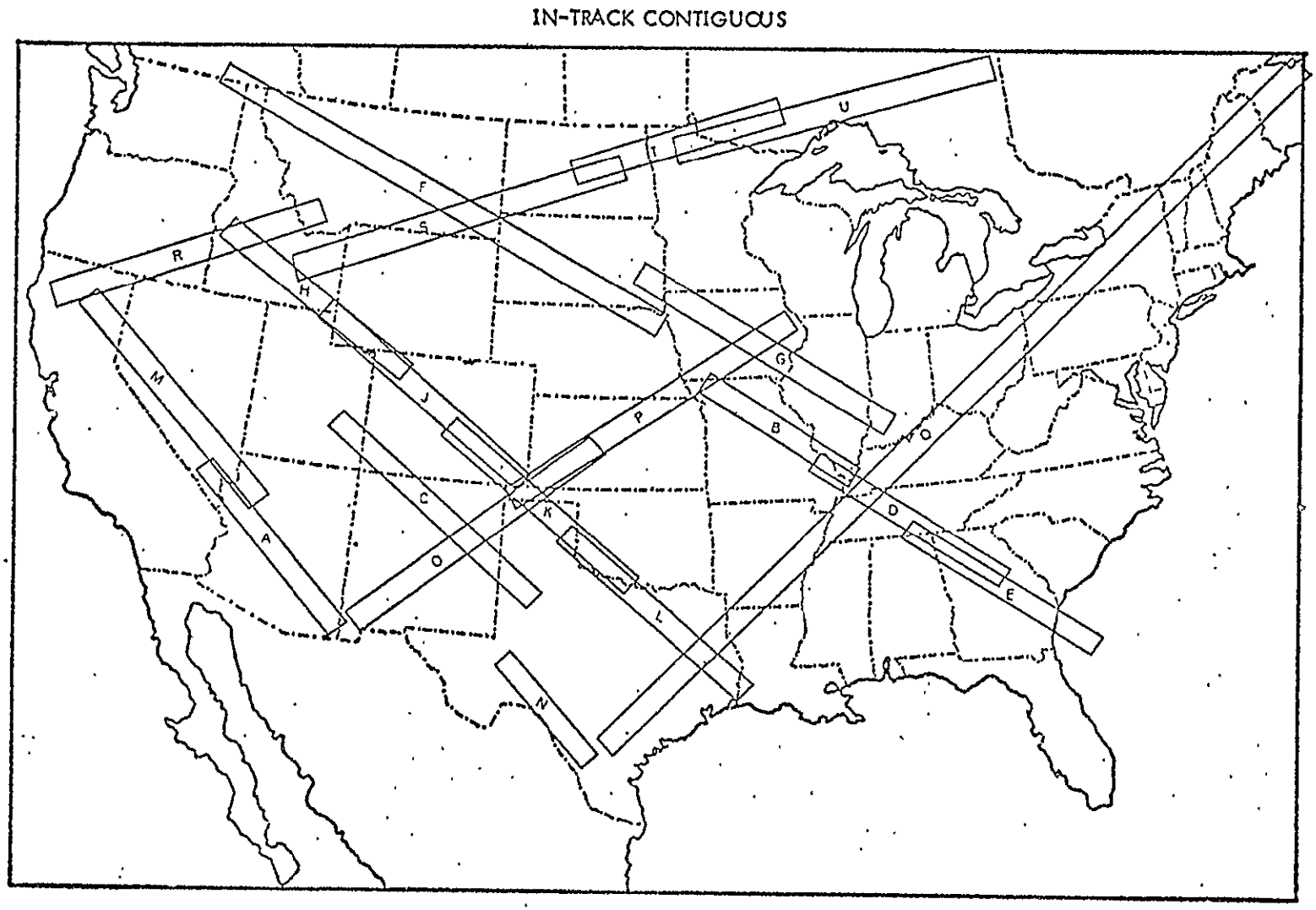

Figure B-2b. In-track contiguous data segments over U.S.A. during SL2 and SL3 missions considered in design of data catalogue.

1. The CTC pitch-offset-29° radiometer/scatterometer-mode data including both the backscatter and radiometric temperature for vertical polarization. Only North American targets are included.

2. The CTC pitch-offset-29° backscatter-only data for vertical polarization. North America, South America and Ocean data are all included.

3. The ITC (VV) backscattering coefficient for the middle three angles (17°, 33°, 41°) for all targets which were viewed by all three angles. This included some ocean targets and some targets that were not in the U.S.A.

4. The ITC (VV) backscattering data for the middle three angles (17°, 33°, 41°) for the long Texas-to-Maine pass on Day 253. This pass was also clustered by a spatial clustering procedure for comparison.

Figures B-2a and B-2b show passes from which the ITC and CTC data over North and South America were obtained.

Other clustering exercises were also conducted, using ITNC data over land and using ITC data for other combinations of sensor configurations than those listed above. These showed similar or worse results, although the number of samples to be clustered was in some cases not sufficient for any proper inference. These cases are not reported.

Clustering on Backscattering Coefficient and Radiometric Temperature at 33°

The CTC (VV) rad/scat pitch offset mode was exercised extensively over North America. Many target points were obtained from oceanic surfaces as well, but these were excluded from the data base. K-means clustering using the radiometer response and the backscatter response as the two-dimensional clustering variable produced five significant clusters. The total number of footprints was greater than 3000 so only a few random samples were manually classified for clusters that contained over 100 points.

A summary of the results is shown in Table B-1. The categories are described by alphanumeric codes; an explanation for these are given atop Figures B-3, B-4 and B-5.

Table B-1

D = Desert
R1 = Range - Grassland
R2 = Range - Thornbush
R3 = Range - Savanna
M1 = Range / Agriculrure
A = Agriculture
M2 = Agriculture / Forest
M3 = Range / Forest
F = Forest
T = Tropical Rain Forest
W = Water
U = Urban
n = Non Vegetated Terrain

CLUS-TER	NUMBER OF FOOTPRINTS													TOTAL
	D	R1	R2	R3	M1	A	M2	M3	F	T	W	U	N	
1	—	—	—	—	—	3	11	10	21	—	—	—	—	45
2	—	3	—	—	—	1	23	—	13	—	—	—	—	40*
3	—	—	—	—	2	7	26	—	5	—	—	—	—	40*
4	2	4	—	—	17	1	9	—	7	—	—	—	—	40*
5	10	5	—	—	3	3	4	—	15	—	—	—	—	40*
TOTAL	12	12	—	—	22	15	73	10	61	—	—	—	—	205

Results Of Clustering Analysis Considering Rad / Scat Responses From CTC Pitch 29° Operation.

(* Only A Few Random Samples Were Taken From Each Cluster . The Actual Number Of Points In Each Cluster Was Far Greater.)

Figure B-3

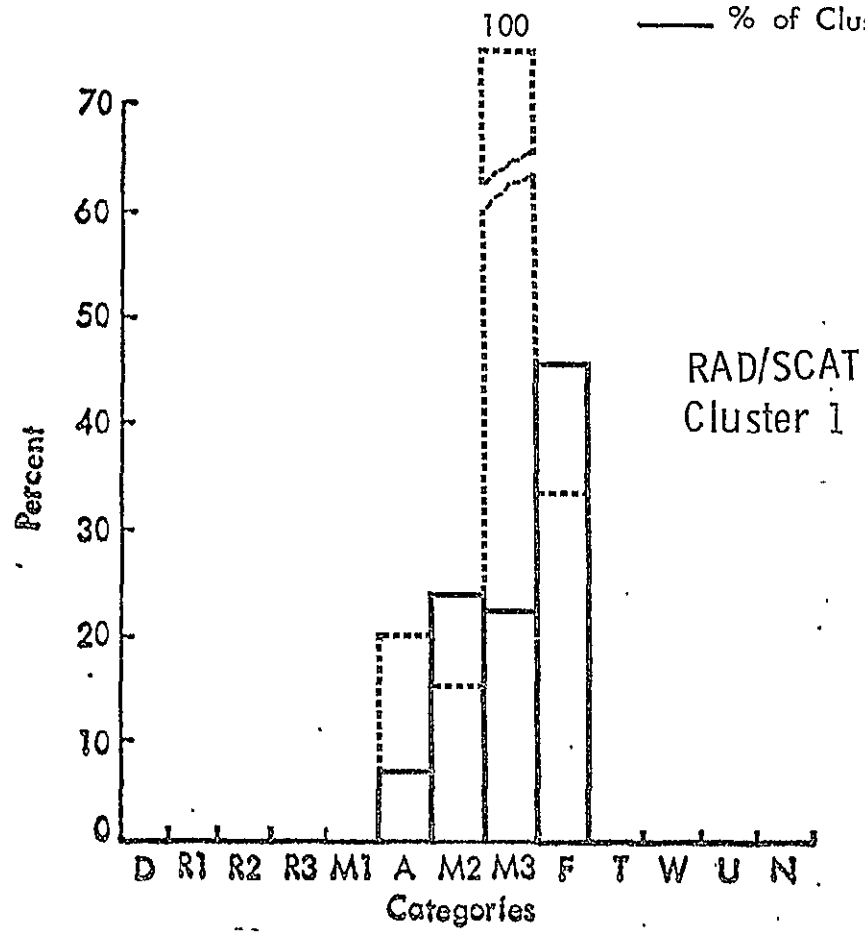

D = DESERT
R1 = RANGE - Grassland
R2 = RANGE - Thornbush
R3 = RANGE - Savanna
M1 = RANGE / AGRICULTURE
A = AGRICULTURE
M2 = AGRICULTURE / FOREST
M3 = RANGE / FOREST
F = FOREST
T = TROPICAL RAIN FOREST
W = WATER BODIES
U = URBAN
N = NON VEGETATED TERRAIN

PROPORTIONS OF MANUALLY CLASSIFIED PHYSIOGRAPHIC AND LAND/USE CATEGORIES IN EACH CLUSTER.
CLUSTERING VARIABLE: σ° AND EMISSIVITY AT 30°, VERTICAL INCIDENCE
DATA BASE: ALL CTC R/S DATA
TOTAL NUMBER OF CLUSTERS: 5

Figure B-4

D = DESERT
R1 = RANGE - Grassland
R2 = RANGE - Thornbush
R3 = RANGE - Savanna
M1 = RANGE / AGRICULTURE
A = AGRICULTURE
M2 = AGRICULTURE / FOREST
M3 = RANGE / FOREST
F = FOREST
T = TROPICAL RAIN FOREST
W = WATER BODIES
U = URBAN
N = NON VEGETATED TERRAIN

—— % of Cluster ..... % of Category

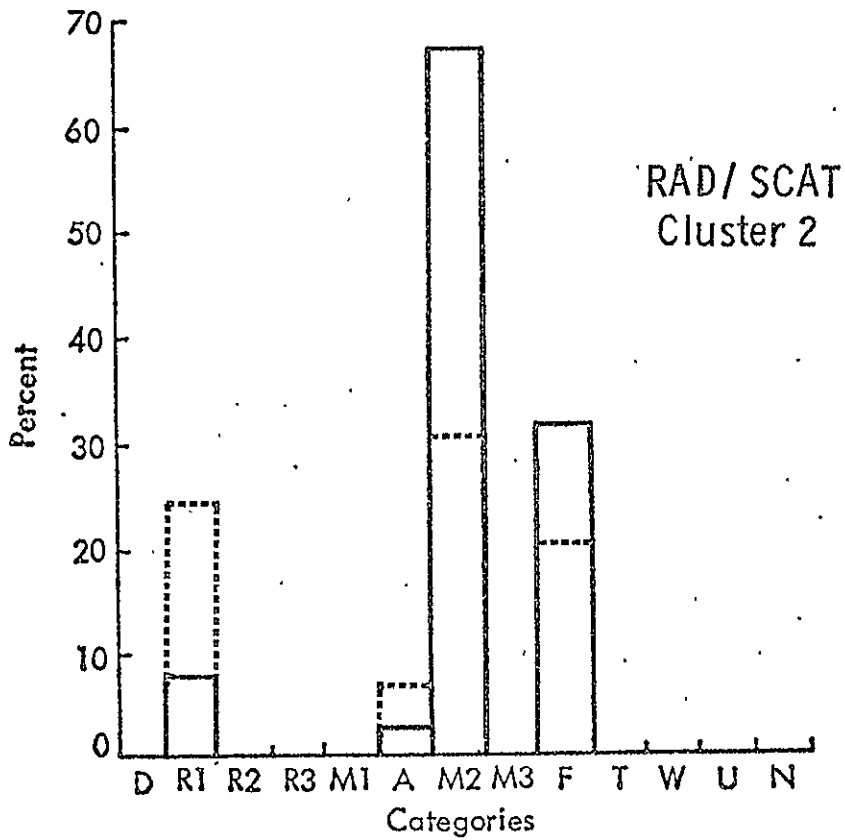

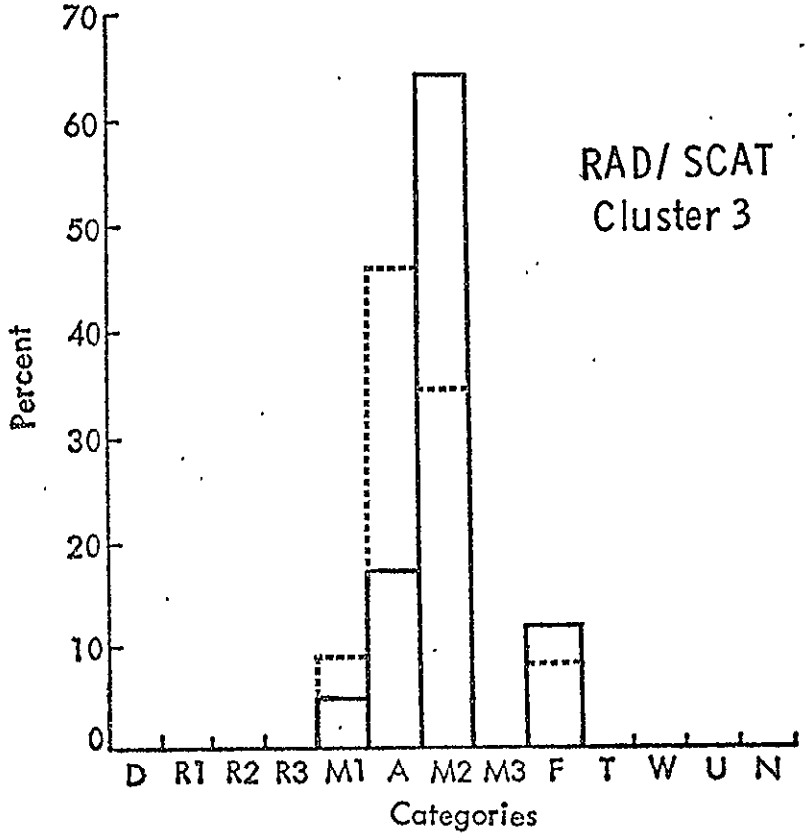

PROPORTIONS OF MANUALLY CLASSIFIED PHYSIOGRAPHIC AND LAND/USE CATEGORIES IN EACH CLUSTER.
CLUSTERING VARIABLE: σ^{o} AND EMISSIVITY AT 30°, VERTICAL INCIDENCE
DATA BASE: ALL CTC R/S DATA
TOTAL NUMBER OF CLUSTERS: 5

Figure B-5

D = DESERT
R1 = RANGE - Grassland
R2 = RANGE - Thornbush
R3 = RANGE - Savanna
M1 = RANGE / AGRICULTURE
A = AGRICULTURE
M2 = AGRICULTURE / FOREST
M3 = RANGE / FOREST
F = FOREST
T = TROPICAL RAIN FOREST
W = WATER BODIES
U = URBAN
N = NON VEGETATED TERRAIN

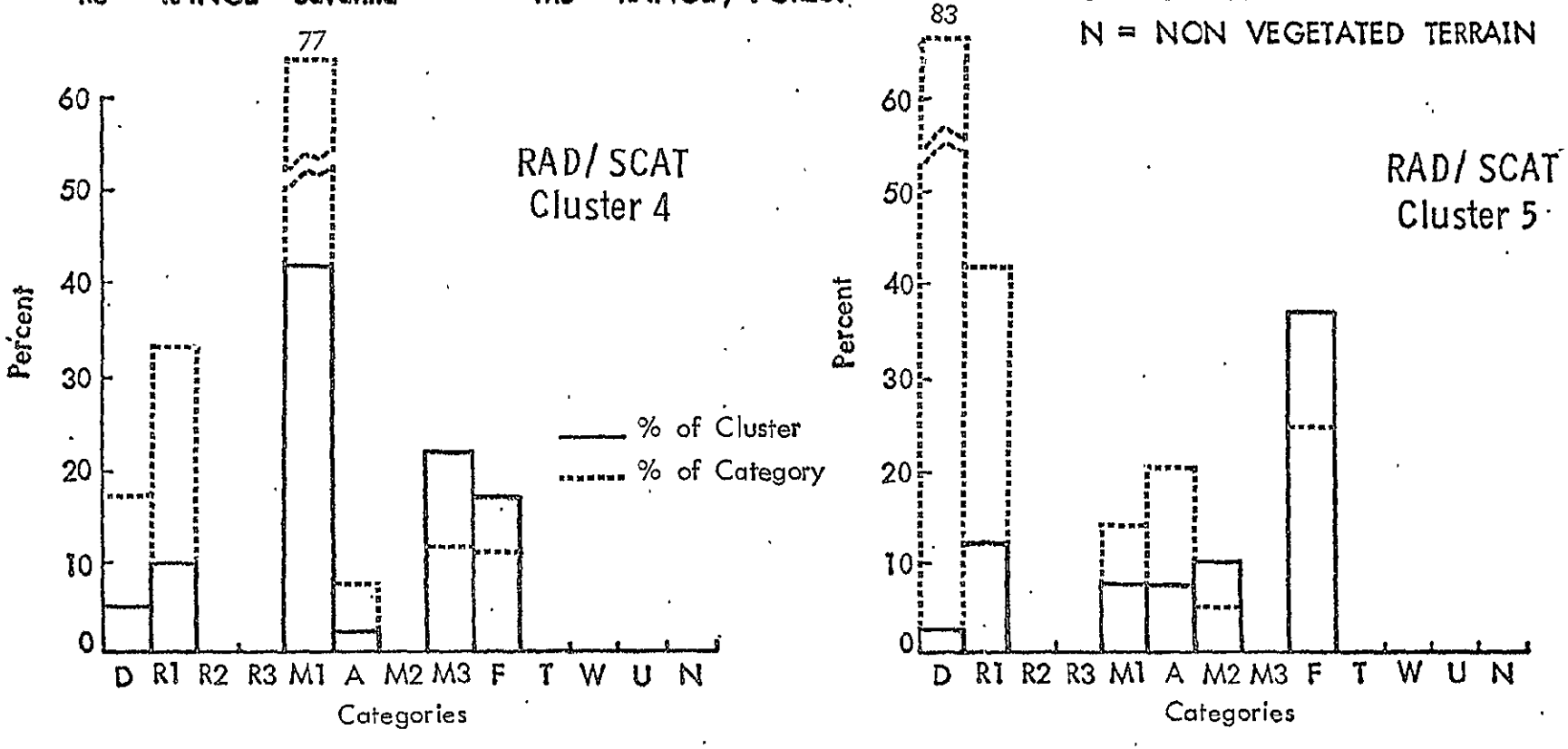

PROPORTIONS OF MANUALLY CLASSIFIED PHYSIOGRAPHIC AND LAND/USE CATEGORIES IN EACH CLUSTER.
CLUSTERING VARIABLE: σ^{o} AND EMISSIVITY AT 30°, VERTICAL INCIDENCE
DATA BASE: ALL CTC R/S DATA
TOTAL NUMBER OF CLUSTERS: 5

Figure B-6

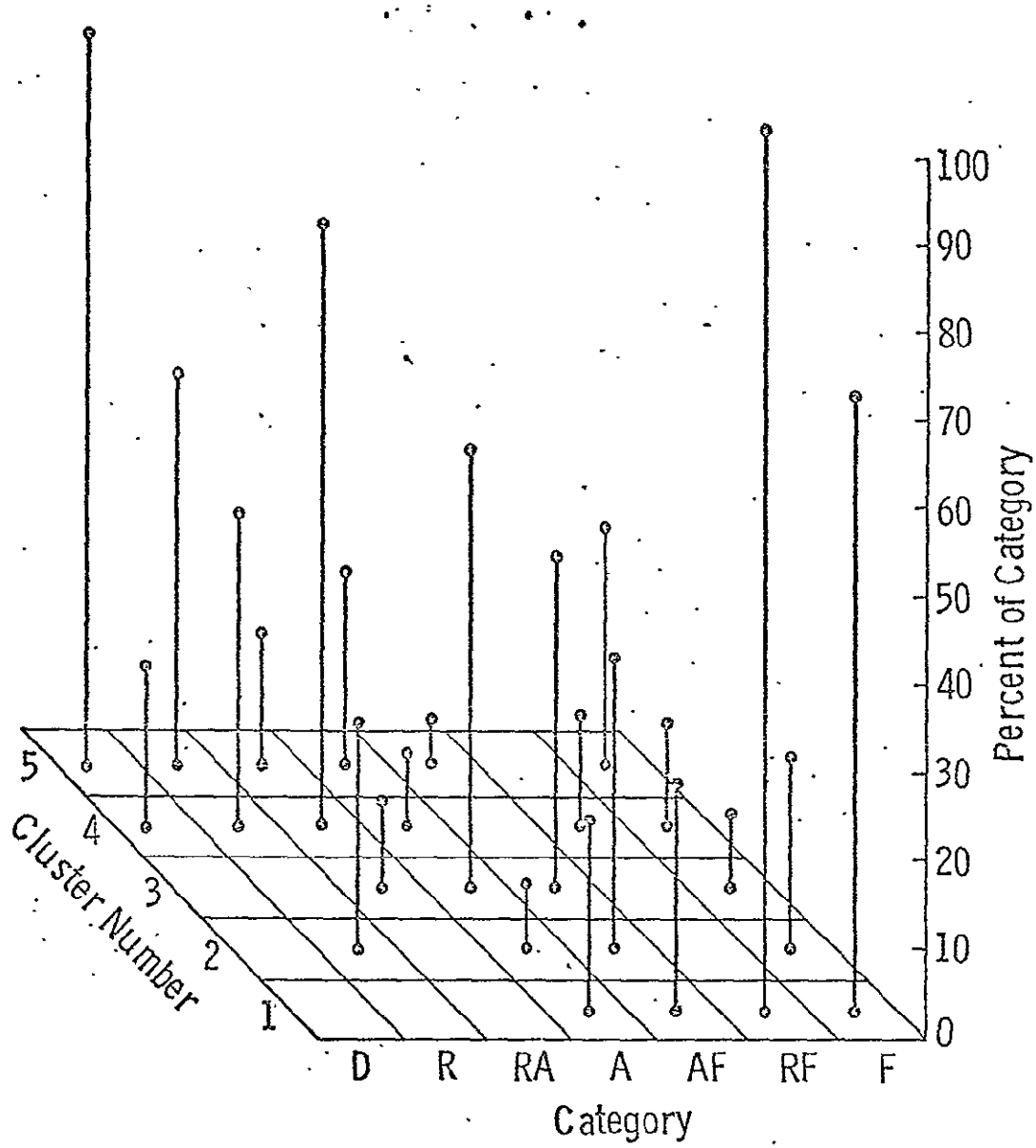

D - Desert
R - Range / Grassland
RA - Range / Agriculture
A - Agriculture
AF - Agriculture - Forest
RF - Range / Forest
F - Forest

Cluster Analysis of Cross-Track-Contiguous Microwave Data.
Clusters Based on Pitch 29° Radiometer and Scatterometer Data.

Except for cluster 1 which only had 45 samples, all the other clusters had samples in excess of a hundred; only 40 samples, randomly chosen were manually classified for these clusters. Figure B-3, B-4 and B-5 show a bar graph presentation of the proportion of each terrain category in each cluster. The bar graphs show the ratio of a particular category to the total number of samples in a cluster and to the total number in that category across all clusters. The first ratio is an indication of the composition of the cluster, the second ratio shows a measure of separability.

These results have been presented another way in Figure B-6, where the three-dimensional presentation makes it somewhat easier to see trends. Note that the horizontal axis is arranged approximately in the order of increasing vegetation amount and size. Clearly the less-vegetated areas are concentrated in the upper left hand of the figure, whereas the forest groups other than agriculture-forest are mostly in clusters 1 and 2. Agricultural terrain is more uniformly spread among the clusters.

These results are more encouraging for the use of microwave sensors than is at first apparent, but clearly better categorization of the "ground truth" is called for. For instance, the areas labelled desert undoubtedly include some range land, and those labelled range would in some cases be called desert by a different categorizer. The category containing both range and agriculture includes areas in which the agriculture is dry-land farming that should look very much like range, or even desert, to the microwave sensors. The general category "agriculture" includes everything from dry pastures and freshly plowed ground to densely vegetated stands of corn and milo. The former are similar in general dryness and roughness to the rangeland and some of the desert, whereas the latter are expected to scatter microwave energy as uniformly as a dense forest. Although it is somewhat surprising that "forest" should appear to a limited extent in category 5 where desert is so strong, it must be remembered that some land is classified as forest when it contains rather sparse stands of scrub trees containing little moisture.

In view of these comments, it seems that more appropriate categeries for use in this study would have been based upon density of vegetation (perhaps the biomass) rather than upon more traditional land-use major categories. After all, a dry-land bean farmer in central New Mexico has more in common with his cattle-grazing neighbor than with an Iowa corn-and-hog operator, and perhaps the categories used should reflect this. Unfortunately, this kind of distinction is more difficult to make from the types of land-use maps available for this study, and even from the space photos, than was the categorization used.

Clustering On Backscatter Response at 33°

The backscatter data from CTC (VV) pitch offset 29° rad/scat and scatterometer-only modes was used as a one-dimensional clustering variable. The number of points was over 7000 and the targets were in North America, South America (Brazil) and in the oceans. The number of significant clusters was 10 and a summary of the results is provided in Table B-2. Once again only a few random samples were classified from the larger clusters.

Without the radiometer data being included, of the four clusters in which there were water bodies, one contained a sizeable number of land targets. Cluster 5 also shown in Figure B-7 in a bar graph representation contained some desert rangeland, and a combination of rangeland, agricultural land and forest. The water targets were in the Gulf of Mexico and the land targets were in Texas, New Mexico and Arizona. The mean backscatter value for this cluster was -15dB and a verification showed that all of the land and ocean samples in this cluster registered very close to this mean value. Figure B-7 also shows a bar graph representation of cluster 7. The non-vegetated terrain category is comprised of a playa surface that appeared on imagery to be totally bare. Once again, there seems to be no particular partitioning of the terrain categories based upon the scattering data.

Figure B-8 shows a three-dimensional plot of these data like that of Figure B-6. The large number of clusters in this case makes discrimination more difficult than it was in Figure B-6. Note, however, that the forest categories F, RF, and T are concentrated in clusters 7, 9 and 10; the only other categories making a significant contribution to this group of clusters are RA, and AF. Conceivably significant portions of the RA and RF categories contained either dense crops like maturing corn or significant number of trees. Regrettably, it was not possible to check these conjectures out point by point because of lack of time.

The tropical rain forest is contained completely in clusters 9 and 10, and it is the only constituent of cluster 9. Thus, the ability to distinguish this type of dense forest seems assured. Most of the water was clearly distinguished into clusters 4, 6, and 8, with the exception of the small contribution in cluster 5. The reason for this is not known. Also somewhat surprising in view of the results of the radscat evaluation is that "Agriculture" appears only in the single cluster, 1. The only explanation seems to be that more of the cells classified as agriculture-only were of the same type in this set of data than in the radscat data.

Table B-2

D = Desert
R1 = Range - Grassland
R2 = Range - Thornbush
R3 = Range - Savanna
M1 = Range / Agriculrure
A = Agriculture
M2 = Agriculture / Forest
M3 = Range / Forest
F = Forest
T = Tropical Rain Forest
W = Water
U = Urban
n = Non Vegetated Terrain

CLUS-TER	NUMBER OF FOOTPRINTS													TOTAL
	D	R1	R2	R3	M1	A	M2	M3	F	T	W	U	N	
1	4	10	11	2	2	4	5	1	—	—	—	—	—	39 *
2	9	19	4	—	—	—	1	3	4	—	—	—	—	40 *
3		M	A	L	F	U	N	C	T	I	O	N		
4	—	—	—	—	—	—	—	—	—	—	40	—	—	40 *
5	6	6	—	1	1	—	2	—	—	—	23	—	—	39 *
6	—	—	—	—	—	—	—	—	—	—	15	—	—	15 *
7	1	6	5	1	2	—	4	14	6	—	—	—	1	40 *
8	—	—	—	—	—	—	—	—	—	—	40	—	—	40*
9	—	—	—	—	—	—	—	—	—	40	—	—	—	40*
10	—	6	5	—	—	—	—	2	—	27	—	—	—	40*
TOTAL	20	47	25	4	5	4	12	20	10	67	118	—	1	333

Results Of Clustering Analysis Considering Scatterometer Responses From CTC Pitch 29° Operation.

(* Only A Few Random Samples Were Taken From Each Cluster . The Actual Number Of Points In Each Cluster Was Far Greater.)

Figure B-7

D = DESERT
R1 = RANGE - Grassland
R2 = RANGE - Thornbush
R3 = RANGE - Savanna
M1 = RANGE / AGRICULTURE
A = AGRICULTURE
M2 = AGRICULTURE / FOREST
M3 = RANGE / FOREST
F = FOREST
T = TROPICAL RAIN FOREST
W = WATER BODIES
U = URBAN
N = NON VEGETATED TERRAIN

—— % of Cluster ------ % of Category

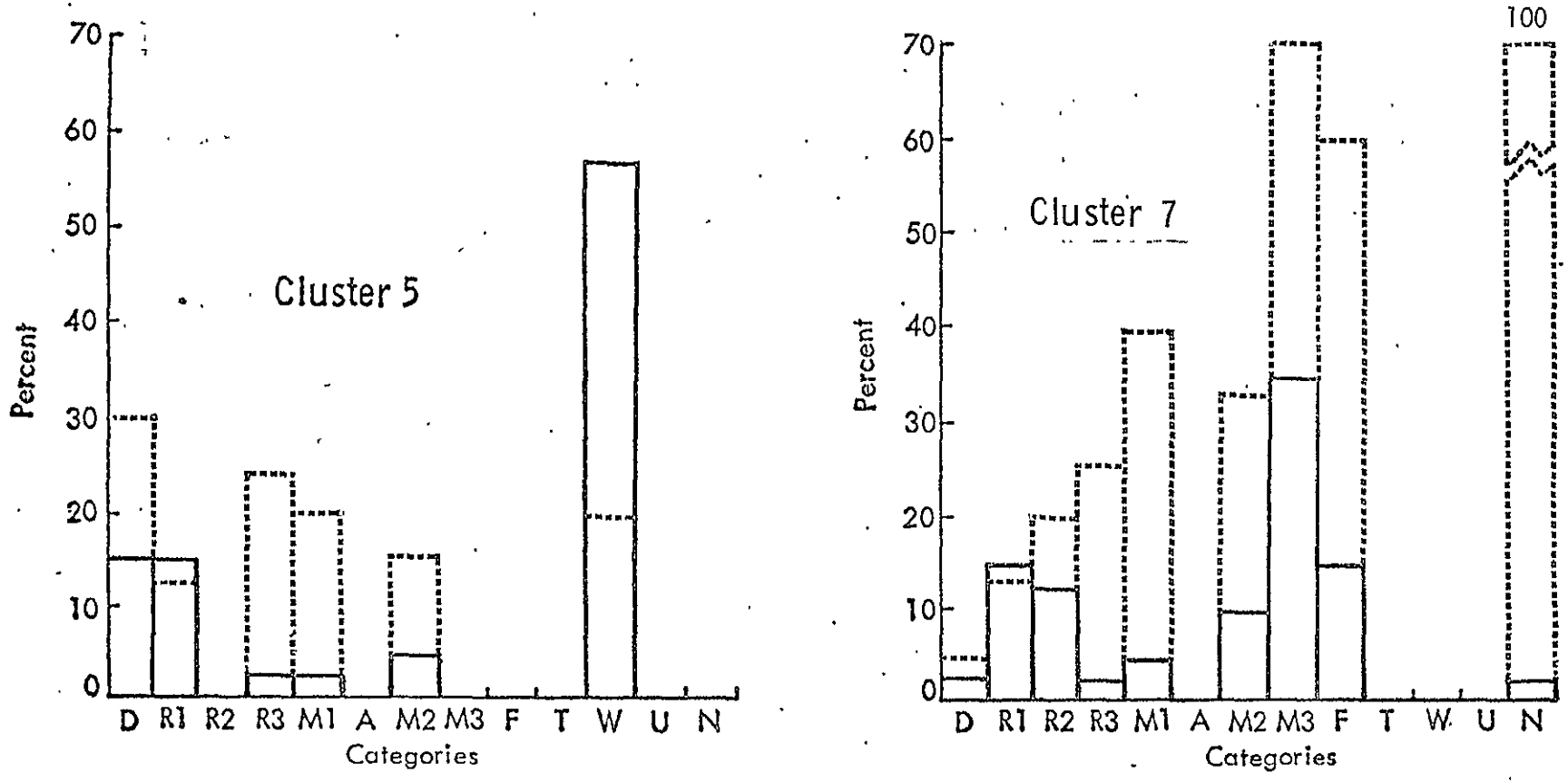

PROPORTIONS OF MANUALLY CLASSIFIED PHYSIOGRAPHIC AND LAND/USE CATEGORIES IN EACH CLUSTER.
CLUSTERING VARIABLE: σ^{o} AND EMISSIVITY AT 30°, VERTICAL INCIDENCE
DATA BASE: ALL CTC SCAT. DATA
TOTAL NUMBER OF CLUSTERS: 10

Figure B-8

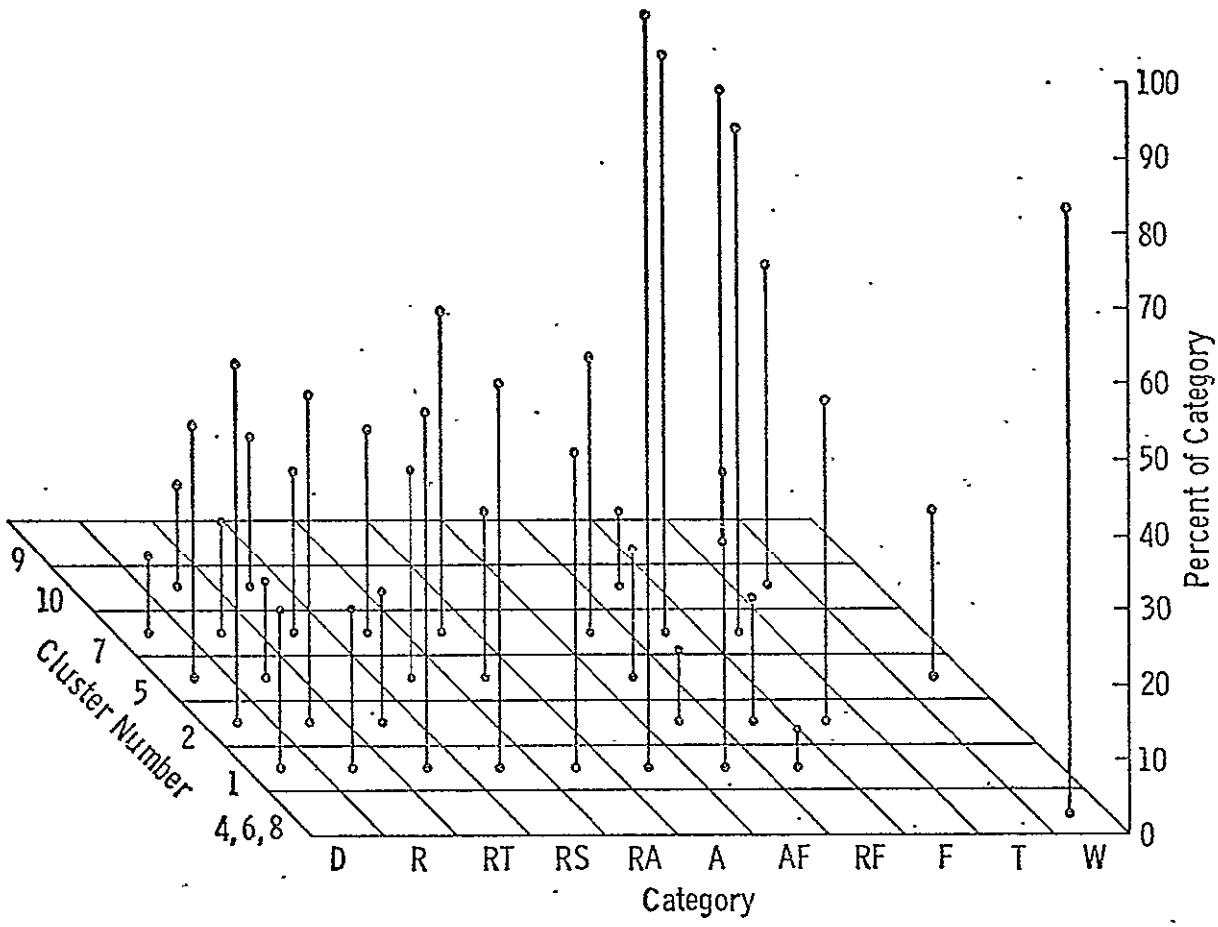

D - Desert
R - Range / Grassland (North America)
RT - Range / Thornbush (Brazil)
RS - Range / Savanna (Brazill)
RA - Range / Agriculture
A - Agriculture
AF - Agriculture / Forest
RF - Range / Forest
F - Forest
T - Tropical Rain Forest
W - Water

Cluster Analysis of Cross-Track-Contiguous Pitch 29° Scatterometer Data.

One conclusion that might be drawn from this data set is that the number of clusters should be deliberately reduced to something less than 10 by increasing the permitted data-space radius. Clearly the sensor is not capable of making real distinctions of this many categories of the type obtained from maps, and allowing the number of clusters to remain large tends to confuse interpretation.

The ITC (VV) data were sorted so that the backscatter responses of a target to the three angles considered were grouped. This was the three-dimensional measurement vector used for clustering. A K-means clustering procedure produced 10 significant clusters. Three others were discarded because of obvious errors in the computation of backscatter or the ephemerides of the target or both. The proportions of the terrain categories in each cluster are shown in Table 3.

One can see that water is always separable from land (clusters 3, 9 and 10). The three clusters of water correspond to distinctly different backscattering coefficients for each. The probable cause of the three separate water clusters is wind speed. Below a wind speed of 4-6 knots the backscattering coefficient at these oblique incidence angles falls very rapidly.

Figure B-9 illustrates in three dimensions the results of this clustering. The clear separation of water is apparent, but it is also apparent that the forested categories are concentrated in clusters 2 and 8, whereas clusters 5, 6, and 7 contain mostly agriculture and range. Cluster 4 contains range alone. The amount of agriculture appearing in cluster 2 is explainable as before is land that contains dense crops, but the presence of range in the same category as the forests cannot be explained.

This data set shows some promise for classification using the scatterometer if better categories were developed, but it is not highly encouraging. Perhaps a combination of better categorization with finer resolution that permits the cells to be more homogeneous would work better, but of course this is conjecture.

Table B-3

D = Desert
R1 = Range - Grassland
R2 = Range - Thornbush
R3 = Range - Savanna
M1 = Range / Agriculture
A = Agriculture
M2 = Agriculture / Forest
M3 = Range / Forest
F = Forest
T = Tropical Rain Forest
W = Water
U = Urban
N = Non Vegetated Terrain

CLUSTER	NUMBER OF FOOTPRINTS													TOTAL
	D	R1	R2	R3	M1	A	M2	M3	F	T	W	U	N	
1	—	4	—	—	—	1	—	—	—	—	—	—	—	5
2	—	7	—	—	—	4	25	—	15	—	—	—	—	51
3	—	—	—	—	—	—	—	—	—	—	3	—	—	3
4	—	12	—	—	—	—	—	—	—	—	—	—	—	12
5	—	3	—	—	—	3	9	—	—	—	—	—	—	15
6	—	13	—	—	—	8	—	—	—	—	—	—	—	21
7	—	10	—	—	—	4	—	—	—	—	—	—	—	14
8	—	6	—	—	—	1	19	—	16	—	—	—	—	42
9	—	—	—	—	—	—	—	—	—	—	9	—	—	9
10	—	—	—	—	—	—	—	—	—	—	15	—	—	15
TOTAL	—	55	—	—	—	21	53	—	31	—	27	—	—	187

Proportions Of Land/Use And Physiographic Categories In Clusters Produced By Considering Backscatter Coefficients At 42^0, 33^0 And 17^0 From ITC (VV) Data. Only U.S. And Some Ocean Targets Are Considered.

Figure B-9 .

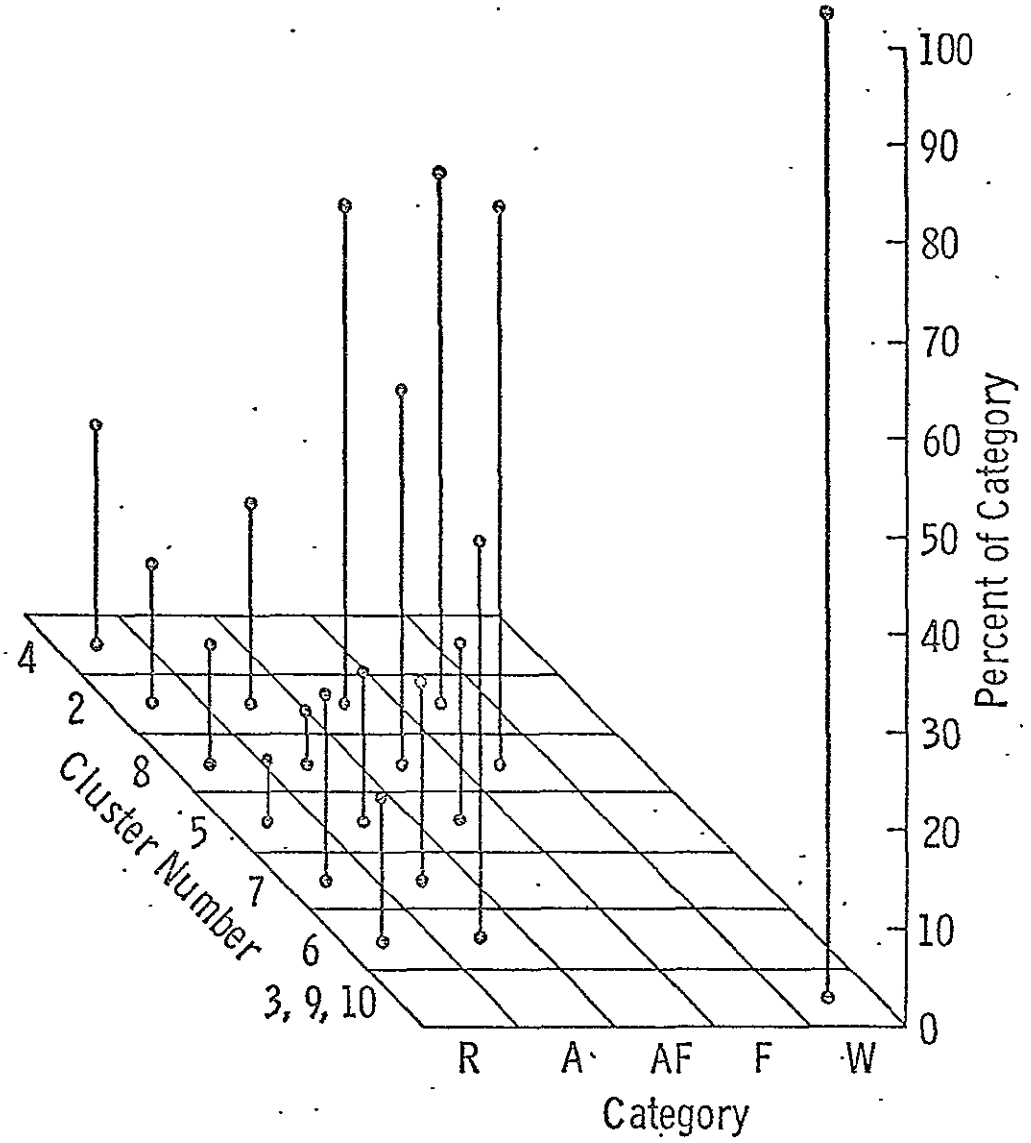

R - Range / Grassland
A - Agriculture
AF - Agriculture / Forest
F - Forest
W - Water

Cluster Analysis of In-Track-Contiguous Microwave Data. Clusters Based on Multi-Angle Scatterometer Data.

Comparison of K-Means and Spatial Clustering Using Backscattering Coefficient at 42°, 33° and 17°

An ITC (VV) pass on September 10, 1973 which viewed regions from Texas to Maine (see Figure B-1) was considered as a sample where two clustering approaches were compared. The middle three angles (42°, 33° and 17°) backscatter response was considered as the three-dimensional variable. K-means clustering results were obtained from the clustering exercise described above. Only clusters with a significant number of samples were chosen. The clusters which contained only one or two samples in a particular category and for which the targets were from this sample pass were ignored because they would be misleading if shown. The three clusters produced are shown in Table B-4.

The backscattering coefficient at each of the angles considered was then quantized separately by an equal probability quantizing algorithm. This three angle backscatter was then considered as the three-dimensional variable for spatial clustering. Spatial clustering has been used primarily on images, therefore to make our data appear in an image-like format we repeated the variables n times to create n columns of the image.

Two approaches with spatial clustering were attempted: for one, the gradient threshold was set at unity and regions of homogeneity were first found before the clustering procedure was applied; and two, each row of the psuedo-image (corresponding to each original measurement vector) was considered to be an independent quantity for clustering. Note that in the first case regions of transition (when the gradient threshold has been exceeded) would not register and those data points would not be considered in the subsequent clustering procedure.

Tables B-4, B-5 and B-6 show the results for the K-means clustering, spatial clustering with each element considered in the clustering and with a gradient threshold set at unity respectively. Although the ratio of the elements in the columns for agriculture, agriculture/forest and forest vary there is no clean-cut differentiation of terrain types possible with any of the three.

D = Desert
R1 = Range - Grassland
R2 = Range - Thornbush
R3 = Range - Savanna
M1 = Range / Agriculrure
A = Agriculture
M2 = Agriculture / Forest
M3 = Range / Forest
F = Forest
T = Tropical Rain Forest
W = Water
U = Urban
n = Non Vegetated Terrain

CLUS-TER	NUMBER OF FOOTPRINTS													TOTAL
	D	R1	R2	R3	M1	A	M2	M3	F	T	W	U	N	
2	–	–	–	–	–	3	22	–	14	–	–	–	–	39
5	–	–	–	–	–	–	6	–	–	–	–	–	–	6
8	–	–	–	–	–	–	19	–	11	–	–	–	–	30
TOTAL	–	–	–	–	–	3	47	–	25	–	–	–	–	75

Table B-4 Results of K-means Cluster Analysis Using σ° at 42°, 33° and 17° From ITC (VV) Mode for Texas-to-Maine Pass on Day 253

CLUS-TER	NUMBER OF FOOTPRINTS													TOTAL
	D	R1	R2	R3	M1	A	M2	M3	F	T	W	U	N	
A	–	–	–	–	–	1	24	–	15	–	–	–	–	40
B	–	–	–	–	–	4	31	–	12	–	–	–	–	47
C	–	–	–	–	–	–	9	–	–	–	–	–	–	9
TOTAL	–	–	–	–	–	5	64	–	27	–	–	–	–	96

Table B-5 Results of Spatial Clustering Analysis for Same Data Set Used for Table B-4. No Gradient Threshold.

CLUS-TER	NUMBER OF FOOTPRINTS													TOTAL
	D	R1	R2	R3	M1	A	M2	M3	F	T	W	U	N	
A	–	–	–	–	–	–	15	–	14	–	–	–	–	29
B	–	–	–	–	–	2	4	–	–	–	–	–	–	6
C	–	–	–	–	–	–	9	–	–	–	–	–	–	9
D	–	–	–	–	–	–	15	–	7	–	–	–	–	22
TOTAL	–	–	–	–	–	2	43	–	21	–	–	–	–	66

Table B-6 Results of Spatial Clustering Analysis for Same Data Set Used for Tables B-4 and B-5. Gradient Threshold = 1.

Conclusion

Based upon the results of a few clustering exercises using certain combinations of Skylab radiometer/scatterometer responses, it appears that the terrain features identified by maps and imagery are not necessarily separable in their microwave response. It may very well be that the microwave response to other combinations of sensor configurations could produce results which can allow a separation of terrain based upon the microwave response. The Skylab radiometer/scatterometer has a gross resolution and the assignment of observations into terrain categories was based upon examination of maps (supplemented by spacecraft imagery) which calls for a subjective decision. Furthermore, the use of land-use rather than vegetation-density categories was probably a mistake. These may have been factors which contributed to the results reported here.

Variation in vegetation biomass and particularly variations in soil moisture within and among categories could have been a factor, but these are not obtainable from the ground information available.

Clearly the microwave responses do separate into different clusters. Proper descriptions of the content of these clusters would be extremely interesting, but this must be deferred until later experiments for which more extensive ground information can be collected specifically for the experiment. These as yet undescribed categories may be very useful for some applications, but apparently gross land-use determination is not one of the suitable applications.

REFERENCES

1. Anderson, J. R., E. E. Hardy and J. T. Roach, "A Land-Use Classification System for Use With Remote-Sensor Data," Geological Survey Circular. 671, Washington, 1972.

2. Haralick, R. M. and I. Dinstein,"A Spatial Clustering Procedure for Multi-Image Data," IEEE Trans. on Circuits and Systems, v. CAS-22, May, 1975.

3. Kuchler, A. W., "Potential Natural Vegetation of the Conterminous U.S.,: Manual to Accompany the Map," American Geographical Society Special Publication No. 36, 1964.

4. MacQueen, J., "Some Methods for Classification and Analysis of Multivariate Observations," Fifth Berkeley Symposium on Probability and Statistics, 1972.

5. Sobti, A., "A Simulation Study of the S193 RADSCAT in Orbit," Technical Report 190-2, The University of Kansas Center for Research, Inc., Remote Sensing Laboratory, Lawrence, May, 1973.

6. United States Department of Interior, Geological Survey, "The National Atlas of the United States of America," Washington, D.C., 1970.

APPENDIX C

BACKSCATTER RESPONSE AT 13.9 GHz

FOR MAJOR TERRAIN TYPES AS SEEN FROM ORBIT

Technical Report 243-4

BACKSCATTER RESPONSE AT 13.9 GHZ FOR MAJOR TERRAIN TYPES AS SEEN FROM ORBIT

by

A. Sobti, R. K. Moore and S. T. Ulaby

August 15, 1975

Prepared for

National Aeronautics and Space Administration
Lyndon B. Johnson Space Center
Houston, Texas

Organization Full Name:	The University of Kansas Center for Research, Inc. 2291 Irving Hill Drive - Campus West Lawrence, Kansas 66045
Title of Investigation:	Design Data Collection with SKYLAB/EREP Microwave Instrument S-193
Title of Report:	Backscatter Response at 13.9 GHz for Major Terrain Types as Seen from Orbit
Period Covered:	3-26-73 through 12-31-75
NASA Contract:	NAS 9-13331
EREP Investigation:	549M
Principal Investigator:	Professor Richard K. Moore
Date Written:	August 15, 1975
Monitor and Address:	Mr. Larry York Earth Observations Division Science and Applications Directorate NASA Manned Spacecraft Center Code TF 3 Houston, Texas 77058
Type of Report:	Advanced Report of Significant Results

APPENDIX C

BACKSCATTER RESPONSE AT 13.9 GHZ FOR MAJOR TERRAIN TYPES AS SEEN FROM ORBIT

A. Sobti, R.K. Moore, and S.T. Ulaby
RSL TR 243-4

ABSTRACT

The S-193 radar scatterometer that flew aboard Skylab provided information on radar returns from many kinds of terrain. Many of the "footprints" of the scatterometer have been classified into terrain types, primarily in terms of land use, by examination of physiographic and land-use maps along with Skylab photographs where clouds did not interfere. The mean scattering coefficients for vertical polarization observed at angles of incidence between 1.5° and 46° are reported here for water bodies. The standard deviations of the measurements are also reported. Means vary from about 13 dB at 1.5° for the salt flats of Utah to about -18 dB for water at 46°. For more normal land categories they range from about +2 dB at 1.5° for desert to -12.5 dB for rangeland at 46°. Since the categories are broad and not based upon expected microwave response, but rather on physiographic and land use descriptions, the ranges between upper and lower standard deviations overlap for most categories.

INTRODUCTION

The space operation of the S-193 scatterometer, operating at 13.9 GHz (2.16 cm wavelength) on board Skylab provided data over many regions of the world. Statistics of the backscatter response from various regions of the world have been reported elsewhere. Comparisons are made here of the backscattering coefficients measured for various terrain categories which were identified by an examination of physiographic and land use maps and spacecraft imagery (from S190A and S190B cameras on board Skylab). The terrain categories chosen are rather gross because the target resolution size of the S-193 scatterometer is large (ranging from 100 square kilometers to 400 square kilometers). Since this effort involves comparisons of backscatter response over "footprints" that were classified by manual interpretation, the data base consists of only a small sample from the many passes made by the S-193 scatterometer. The emphasis in selecting candidate passes has been on finding areas where the land use and physiographic features were easily accessible and where large areas of homogeneous terrain were known to exist. The large extent of rain forests in

Brazil is a prime example of the latter case. The backscatter response from ocean surfaces, computed by considering many passes over the ocean, is shown for comparison. The data presented here are for vertical polarization only.

THE SKYLAB RADAR SCATTEROMETER EXPERIMENT

One of the sensors observing the earth from Skylab was a radar scatterometer (termed the S-193), operating at 13.9 GHz. Characteristics of this instrument have been described in various NASA publications and in some journals, so only the briefest summary will be included.

The Skylab scatterometer was part of a composite radiometer/scatterometer and altimeter all operating at 13.9 GHz and sharing the same parabolic antenna and much of the rf hardware. The beamwidth (two-way) of the mechanically scanned dual-polarized antenna was 1.45°. The scan of the antenna was programmed and selection of one of four possible modes was made by the astronaut.

1. In-Track Non-Contiguous (ITNC--overlapping measurements at angles of 0°, 15°, 29°, 40° and 48° from nadir, with 100 kilometers spacing between each set of targets with measurements at all five angles).

2. Cross-Track Non-Contiguous (CTNC--measurements at the same angles of incidence as ITNC but perpendicular to the track so that there is a 100 kilometer spacing between every target point and no overlap).

3. In-Track Contiguous (ITC--measurements at the same angles as the non-contiguous modes but in pitch (along track) and at a spacing of 25 kilometers between adjacent targets with all five angles).

4. Cross-Track Contiguous (CTC--measurements within $\pm 11°$, perpendicular to track about a scan initialized point. The scan could be initialized at nadir, or 15°, 30°, 40° in pitch or roll but not both).

The non-contiguous modes were exercised mainly over the ocean although some were also flown over land. For this study the contiguous modes were the major sources of data over land and the non-contiguous modes were the exclusive sources for data over the ocean. The non-contiguous modes provided coverage with all four transmit-receive polarization pairs while the contiguous modes provided coverage with any selected polarization pair. The target size varied with incidence angle and ranged from a minimum of 97 square kilometers (a circle with a diameter of approximately 11 kms) to to a maximum of approximately 387 sq. kms (an ellipse 17.3 by 28 kilometers).

Data from the first and second occupancies of Skylab were used in this study. The passes chosen over land are shown in Table 1. These passes are predominantly over the continental U.S.A. although there are a few over South America. There were a total of 10 passes with the ITNC mode configuration over ocean surfaces which were used to compute the statistics of the backscattering coefficients over the ocean.

The major terrain categories into which all terrain was to be classified were:

1. A -- Agriculture
2. D1 -- Desert (Nevada, Arizona)
3. D2 -- Desert (New Mexico, Texas)
4. F -- North American Forest
5. R -- Rangeland
6. SF -- Salt Flats, Utah
7. SH -- Sand Hills, Nebraska
8. TF -- Tropical Forest, Brazil
9. W -- Water, Ocean

The comparisons were made by considering a number of samples for each polarization and angular group.

CHARACTERISTICS OF BACKSCATTER FOR VARIOUS TERRAIN

For terrain categories with sufficient samples in a particular 2° incidence-angle group centered at 1.5°, 17°, 33° and 46°, histograms of the distribution of the backscattering coefficient were generated. Along with these histograms, standard deviations of the mean backscattering coefficient were also computed. Where the sample size for a particular terrain category and incidence angle group was insufficient to warrant a histogram, only the mean value is provided. Some terrain categories had enough samples at each of the four angles considered to produce histograms, while others only had sufficient data at one angle.

The angles chosen for describing the backscatter coefficient are dictated by the availability of data. These angles are the true incidence angles for the in-track modes of operation; the cross-track contiguous mode with the appropriate pitch- or roll-offset also provides data at or near these angles. Over land, the number of samples ranges from a maximum of 99 for Forest at 46° to a minimum of 8 for Desert (Nevada, Arizona) at 1.5°. The number of samples over the ocean surface always exceeded 82 for all four angles of incidence considered.

The backscattering coefficients for the various terrain categories are presented for each of the four incidence angle groups separately. Figure 1 shows the distribution

of backscattering coefficient for the different categories for an incidence angle centered at 1.5°. The range between the upper and lower values that are one standard deviation from the mean at this angle are greater than for any of the other angles for every surface. The range between these upper and lower bounds for the ocean are greater at all angles than for any land category. The mean for the ocean is lower than that for the Salt Flats in Utah but the upper bound (hereinafter the one sigma value is called the bound) for ocean is higher than the mean for the Salt Flats. As an example, the histogram of the distribution for the ocean for vertical polarization and for the angle group considered here is shown in Figure 2. The mean value for σ^o (the backscattering coefficient) is 12.32 dB. This is about 10 dB higher than the backscatter over an ensemble of targets over North America. The mean value for Utah Salt Flats (13.5 dB) is quite expected because the Utah Salt Flats appear like a smooth reflector at 2 cms wavelength.

The backscatter responses for the remaining five terrain categories which registered data for this angle (see Figure 1) show a great amount of overlap. Rangeland, Forest, and Agriculture had enough samples to produce histograms. The spread between the upper and lower bounds for all three of these groups is approximately 7 dB. The range between upper and lower bounds for these categories overlap the means for desert in Nevada, Arizona, and the sand-hills region in Nebraska. In fact, the lower bound of responses over the ocean falls within these ranges. The difference in the means for these land categories is very small.

At 17° incidence (Figure 3) the range between the upper and lower bounds becomes smaller for all terrain categories. The means for all terrain categories are much lower than at 1.5° (as expected). The mean backscatter over the ocean still registers higher than land categories. The difference between the means for forest and for rangeland at 1.5° was approximately 1.9 dB, at 17° the mean for the two categories is almost the same.

The maximum number of data included in this study is for an incidence angle group centered at 33°, with seven of the nine categories containing enough samples to permit the generation of histograms. There is a reversal in the comparative level of the ocean backscatter (Figure 4). The mean for the ocean at 33° is now seen to be roughly 5 dB lower than most land targets. There is a wide spread between the upper and lower bounds (8 dB) for ocean; the corresponding spread for all land targets is much less. Once again the means for all land targets except the tropical forest in Brazil lie within or very close to the bounds between upper and lower values for all land categories.

The tropical rain forest with its dense vegetation canopy seems to appear rougher to the scatterometer and registers a backscatter higher than the corresponding North American forest.

Less data exist at 46° than at 33°. The range between upper and lower bounds for the ocean surfaces is seen to be very large (10 dB). This range is probably larger than would be expected for only a 2° interval of incidence angle around 46°. To increase the sample size, incidence angles from 42° to 50° were included in this angle group. The mean for the oceanic backscatter is now seen to be some 10 dB below that for agricultural terrain and about 7 dB below that for rangeland. The range between upper and lower bounds for rangeland is quite large (9 dB). Surprisingly the mean for the agricultural terrain is higher than that for forest and rangeland. Perhaps, the small range between upper and lower bounds for agricultural terrain must be due to small sample size (48 samples).

TABLE 1. S-193 DATA PASSES CONSIDERED

	Mode/Angle	Area	Description of Area
156	CTC P00	Utah	Salt Flats and Great Salt Lake and Desert
156	CTC P29	Texas	Woodland, Agriculture, Grassland
161	CTC P29	Brazil	Mostly Tropical Forest
162	CTC P29	Oregon	Agriculture, Rangeland and Forest
162	CTC P29	Venezuela, Brazil	Mostly Tropical Forest
165	CTC P29	Brazil	Mostly Tropical Forest
165	CTC P29	Nevada, Arizona	Mostly Desert
215	CTC P29	Nevada, Utah	Forested Mountains, Rangeland and Portions of Salt Lake
220	CTC P29	New Mexico, Texas	Woodland, Agriculture and Rangeland
221	CTC P00	North Dakota	Agriculture and Range
249	CTC P00	Colorado, Nebraska	Rangeland, Agriculture
250	CTC P29	S.W. Mexico to New Mexico	Mostly Desert
253	CTC P00	Colorado, Nebraska	Forest, Agriculture and Sand Hills
223	ITC	Nevada	Mostly Desert, Little Forest and Mountains
250	ITC	New Mexico to Kansas	Agriculture and Forest and Rangeland
253	ITC	Texas to Maine	Farmland, Rangeland, Forest, Some Lakes
217	ITNC	Washington Coast to Idaho	Agriculture and Forest
217	ITNC	Idaho to Oklahoma	Agriculture, Mountains, Sand Hills, Rangeland

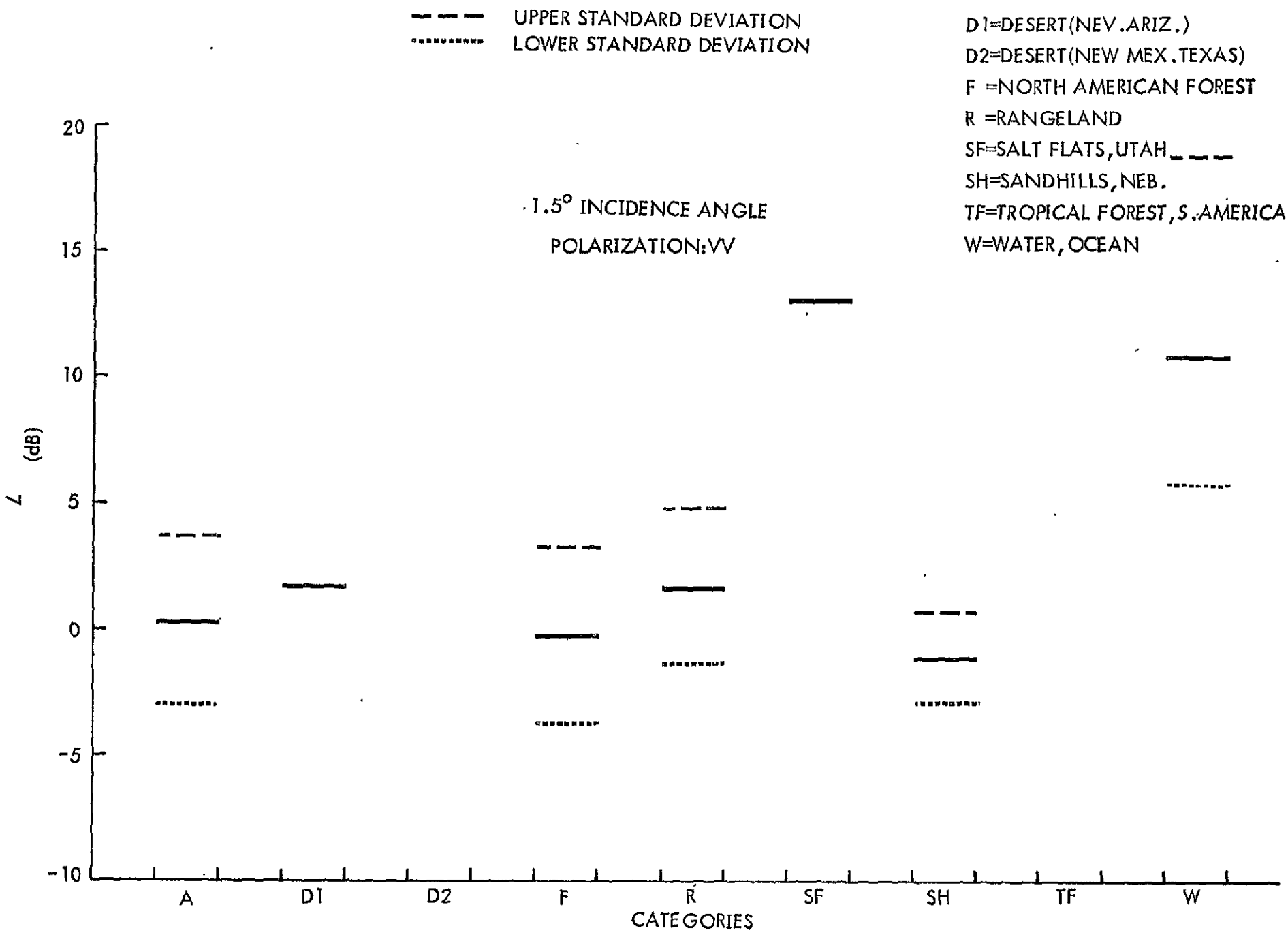

Figure 1. Comparison of Backscattering Coefficient for Various Terrain Categories from SL2-SL3 Missions of S-193 Scatterometer.

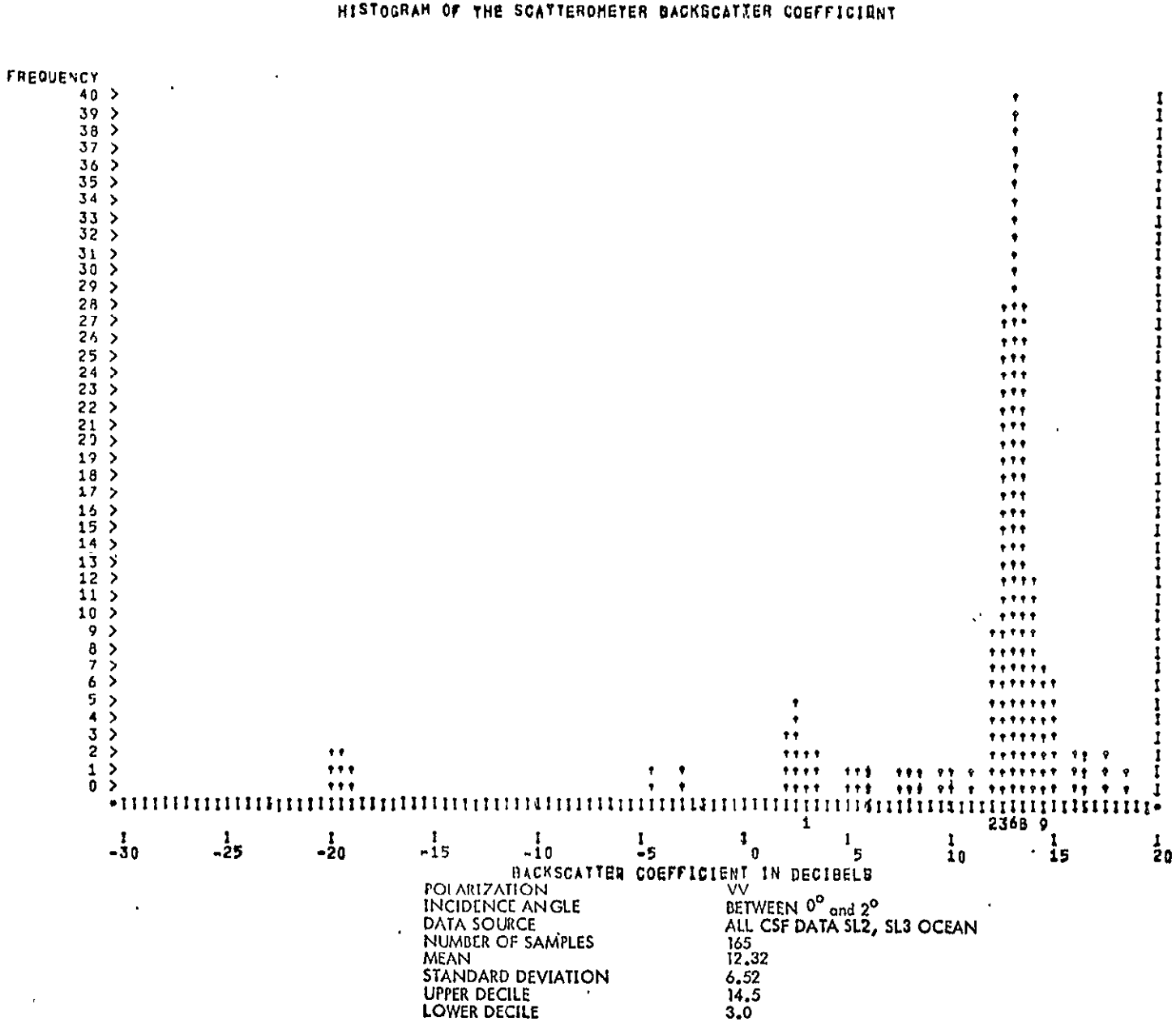

Figure 2. Example of Computer-Generated Backscatter Histogram

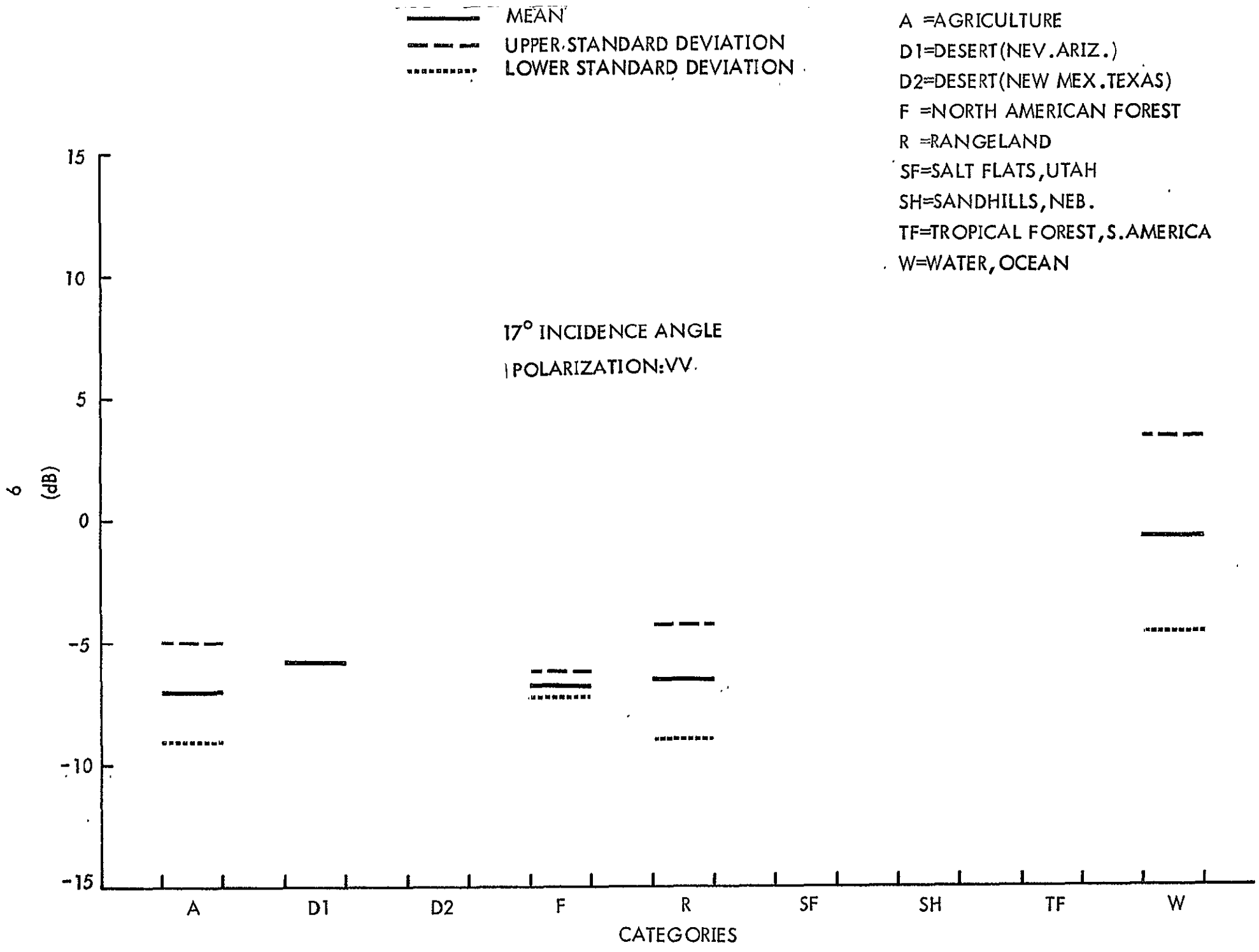

Figure 3. Comparison of Backscattering Coefficient for Various Terrain Categories from SL2-SL3 Missions of S-193 Scatterometer.

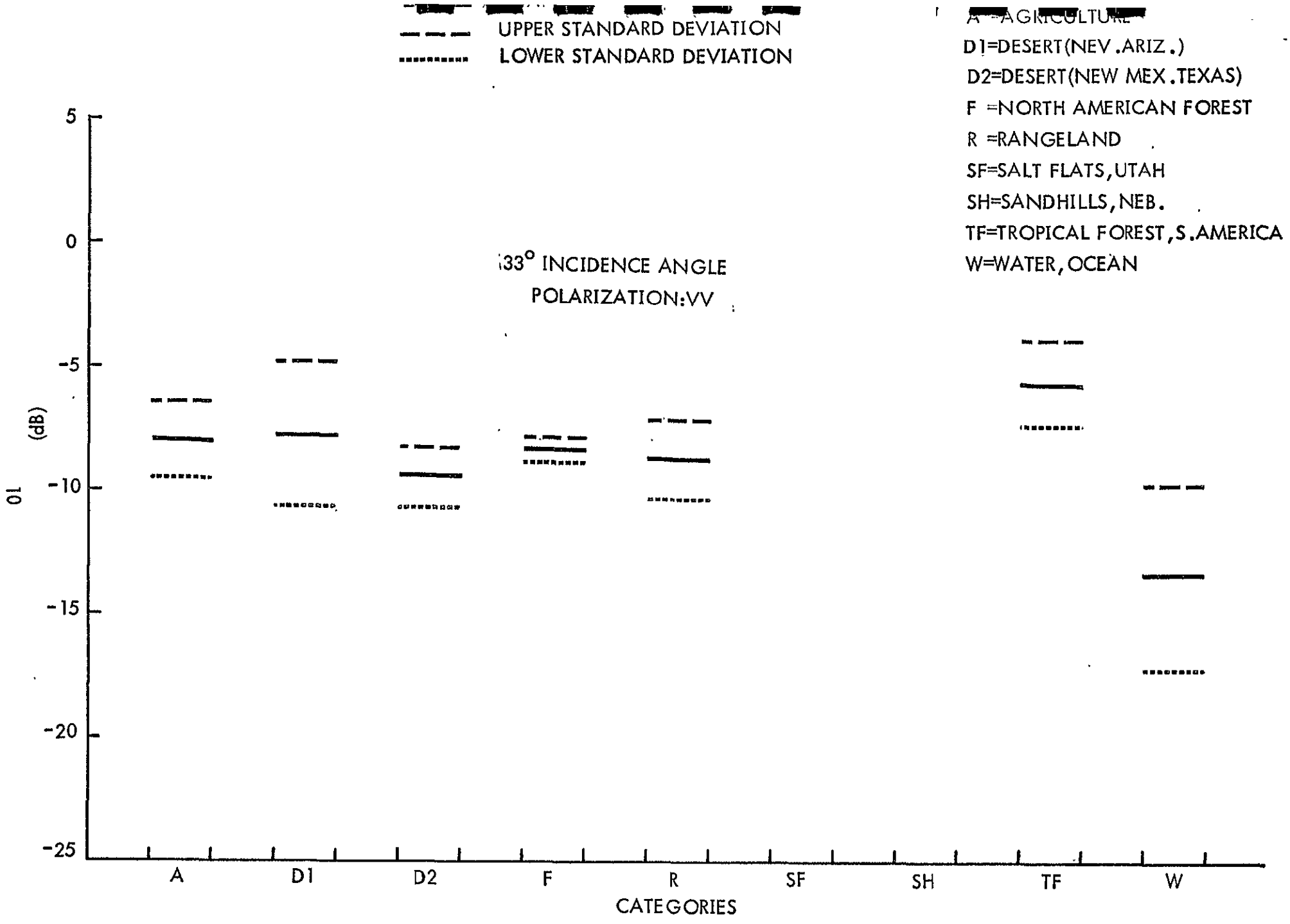

Figure 4. Comparison of Backscattering Coefficient for Various Terrain Categories from SL2-SL3 Missions of S-193 Scatterometer.

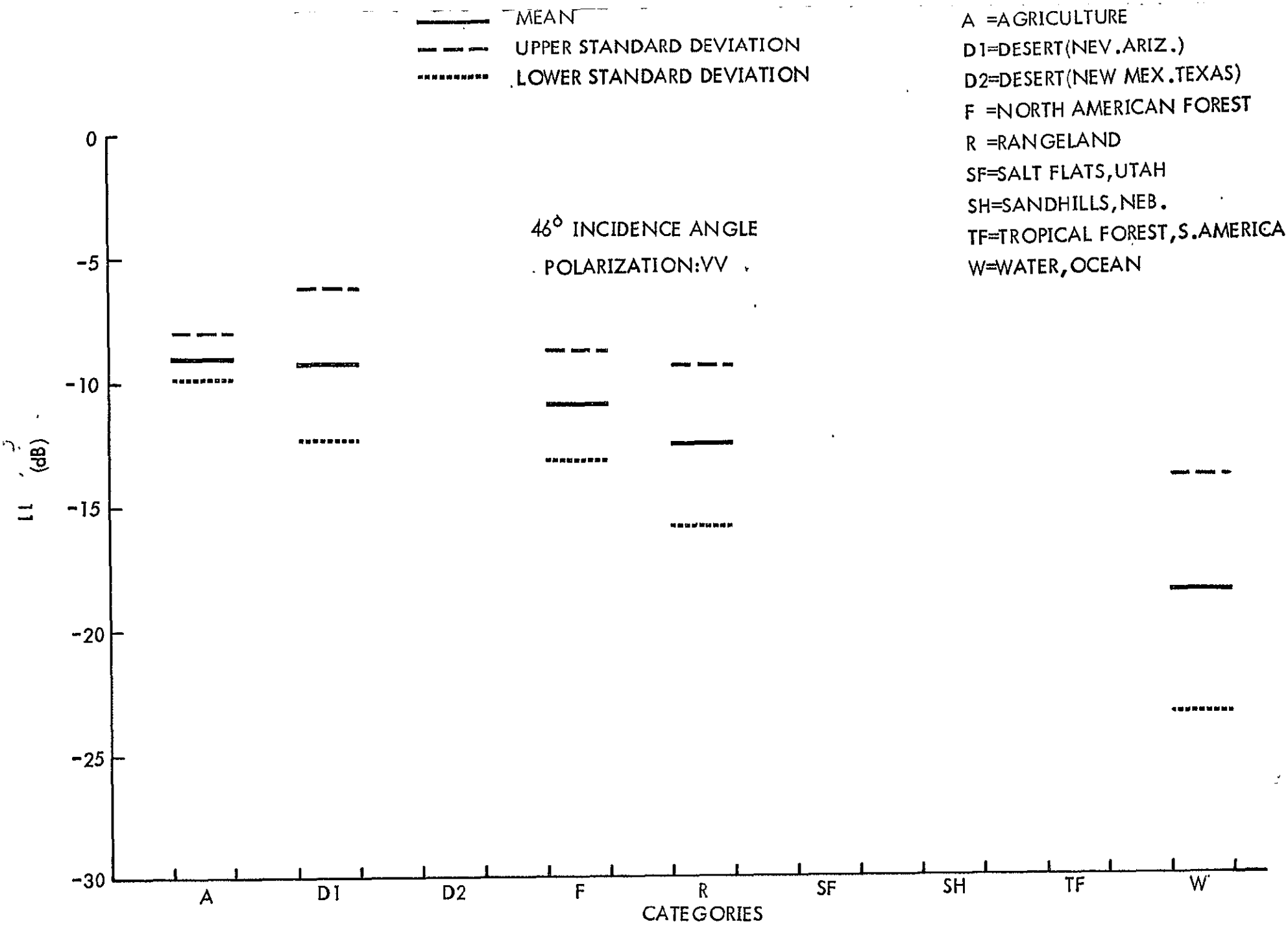

Figure 5. Comparison of Backscattering Coefficient for Various Terrain Categories from SL2-SL3 Missions of S-193 Scatterometer.

COMPARISON OF SKYLAB SCATTEROMETER DATA WITH PRIOR MEASUREMENTS

King and Moore[1] conducted a survey of terrain scattering measurement programs. The categories and angles for which they provided data during the pre-Skylab era were selected so that a ready comparison with data obtained from the Skylab scatterometer could be made. Due to the extensive effort involved in locating and identifying homogeneous targets by imagery and maps, only a few categories could be represented by the Skylab data. The incidence angles which King and Moore used in their comparisons were the design values of the incidence angles expected during the space operation of the Skylab scatterometer. The incidence angles actually achieved during the space operation deviated slightly from these design values. This should have minimal effect for the angles away from nadir but for the angles near vertical, one must allow for a variation due to incidence angle. The pre-Skylab data have been reported at 0° whereas the Skylab data are reported at 1.5°.

King and Moore reported on both vertical and horizontal polarization. In this study we have considered only vertical polarization. The fact that the response for the two polarizations is quite similar and correlated allowed us to spend more time getting a larger data base for just one polarization. The categories considered by King and Moore are somewhat different from ours, e.g., they make no distinction between types of forest whereas we find that Brazilian Tropical Forest formations show decidedly different backscatter characteristics than any of the less dense North-American forests. The categories used by King and Moore are necessarily designed so that the bulk of backscatter data collected by programs (aircraft-based and ground-based) could be reported. For example, categories like road surface, which could not possibly show up in the gross resolution of the Skylab scatterometer, were reported.

We have taken the data from King and Moore's report for the categories for which we could locate Skylab scattering coefficient data. The presentation of the comparisons is given in a manner similar to theirs, i. e., in a bar graph representing the bounds* (where available) and the mean values. The bounds as reported by King and Moore are also one sigma spreads.

---

*"Bounds" is used as in the preceding section to mean values lying one standard deviation from the mean.

Figure 6 shows a comparison of the backscatter response at nadir with the Skylab scatterometer and measurements by other programs. Naval Research Laboratories conducted two experiment programs, one from aircraft-based sensors[2] and the other from bridge-mounted sensors[3]. The frequency for which the comparison is shown with Skylab data is X-band (8.9 GHz). NRL did not provide bounds for their data for grassland; their average value estimated at nadir is approximately -12 dB. This is much lower than the Skylab-obtained value. Sandia Corporation[4] conducted measurements near vertical at 3.8 GHz. A comparison can be made between Sandia data over farmland, and data obtained from a fan-beam scatterometer operating at 13.3 GHz on an aircraft over agricultural terrain in Kansas, with the Skylab data. It is seen that the bounds all overlap, but, the mean for the Skylab data is a little lower, and, the range between upper and lower bounds for the Skylab data is much less than the ranges shown for the finer resolution sensors. There is a great variation between different types of farmland, but with the great spatial averaging involved in the Skylab scatterometer measurements, the dynamic range seems to have been reduced.

The response over forests is reported by NRL, land and air, and the difference between the mean values for these two programs is about 30 dB for the same target category. Sandia Corporation's measurements (3.8 GHz) show a mean value and range comparable to that for the Skylab radar. The forests in Sandia's measurements are of two densitites (Maine and Minnesota). The Skylab radar viewed regions which were registered on the topographic maps as forests but no density of the foliage can be estimated. A comparison of the mean desert response at 0° to the NRL airborne measurement shows a difference of 4 dB.

The comparisons at around 16° are given in Figure 7. Once again the mean over grassland obtained by NRL is much lower than that from the Skylab scatterometer. Over farmland, we find again that the dynamic range of values from the Skylab radar is much smaller than reported by aircraft and land-based measurement programs. There seems to be a variation in the means as well. The Ohio State data[5] is at X-band. The resolution cell size for these data is of the order of one foot on a side! Notice the extremely narrow range between upper and lower deciles for the forest category for the Skylab data. The mean is lower than those measured by NRL and Sandia. The desert response from the Skylab radar compares very well with that reported by NRL (airborne) measurements.

Comparisons at 31° are shown in Figure 8. As usual NRL measurements over rangeland are over 10 dB lower in the mean than the Skylab data. A significant

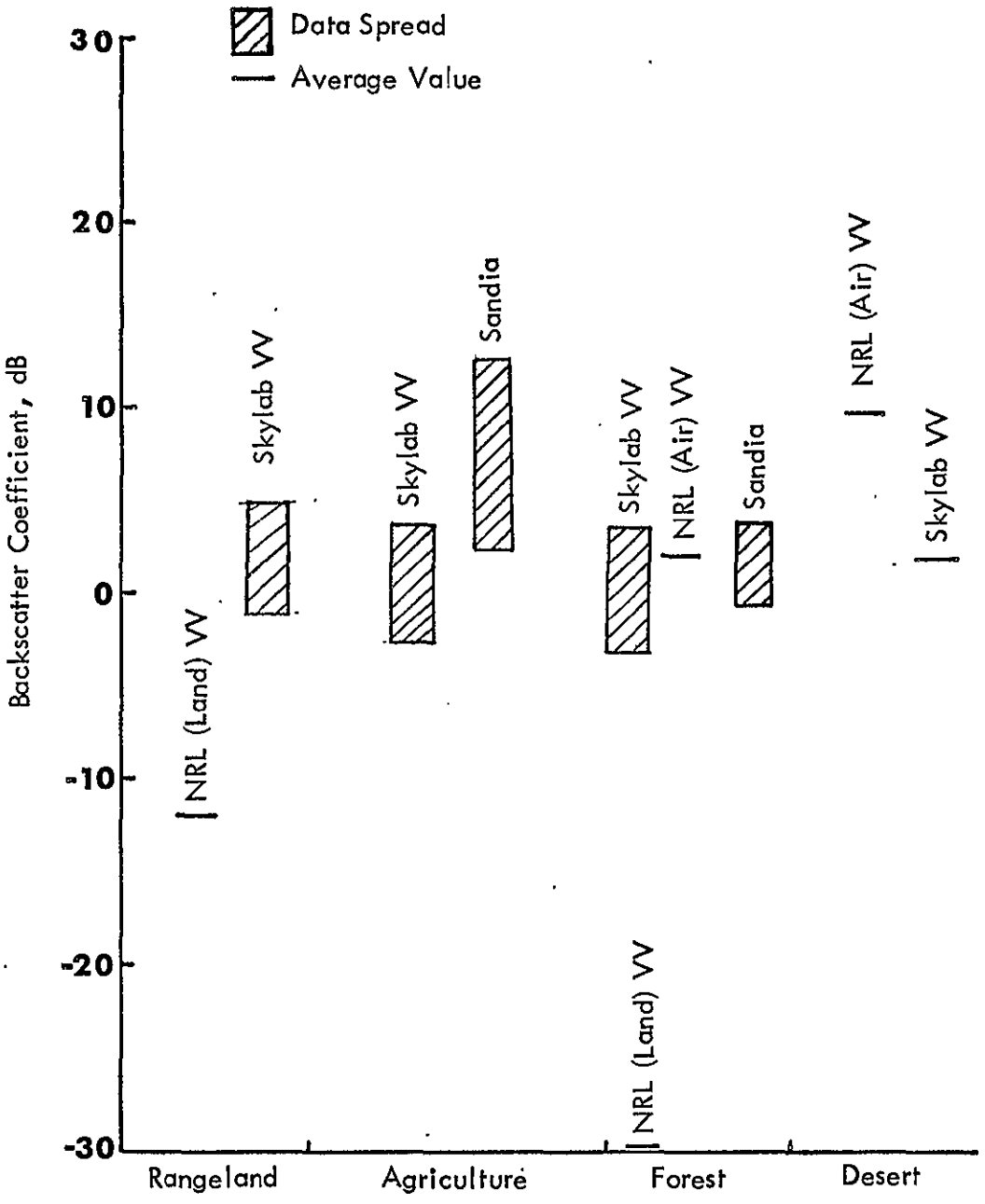

Figure 6. Comparison of Skylab Results with Previous Aircraft and Ground Scattering Measurments. Angle of Incidence 0^{o}.

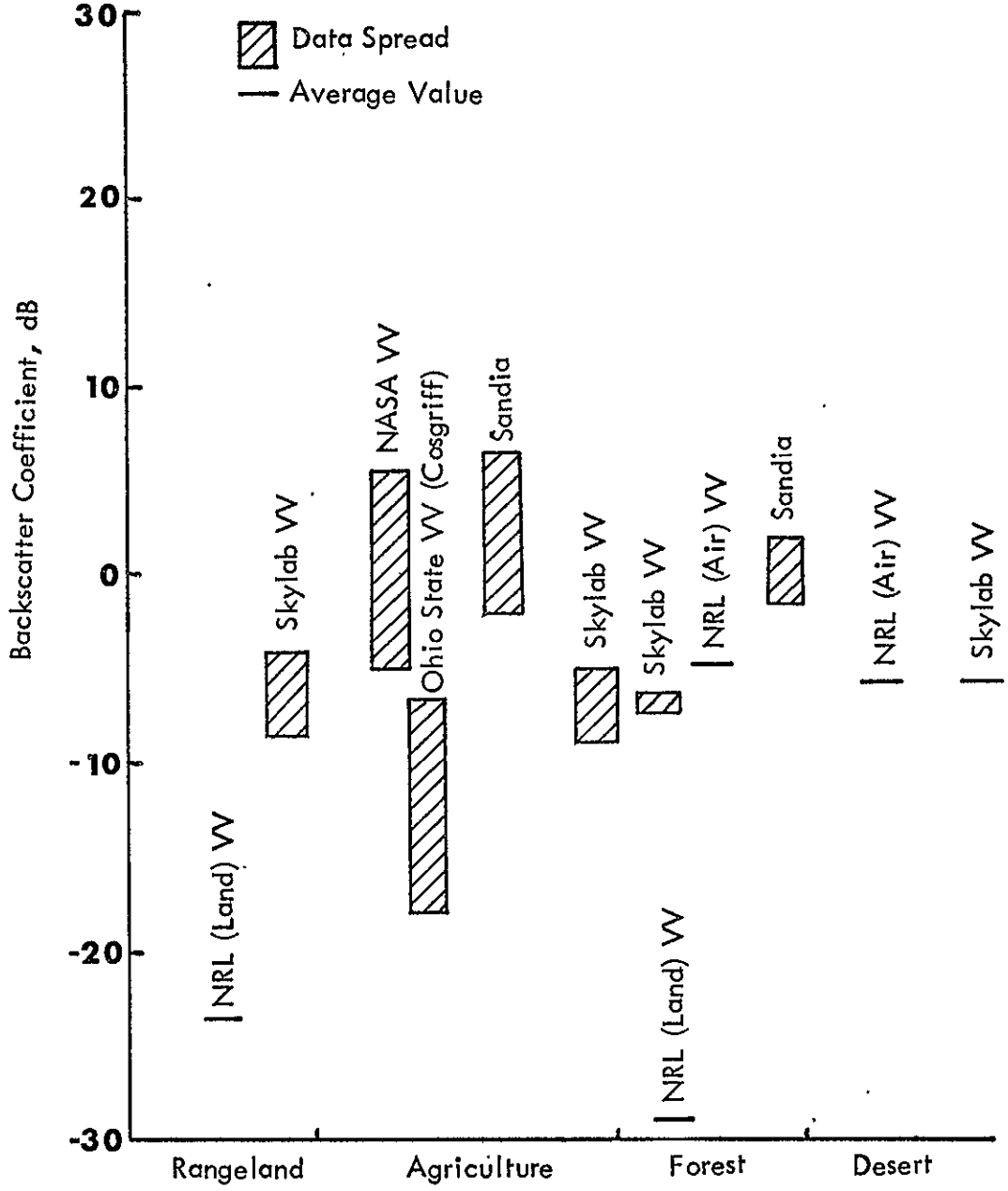

Figure 7. Comparison of Skylab Results with Previous Aircraft and Ground Scattering Measurments. Angle of Incidence 16°.

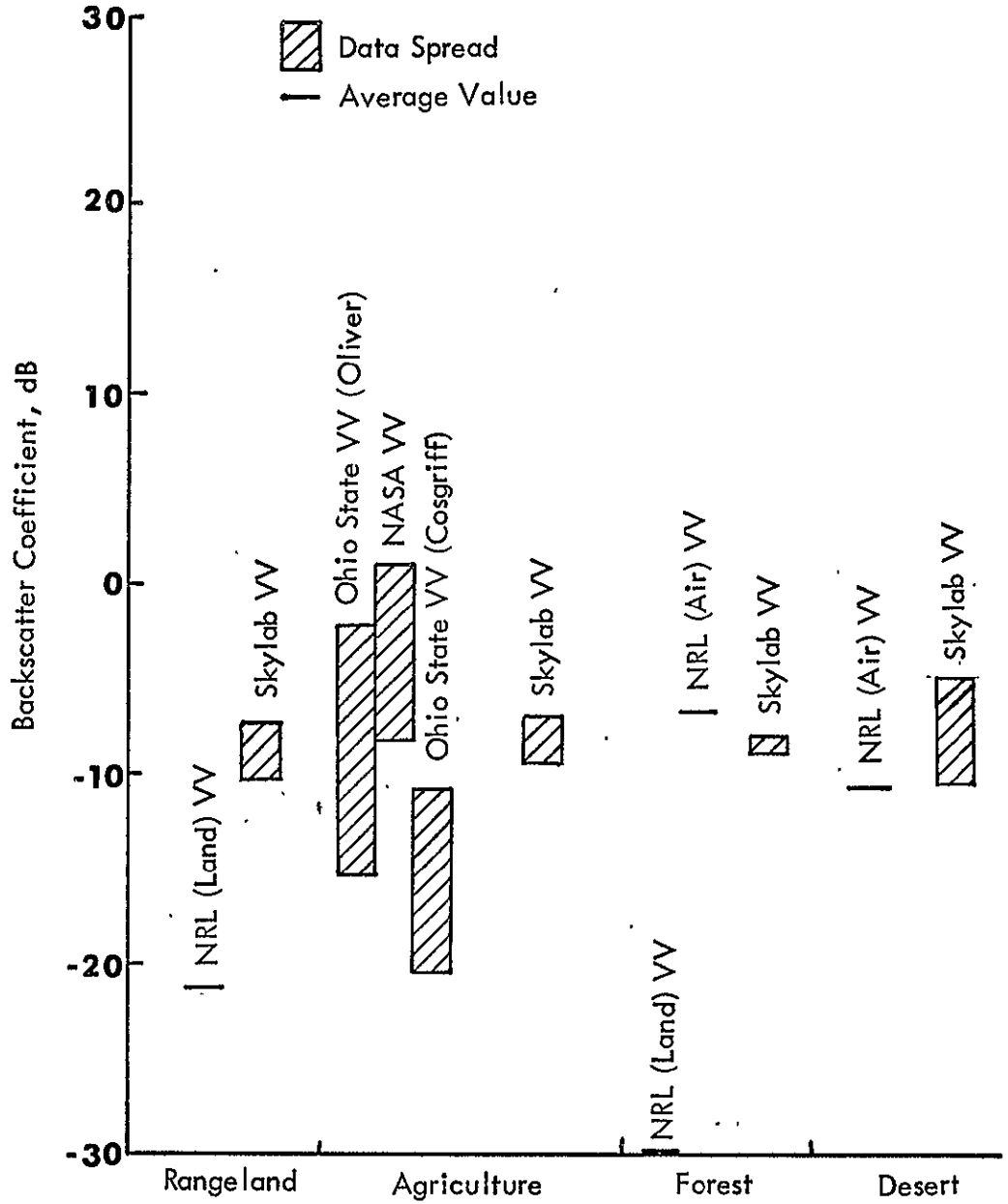

Figure 8. Comparison of Skylab Results with Previous Aircraft and Ground Scattering Measurments. Angle of Incidence 31°.

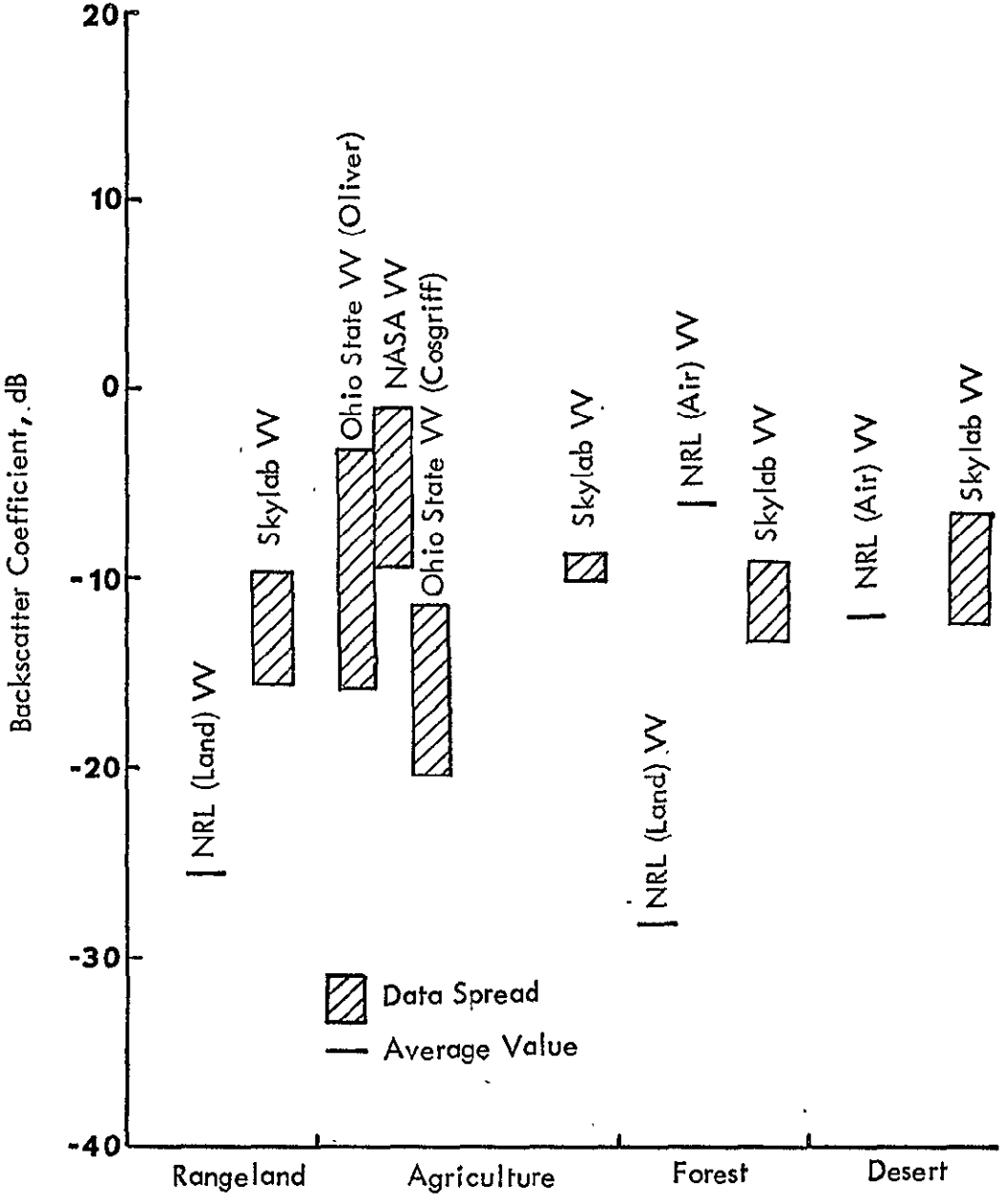

Figure 9. Comparison of Skylab Results with Previous Aircraft and Ground Scattering Measurments. Angle of Incidence 43°.

reduction in the dynamic range can be seen in the backscatter response measurements over agricultural terrain. The range between upper and lower bounds for Skylab data is only 3dB. This compares with ranges in the neighborhood of 10 dB for the finer-resolution measurement programs. Once again forest has a very small range between upper and lower bounds (1 dB). Desert has a mean value comparable to that of the NRL measurements but a spread which is much more than that for forests.

Figure 9 shows a comparison of 43°; the ranges between upper and lower bounds for rangeland is larger at this angle than at any other angle. The mean is again approximately 10 dB higher than the NRL value. This implies that if one discounts the 10-or-so dB bias between the two measurement programs, the trends of the backscatter response are quite similar for the NRL and Skylab data. The range between upper and lower bounds for agriculture is only 5 dB; this compares with ranges in excess of 10 dB for the finer-resolution sensors. Forest at 43° had twice as many samples of Skylab data as for the other angles; its range between upper and lower bounds is 5 dB. The mean falls between the NRL land-based and aircraft-based values for forest, which show a difference of over 20 dB. Desert had a mean comparable to the NRL values.

SUMMARY OF SKYLAB SCATTEROMETER RESPONSE FOR TERRAIN CATEGORIES

For the terrain categories considered and for almost all angles of incidence, the range between upper and lower one sigma values for the Skylab scatterometer data is less than the corresponding range measured by the finer-resolution aircraft-and land-based sensors. There is a wide discrepancy between the mean values among the aircraft and land-based sensors for each terrain category at each angle. The Skylab data usually fall within the upper and lower values presented by the prior measurements. For rangeland and desert, where only one prior measurement program has reported data, the Skylab data show a difference of 10 dB for the former and are comparable for the latter.

There is a great deal of overlap in the backscatter response from the various categories. Figure 10 shows the bounds between upper and lower deciles and the mean values for various terrain categories for angles of incidence from 0° to 47°. The categories included in this composite figure are those for which enough samples existed for statistical validity. It can be seen from the figure that the range between upper and

lower deciles for the ocean is much wider than all the land categories. There is a difference between some land and the ocean targets below 10° incidence and again beyond 30°. The region between 10° and 30° seems to have a total overlap between the response from all kinds of terrain. This would imply that a radar designed for discriminating/identifying terrain would not be very capable between 10° and 30° of incidence. The response below 10° incidence shows that, apart from regions like the Utah Salt Flats which appear like mirror reflectors at 2 cms wavelength, land targets register a backscatter response lower than the ocean surface. The tropical rain forests in Brazil show the highest backscatter of any targets at 33°. This is in accordance with the expected response from rough surfaces. Notice that the range between upper and lower deciles for the tropical forests in Brazil and the forests in North American do not ever overlap. Surprisingly, the response from desert surfaces is quite high at the greater angles of incidence.

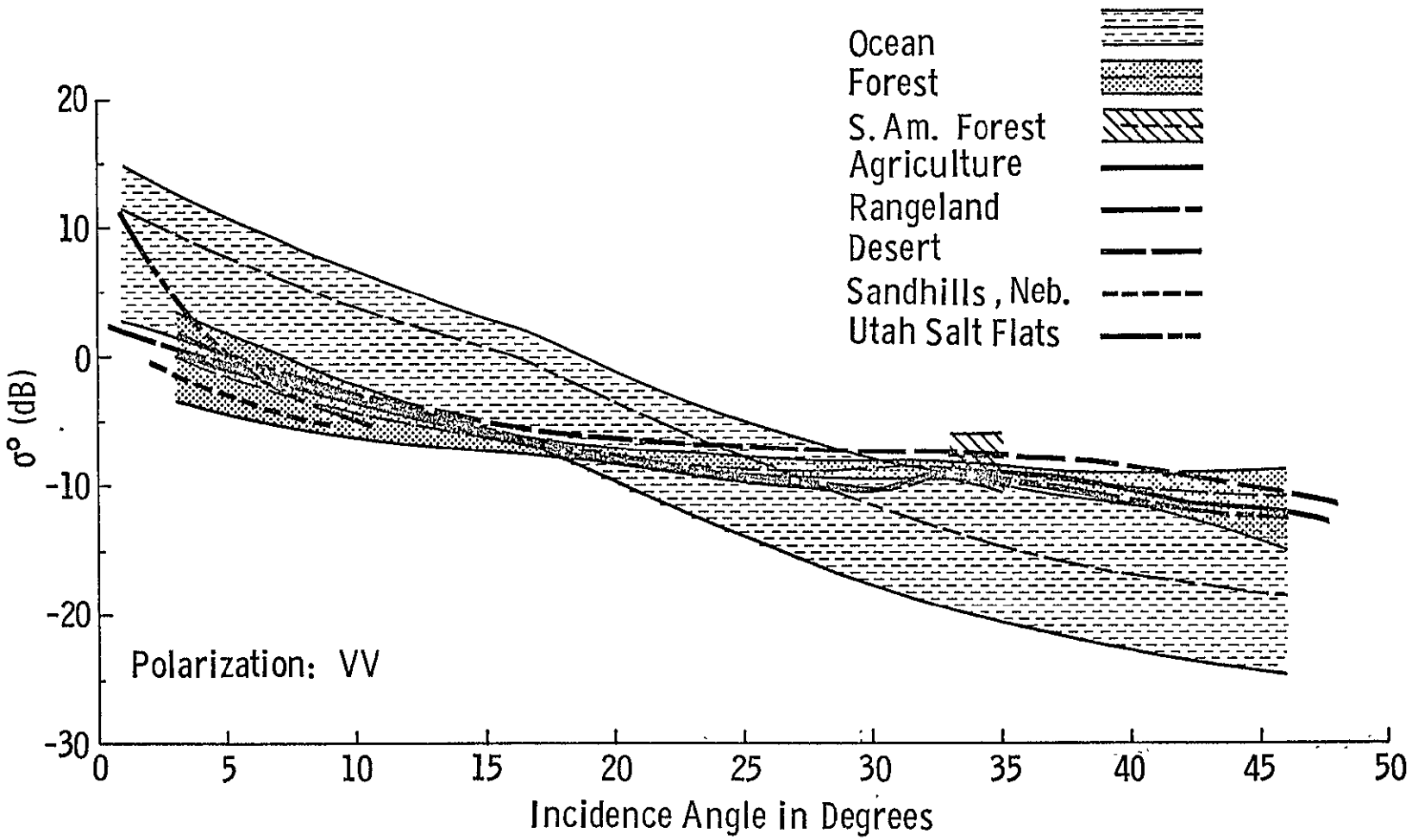

Figure 10. Comparison of angular backscatter response from various categories. Ranges, where shown, are between upper and lower deciles, not standard deviation.

REFERENCES

1. King, C., and R. K. Moore, "A Survey of Terrain Radar Backscatter Coefficient Measurement Programs," University of Kansas Center for Research, Inc., CRES Tech. Report 243-2, December 1973.

2. Ament, W. S., F. C. MacDonald, and R. D Shewbridge, "Radar Terrain Reflections for Several Polarizations and Frequencies," U.S. Naval Research Laboratory, unpublished report, 1959.

3. Grant, C. R., and B. S. Yaplee, "Backscattering from Water and Land at Centimeter and Millimeter Wavelengths," Proc. IRE, vol. 45, pp. 976-982, 1957.

4. Edison, A. R., R. K. Moore, and B. D. Warner, "Radar Terrain Return Measured at Near-Vertical Incidence," Trans. IRE, vol. AP-8, pp. 246-254, 1960.

5. Cosgriff, R. L., W. H. Peake, and R. C. Taylor, "Terrain Scattering Properties of Sensor System Design," Terrain Handbook II, Engrg, Expt. Sta., Ohio State University, Bulletin 181, May 1960.

APPENDIX D

SATELLITE MICROWAVE OBSERVATIONS OF THE UTAH GREAT SALT LAKE DESERT

Fawwaz T. Ulaby and Louis F. Dellwig
University of Kansas Center for Research, Inc.
Remote Sensing Laboratory
Lawrence, Kansas 66045

Thomas Schmugge
NASA Goddard Space Flight Center
Hydrology and Oceanography Branch
Greenbelt, Maryland 20771

THE UNIVERSITY OF KANSAS SPACE TECHNOLOGY LABORATORIES
2291 Irving Hill Dr.— Campus West Lawrence, Kansas 66044

Telephone:

SATELLITE MICROWAVE OBSERVATIONS OF THE UTAH GREAT SALT LAKE DESERT

Remote Sensing Laboratory
RSL Technical Report 243-6

Fawwaz T. Ulaby
Louis F. Dellwig
Thomas Schmugge

August, 1975

Supported by:

NATIONAL AERONAUTICS AND SPACE ADMINISTRATION
Johnson Spacecraft Center
Houston, Texas 77058

Contract NAS 9-13331

Organization Full Name:	The University of Kansas Center for Research, Inc. 2291 Irving Hill Drive - Campus West Lawrence, Kansas 66045
Title of Investigation:	Design Data Collection with SKYLAB/EREP Microwave Instrument S-193
Title of Report:	Satellite Microwave Observations of the Utah Great Salt Lake Desert
Period Covered:	3-26-73 through 12-31-75
NASA Contract	NAS 9-13331
EREP Investigation:	549 M
Principal Investigator:	Professor Richard K. Moore
Date Written:	August 13, 1975
Monitor and Address:	Mr. Larry York Earth Observations Division Science and Applications Directorate NASA Manned Spacecraft Center Code TF 3 Houston, Texas 77058
Type of Report:	Advanced Report of Significant Results

app. 21 c

TABLE OF CONTENTS

LIST OF FIGURES

Opp. 21 e

SATELLITE MICROWAVE OBSERVATIONS OF THE

UTAH GREAT SALT LAKE DESERT

Fawwaz T. Ulaby and Louis F. Dellwig
University of Kansas Center for Research, Inc.
Remote Sensing Laboratory
Lawrence, Kansas 66045

Thomas Schmugge
NASA Goddard Space Flight Center
Hydrology and Oceanography Branch
Greenbelt, Maryland 20771

ABSTRACT

Microwave data acquired over the Great Salt Lake Desert area by sensors aboard Skylab and Nimbus 5 indicate that the microwave emission and backscatter were strongly influenced by contributions from subsurface layers of sediment saturated with brine. This phenomenon was observed by Skylab's S-194 radiometer operating at 1.4 GHz, S-193 RADSCAT (Radiometer-Scatterometer) operating at 13.9 GHz and the Nimbus 5 ESMR (Electrically Scanning Microwave Radiometer) operating at 19.35 GHz. The availability of ESMR data over an 18 month period allowed an investigation of temporal variations. Aircraft 1.4 GHz radiometer data acquired two days after one of the Skylab passes confirm the satellites' observations. ESMR data reveal similar responses over the Bolivian deserts, which have geologic features similar to those of the Utah desert.

1.0 INTRODUCTION

The microwave emissivity, ϵ, and backscattering coefficient, σ^o, of terrain surfaces are functions of the dielectric properties and surface roughness (relative to the wavelength) of the ground. The dielectric properties are in turn strongly influenced by the soil moisture content. Microwave observations of soil surfaces by active [Ulaby, 1974a,b; Ulaby et al., 1975a] and passive [Schmugge et al., 1974; Newton et al., 1974; Eagleman and Ulaby, 1974] sensors indicate a high degree of sensitivity to soil moisture variations. Due to the nature of the scattering and emission phenomena, the scattering coefficient exhibits a positive correlation with soil moisture content, whereas the emissivity (and hence brightness temperature) decreases with soil moisture content. In both cases [Ulaby et al., 1975a; Newton et al., 1974] longer wavelengths have been observed to yield more satisfactory results (in terms of sensitivity to moisture variations) simply because, for a given terrain surface, the effects of surface roughness on the microwave response (backscatter and emission) are reduced as the wavelength is made longer since the surface would appear electromagnetically smoother.

Brightness temperature data acquired by Skylab and Nimbus 5 microwave radiometers over Utah indicate a consistent difference in temperature between the Great Salt Lake Desert area and neighboring land surfaces. The Skylab microwave sensors include a 13.9 GHz Radiometer-Scatterometer (RADSCAT) designated S-193 and a L-band radiometer operating at 1.4 GHz designated S-194. The microwave sensor aboard Nimbus 5 is a 19.35 GHz Electrically Scanning Microwave Radiometer (ESMR).

During Skylab Pass 5 on June 5, 1973, S-193 measured brightness temperature values as low as 200°K for some parts of the Great Salt Lake Desert in comparison to a 270°-280°K range for areas outside the desert. In conjunction with the low temperature values, the measured scattering coefficient of the same general area was more than 15 dB higher than the scattering coefficient of areas outside the desert. Similar observations to those indicated by the S-193 radiometer were also evident in the data acquired by S-194 and ESMR for the same date. Another Skylab pass on August 8, 1973 and numerous ESMR passes over an 18 month period confirm that these observations are in response to specific characteristics of the Great Salt Lake Desert soil material. Detailed analysis of the data and the hydrology of the region has led us to believe that a significant contribution to the measured emitted and backscattered energy is from subsurface layers of brine.

As will be discussed in this paper, the availability of microwave data over the Great Salt Lake Desert at three different wavelengths has proven very useful in the analysis and interpretation. Moreover, the scatterometer data at 13.9 GHz has also served to complement the observations made with the passive sensors. The daily global coverage of the Nimbus 5 ESMR make possible observation of other salt deserts. In particular, low brightness temperatures have been observed over the salt deserts of the Alti Plano region of Bolivia.

2.0 DEVELOPMENT AND CHARACTERISTICS OF THE GREAT SALT LAKE DESERT

The test site under investigation trends in a northwest-southeast direction across the Great Salt Lake Desert (Figure 1). The narrow side represents the coverage on the ground by S-193 RADSCAT as the antenna was scanned in the cross-track-contiguous mode at 0° forward pitch during the Skylab June 5, 1973 descending pass (northwest to southeast direction) over Utah. S-194 coverage comprised approximately 74 per cent of the test site and complete coverage by ESMR is available for numerous passes. Two lines are shown in Figure 1, a horizontal line representing a transect across the desert at 40° 30' North latitude, the elevation profile of which is shown in Figure 2, and a NW-SE line indicating the coverage by the NASA airborne 1.4 GHz radiometer flown on August 10, 1973. Several types of terrain are also shown including lakes (Great Salt Lake and Utah Lake), saltflats, mud flats, mountains, and the Great Salt Lake Desert.

2.1 Hydrologic Properties

Fifteen to twenty thousand years ago, coincident with the beginning of the retreat of the most recent glacial advance over the northern portion of the North American continent, a large area of northwestern Utah was covered by ancient Lake Bonneville which, through a complex history of contractions and expansions, ultimately was reduced to the 4270 km^2 now occupied by the Great Salt Lake. To the southwest of the lake and connected to it by a narrow threshold is the Great Salt Lake Desert (Figure 1), approximately 9 m above the present level of the lake. Until approximately 10,000 years ago [Eardley, 1962], this area was covered by the waters of Lake Bonneville into which were washed the sediments now composing the lake bed deposits which underlie the salt encrusted surface. These deposits underlie the major portion of the Great Salt Lake Desert below altitudes of approximately 1300 meters

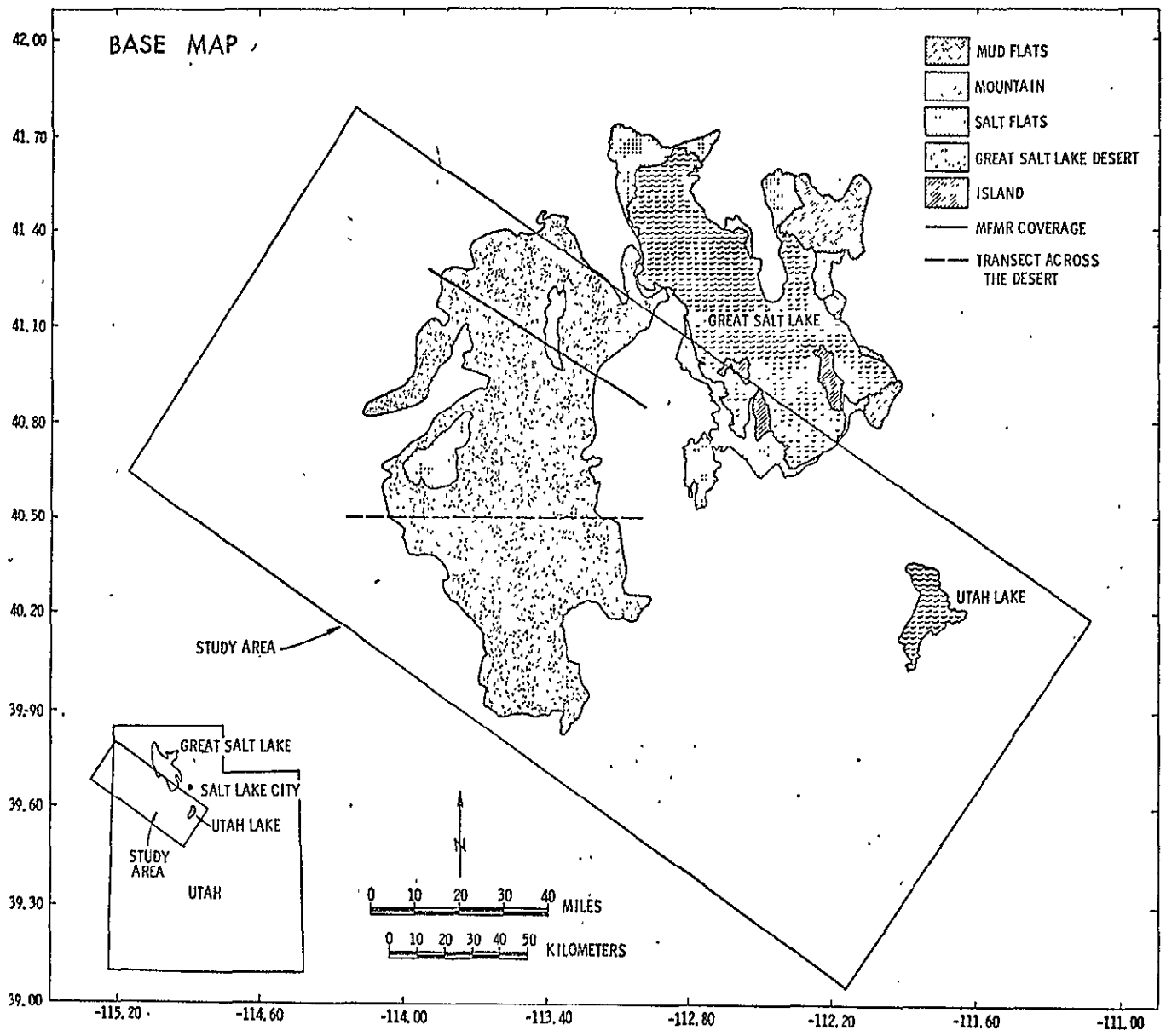

Figure 1. Great Salt Lake Desert test site. Elevation profile of the horizontal transect is shown in Figure 2 and the MFMR coverage refers to Figure 9.

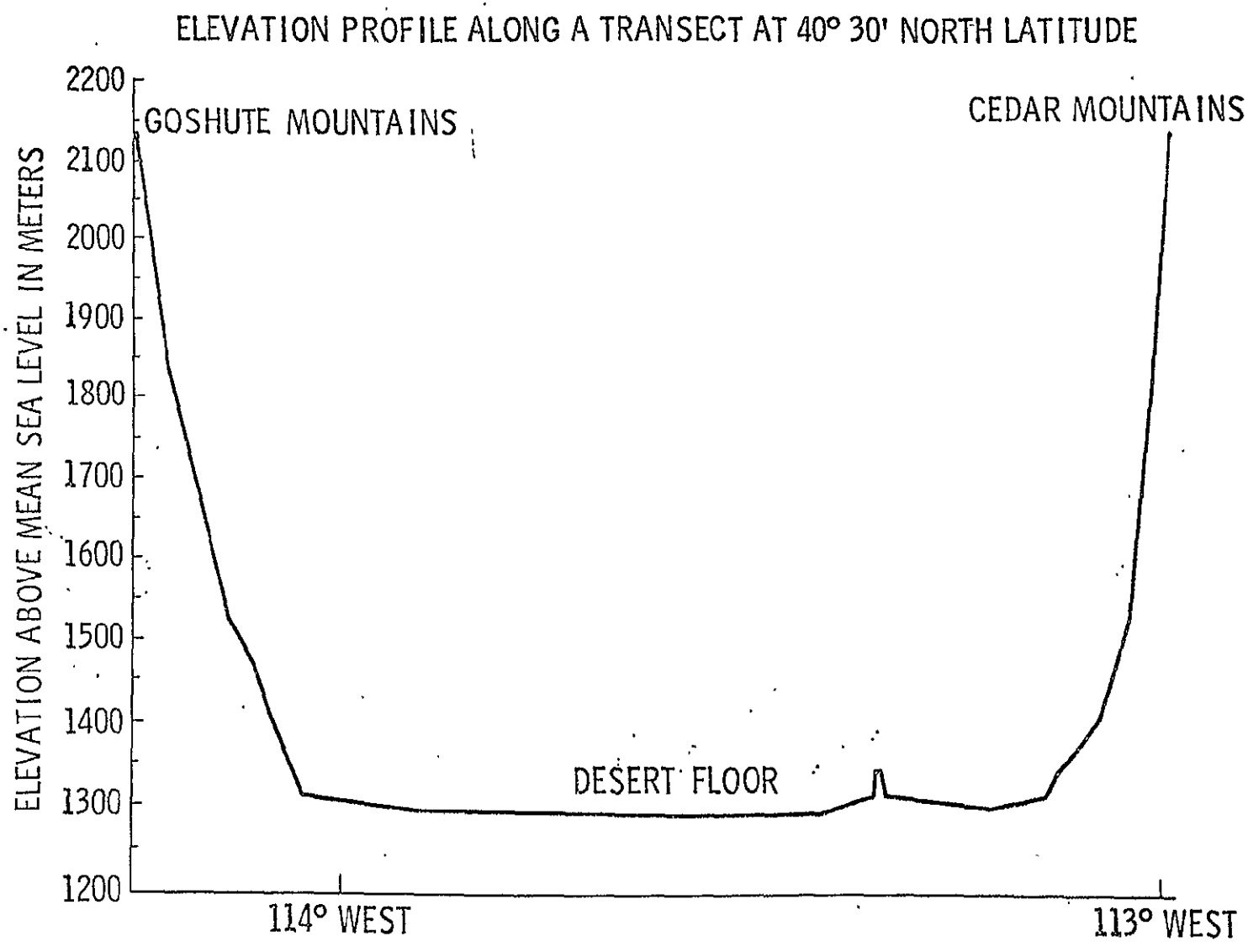

Figure 2. Elevation profile along a transect at 40°30' North latitude.

and are predominately clay and silt with variable salt content [Stephens, 1974]. From this bleak terrain surface rimmed by mountains (Figure 2) several areas show deviation: to the west in the general vicinity of Wendover, Utah lay the Bonneville Salt Flats and along the east side of the desert are gypsum sand dunes which have developed through the ablation of the desert surface by the westerly winds. In addition, isolated masses of bedrock protrude upward from the central and marginal areas of the Great Salt Lake Desert.

Lake bed clays and silts and crystalline salt form a shallow brine aquifer a maximum of 7.6 meters thick which covers the bulk of the surface of the Great Salt Lake Desert (Figure 3), only the northern portion of which has been studied in detail [Stephens, 1974].

Generally, in the area where lake clays form the surface, the depth to brine is estimated to range between 60 and 90 cm near the center of the desert floor and 2.1 - 2.7 m at the margins [Nolan, 1928], although capillary action in the fine grained sediments may raise the water in excess of one-half meter above the water table which causes the surface to remain perpetually moist. In the Bonneville Salt Flats, although the surface of the salt bed is rigid, the salt remains saturated with brine to within a few inches of the surface [Stephens, 1974], the water table ranging between approximately 15 and 20 cm below the surface. With the precipitation in the central part of the desert averaging less than 13 cm per year, the possibility of accumulating standing water on the desert surface or of elevating the water table above its normal 60-90 cm position below the desert's surface is minimal. Runoff from the highest parts of the mountains in the area averages less than 2.5 cm annually [Badgley et al., 1964; Busby, 1966] and runoff during the brief periods of rapid snow melt generally infiltrates the stream channels downslope and only locally spreads out over the desert floor, most frequently in the Bonneville Salt Flats area. Recharge is by infiltration of precipitation and lateral subsurface inflow, the brine moving through the lake beds by intergrannular flow through layers of salt impregnated clay and through open joints (Figure 4).

2.2 Dielectric Properties

Except for a few isolated segments, the Great Salt Lake Desert is characterized by a very flat surface. Hence, as a first order approximation, the specular surface model can be applied to calculate the emissivity of the surface in terms of the power reflection coefficient R [Moore, 1975]:

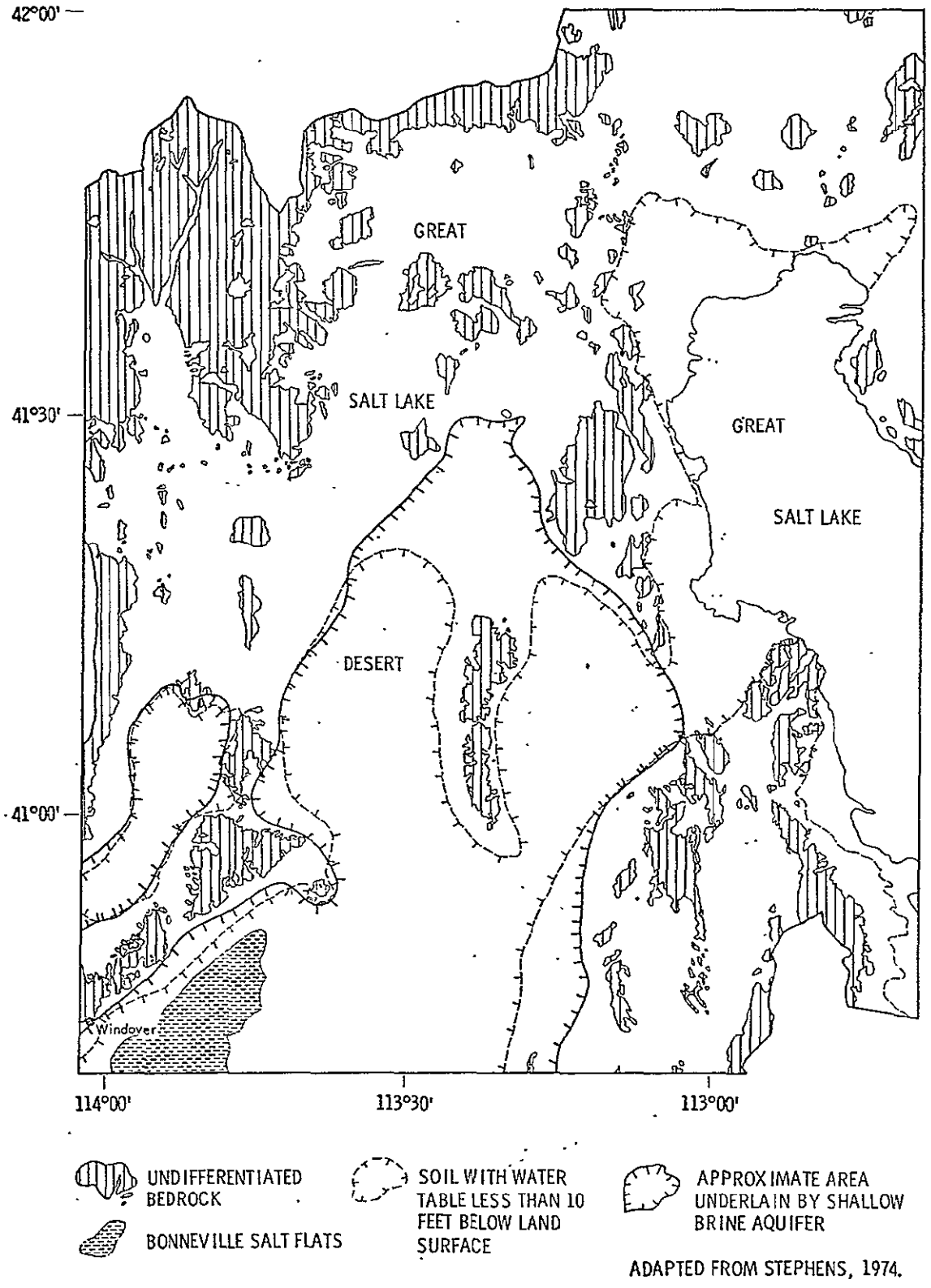

Figure 3. Northern portion of the Great Salt Lake Desert.

INFERRED SUBSURFACE STRATIGRAPHIC RELATIONSHIPS NEAR WENDOVER

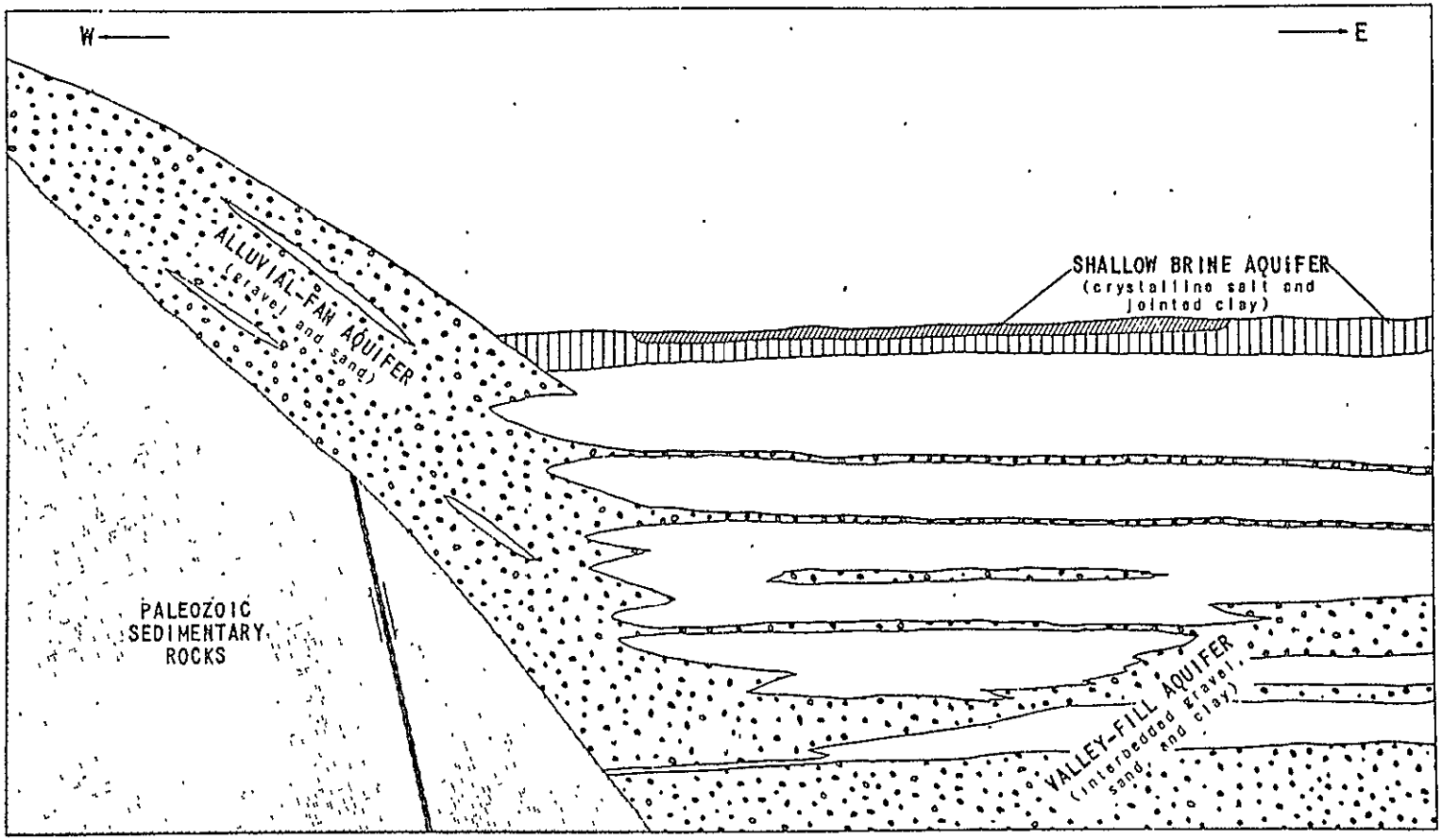

From Stephens, 1974.

Figure 4. Inferred subsurface stratigraphic relationships near Wendover, Utah.

$$\epsilon = 1 - R \tag{1}$$

At nadir, R takes the form:

$$R = \left(\frac{1 - \sqrt{k}}{1 + \sqrt{k}} \right)^2 \tag{3}$$

where k is the relative complex dielectric constant of the ground:

$$k = k_1 - j\, k_2 \tag{3}$$

At microwave frequencies, typical values of k_1 for dry soil lie in the range $2.5 \leq k_1 \leq 3.5$ and $k_2 \approx 0$ [Hoekstra and Delaney, 1974] leading to an emissivity range at nadir of $0.95 \leq \epsilon \leq 0.91$. In contrast, k_1 and k_2 of water are much larger in magnitude and are, in general, functions of frequency, temperature and salinity [Stogryn, 1971]. Shown in Table 1 are calculated k and ϵ values for pure water, saline water with a salinity of 150 °/oo* and saline soil typical of the Great Salt Lake Desert brine layer, all at 23°C. According to Stephens [1974] the salinity of the water under the desert floor is generally 150 °/oo or more and the average porosity of the soil is 45 per cent. Thus the brine layer is a mixture consisting of 45 per cent saline water and 55 per cent soil. Due to the lack of dielectric constant data for such a mixture, the entry in Table 1 for the dielectric constant of saline soil was calculated using the dielectric values calculated for dry soil and saline water [Stogryn, 1971], each weighted by its respective proportion of the combined mixture.

Most of the brightness temperature data presented in the next section was acquired on June 5, 1973. The ground temperature at the time of the Skylab and Nimbus passes was estimated to be 296°K (23°C) [NASA, 1974], hence all values shown in Table 1 were calculated at 23°C.

Whereas the effect of salinity on the emissivity of water is negligible at 13.9 GHz and 19.35 GHz, Table 1 shows that the emissivity of saline water at 1.4 GHz is less than half the emissivity of pure water. Moreover, the calculated emissivity of saline soil (as defined above) is smaller than the emissivity of pure water!

---

* °/oo stands for "parts per thousand".

Table 1. Calculated dielectric constant k and emissivity ϵ of dry soil, pure water, saline water and saline soil at 23°C.

	Dry Soil		Pure Water		Saline Water*		Saline Soil**	
Frequency	k_d	ϵ_d	k_p	ϵ_p	k_s	ϵ_s	k_{ss}	ϵ_{ss}
1.4 GHz	3-j0	0.928	78.63-j5.57	0.364	41.9-j237.4	0.179	20.5-j106.8	0.256
13.9 GHz	3-j0	0.928	52.4-j35.7	0.382	31.4-j40.6	0.394	15.7-j18.3	0.524
19.35 GHz	3-j0	0.928	40.4-j37.2	0.396	25.7-j35.6	0.416	13.2-j16.0	0.549

*Salinity = 150 °/oo

**$k_{ss} = 0.55\, k_d + 0.45\, k_s$

3.0 MICROWAVE OBSERVATIONS

At satellite altitudes, the measured brightness temperature of a flat surface is given by [Moore, 1975]:

$$T_B = \tau_a [T_{BS} + (1 - \epsilon) T_d] + T_u \qquad (4)$$

where τ_a is atmospheric transmittance, T_{BS} is the brightness temperature of the surface, T_d is the brightness temperature of the total downward radiation (atmospheric plus cosmic) and T_u is the brightness temperature of the upward atmospheric radiation. T_{BS} is the product of ϵ and the ground thermometric temperature T_g. Under clear sky conditions, atmospheric effects are negligible for the dry desert atmosphere of the Great Salt Lake Desert area, particularly at 1.4 GHz and 13.9 GHz. After calculating τ, T_u and T_d for the June 5, 1973 atmospheric conditions, the error between the measured brightness temperature T_B and the brightness temperature of the surface T_{BS}:

$$\Delta T = T_B - T_{BS} = T_B - \epsilon T_g \qquad (5)$$

was estimated by calculating ϵ using Eq. 4 for the range of values of T_B measured by the satellite radiometers. The following results were obtained:

$$\Delta T = \begin{cases} \leq 2.3^\circ K & \text{at 1.4 GHz.} \\ \leq 2.5^\circ K & \text{at 13.9 GHz} \\ \leq 9.1^\circ K & \text{at 19.35 GHz} \end{cases}$$

Similar results (within $0.2^\circ K$) were also obtained for the August 8, 1973 Skylab and Nimbus 5 passes over the Great Salt Lake Desert. In addition to these two passes, data reported herein includes Nimbus coverage over a period of 18 months during which the data acquired on some passes were more severely influenced by atmospheric conditions. During the drier winter months, calculations for the mid-latitude winter standard atmosphere profiles yield a smaller difference, $\Delta T \leq 5.9^\circ K$. The value of the difference for the Bolivian salt desert would be less than $5^\circ K$ due to the higher altitude and reduced water vapor content.

If we model the Great Salt Lake Desert as a stratified medium consisting of a relatively dry surface layer of height h (layer 1) covering a substrate consisting of

saline soil (layer 2) with both layers having the same thermometric temperature T_g, the brightness temperature of the surface can be expressed as (adapted from King [1970]):

$$T_{BS} = T_g (1 - R_{1a})(1 - \tau_1^2 R_{12}) \qquad (6)$$

where R is the power reflection coefficient at the interface between two semi-infinite homogeneous media. The subscript "a" refers to the air medium above layer 1. The effect of the attenuation by layer 1 is accounted for by the transmittance τ_1:

$$\tau_1(h) = \exp(-2\alpha h) \qquad (7)$$

where 2α is the power attenuation coefficient of layer 1.

In the absence of the top layer, $R_{1a} = 0$, $R_{12} = R_{a2}$ and $\tau_1 = 1$ which leads to:

$$T_{BS} = T_g (1 - R_{a2})$$

$$= T_g \epsilon_{a2}$$

where in this case ϵ_{a2} is the same as the emissivity of saline soil ϵ_{ss} (Table 1). Since α varies directly with frequency, the effect of attenuation by the top layer would be expected to be negligible at 1.4 GHz in comparison to 13.9 GHz and, especially, 19.35 GHz. Moreover, since h, the depth to brine, varies between about 10 cm near the center of the desert floor and 2.7 m at the margins, the effect of this variation should be reflected in the difference between the measured brightness temperature T_B and the brightness temperature of saline soil, $T_g \epsilon_{ss}$. Due to the lack of exact information on the moisture, salinity and temperature profiles of the Great Salt Lake Desert floor, only qualitative comparisons can be made between the measured brightness temperatures and the inferences drawn from the two-layer model discussed above.

Table 2 is a summary of vehicle, sensor, and test site parameters pertinent to the present study. More detailed information is given in each of the following subsections.

3.1 S-193 Observations

Three different microwave sensors operating at the same frequency of 13.9 GHz are incorporated in S-193: a radiometer, a scatterometer and an altimeter, all sharing the same antenna and some of the receiver front-end. In general, for a given pass (or

Table 2. Summary of Vehicle, Sensor, Pass and Site Information.

	S-194		S-193 RAD		S-193 SCAT		ESMR
Vehicle	Skylab		Skylab		Skylab		Nimbus 5
Altitude	438 km		438 km		438 km		1100 km
Sensor	Radiometer		Radiometer		Scatterometer		Radiometer
Frequency	1.4 GHz		13.9 GHz		13.9 GHz		19.35 GHz
Effective Antenna Beamwidth	15.2°		2.02°		1.56°		*
Beam Scanning	None		Mechanical		Mechanical		Electrical
Pass Information							
Pass Number	5	16	5	16	5	16	*
Pass Date	6-5-73	8-8-73	6-5-73	8-8-73	6-5-73	8-8-73	*
Local Time	10:58 a.m.	9:01 a.m.	10:58 a.m.	9:01 a.m.	10:58 a.m.	9:01 a.m.	12:00-1:00 p.m.
Mode	nadir looking	nadir looking	CTC	CTC	CTC	CTC	CTC
Pitch Angle	0°	0°	0°	17.0°	0°	17.0°	0°
Scan Angle	N/A	N/A	± 10.5°	+10.5°	± 10.5°	± 10.5°	± 50°
Nadir Angle Range	N/A	N/A	0°- 10.5°	17.0°-20.0°	0°- 10.5°	17.0°-20.0°	0°-50°
Ground Resolution at 0° Scan Angle	117 km diameter	117 km diameter	15.5 km diameter	16.2 km x 16.9 km	11.11 km diameter	11.6 km x 12.1 km	25 km diameter
Ground Resolution at End of Scan	N/A	N/A	15.7 km x 16.0 km	16.5 km x 17.5 km	11.3 km x 11.4 km	11.8 km x 12.5 km	160 km x 45 km
Test Site Ground Temperature	296°K	298°K	296°K	298°K	296°K	298°K	*
General Reference	NASA (1974)		Sobti (1973),		Sobti (1973)		Wilheit (1972)

*see section 3.3

**CTC = Cross-Track-Contiguous

parts thereof) either the altimeter or the RADSCAT (Radiometer-Scatterometer) was operated. For the RADSCAT portion several modes of operation were available; each mode specifies the data taking sequences in terms of pitch and roll angles, polarization and sensor. Because of either coverage, incident angle and/or scanning mode considerations, only two S-193 passes were judged suitable for the purposes of the present study. These are Pass 5 on June 5, 1973 and Pass 16 on August 8, 1973. Detailed discussion of the data recorded on Pass 5 will be presented next followed by a brief summary of the observations noted from the data of Pass 16.

Pass 5 was a North-West to South-East descending pass during which S-193 RADSCAT was operated in a cross-track contiguous mode with the radiometer and scatterometer measurements interlaced in time. Other mode parameters include: linear polarization in a direction parallel to the spacecraft velocity vector, approximately 0° pitch, and roll scan between $+10.5^{\circ}$ and -10.5° relative to nadir in the cross-track direction. In this mode, the signal polarization relative to the ground is horizontal. During each scan 12 data points are recorded by each sensor. Figure 5 shows the radiometer footprints (calculated on the basis of the antenna beamwidth) enclosed in the test site frame chosen for this investigation. For reference considerations, the scans have been designated by alphabetical letters and the footprints within each scan are numbered. The position accuracy of the center of a footprint is estimated to be approximately equal to one half of a footprint diameter.

In Figure 5, scans a-d, which fall completely outside the desert area, show brightness temperatures between $270^{\circ}K$ and $279^{\circ}K$. As the spacecraft moved towards the southeast, lower T_B values were observed over the desert, the lowest being $200^{\circ}K$ at footprints 6h and 8h, situated approximately in the central part of the desert. Furthermore, the radiometer shows a drastic change as it crosses boundaries; viz., 3g($264^{\circ}K$) outside the desert, 4g ($220^{\circ}K$) at the boundary, and 5g ($206^{\circ}K$) inside the desert. In scan m, as the antenna scanned between 10m and 12m, two different boundaries are crossed; 10m is at $260^{\circ}K$, 11m is $205^{\circ}K$ (saltflats) and 12m is $154^{\circ}K$ (lake). Keeping in mind the position accuracy of these footprints and the topographic accuracy of the terrain map, it is clear that the radiometer response is fairly consistent throughout. Consider, for example, footprint 10S. Its relatively low brightness temperature of $198^{\circ}K$ leads us to suspect that a larger portion of Utah Lake is enclosed in 10S than is shown.

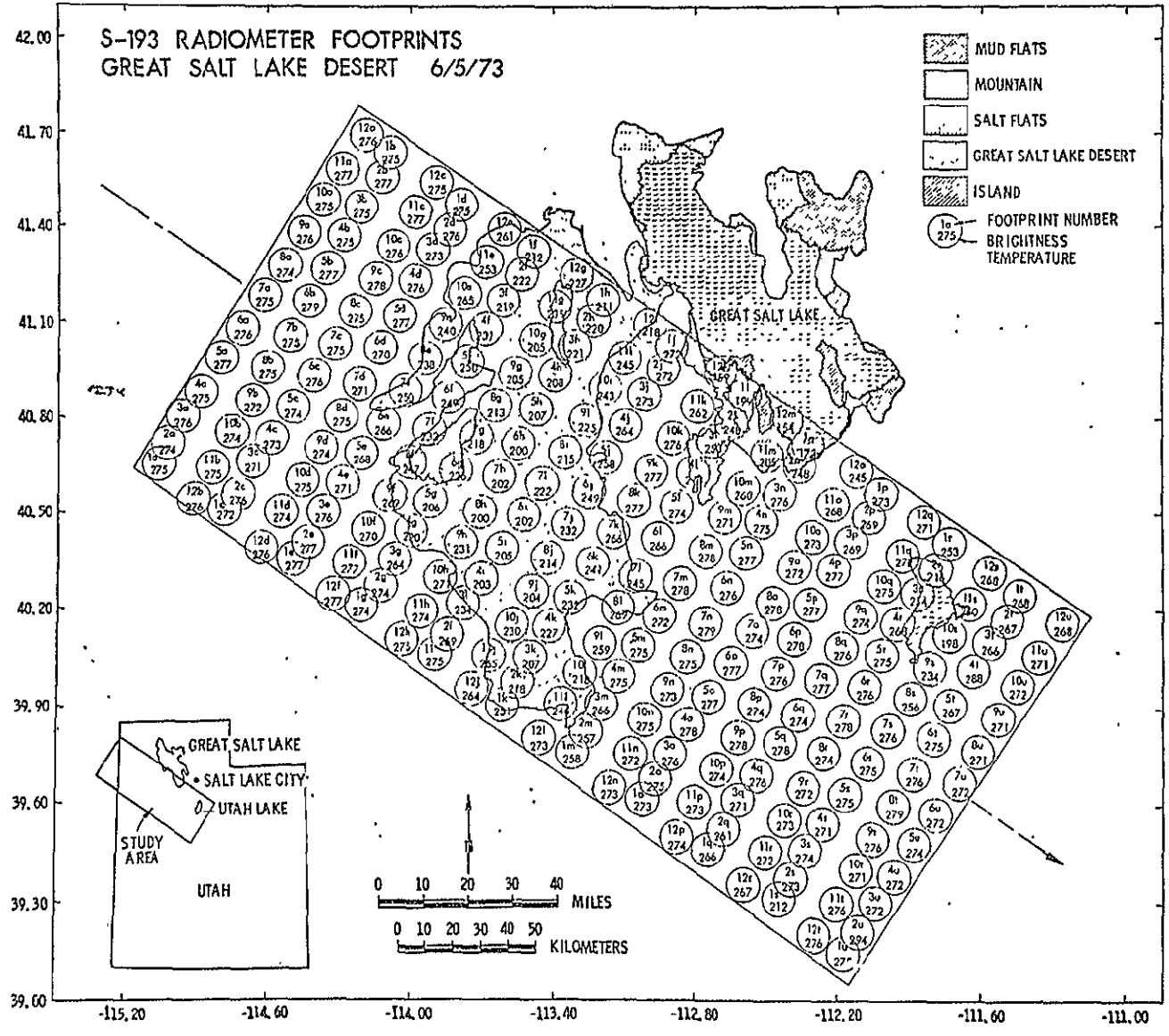

Figure 5. S-193 radiometer footprints, Pass 5, 6/5/73.

For a closer understanding of the spatial variation of the brightness temperature within the Great Salt Lake Desert area, Figure 6 shows a contour map generated on the basis of the data shown in Figure 5.. Based on our earlier discussion of the desert hydrology, we propose that the contour map represents a gross "mapping" of the depth to the brine layer beneath the surface.

Whereas the microwave emissivity is almost insensitive to incident angle variation between nadir and 10.5°, the radar scattering coefficient experiences its largest drop in magnitude in precisely this range of angles. Hence for the purposes of this study, only the data within the $\pm$ 2.5° range around nadir was included in the contour map of Figure 7. The radar data confirms the observations made by the radiometer in that its measured scattering coefficient changes from values smaller than 0 dB for footprints outside the desert to values as high as 17.7 dB over the central part of the desert.

During the early stages of this study, it was suggested that perhaps the response observed by S-193 over the Great Salt Lake Desert might be due to spots of standing water formed by a previous rainfall. No such evidence was observed on the Skylab photography (S 190A) of this area. The next step was to determine whether or not this phenomenon is also evident from data acquired by a) other Skylab passes or b) other satellites carrying microwave sensors. The answer to the latter was provided by ESMR (section 3.3) while the answer to the earlier was provided by Skylab Pass 16 on August 8, 1973, approximately two months after Pass 5. The subsatellite track of Pass 16 was approximately parallel to that of Pass 5 but was shifted towards the North-East by about 52 km.

During Pass 16 over Utah, S-193 RADSCAT was operated in a cross-track contiguous mode similar to Pass 5, except that the pitch angle was about 17° (0° for Pass 5). Corresponding to a roll scan of $\pm$ 10°, the incident angle varied between about 17° (at 0° roll) and 20° (at 10° roll). Thus, for all practical purposes, the incident angle was almost a constant. Due to the larger pitch angle employed in Pass 16, the scatterometer and radiometer footprints were slightly larger (than those of Pass 5). The Pass 16 data were used to generate footprint and contour maps similar to those shown in Figures 5 and 6. Over the test site area, the radiometer recorded a high of 273°K and a low of 199°K [Figures 8 and 9]. The general shape of the contours are similar to those produced from the June 5, 1973 data. Footprints over the Salt Lake itself recorded brightness temperatures as low as 146°K. The point to be made here is that indeed the phenomenon observed in June was also evident in August.

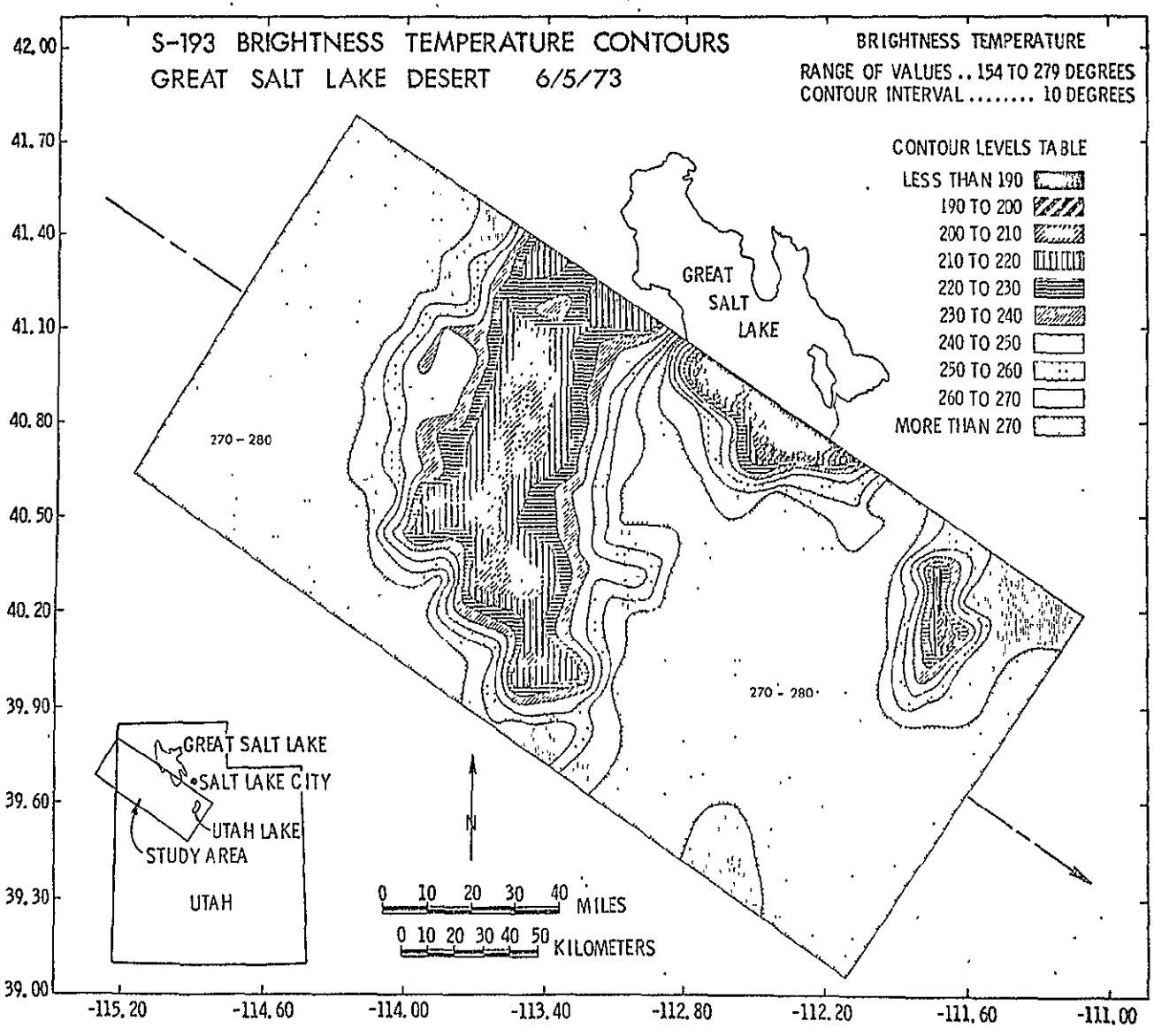

Figure 6. S-193 brightness temperature contours based on the data of Figure 5.

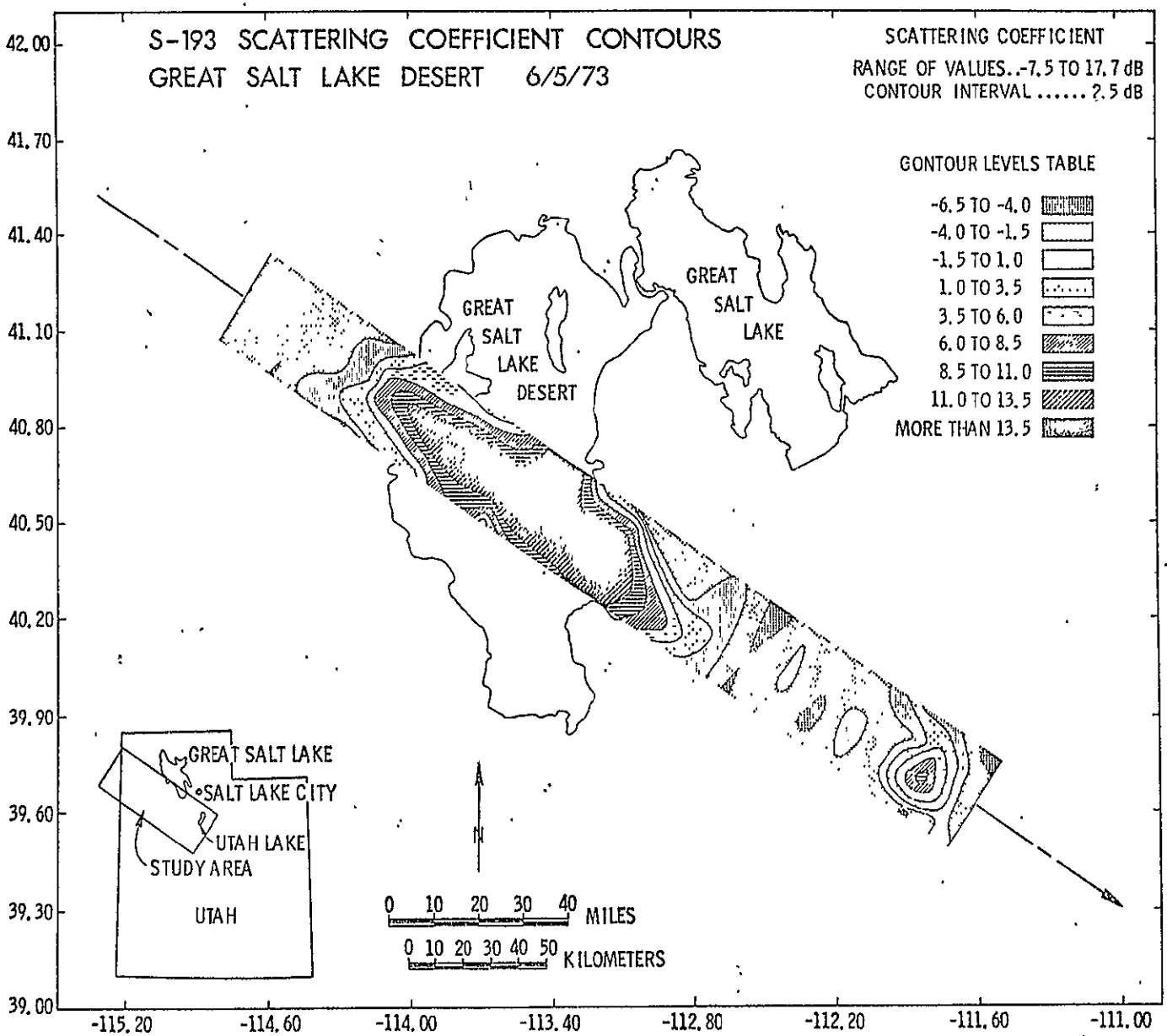

Figure 7. S-193 scattering coefficient contours, Pass 5, 6/5/73.

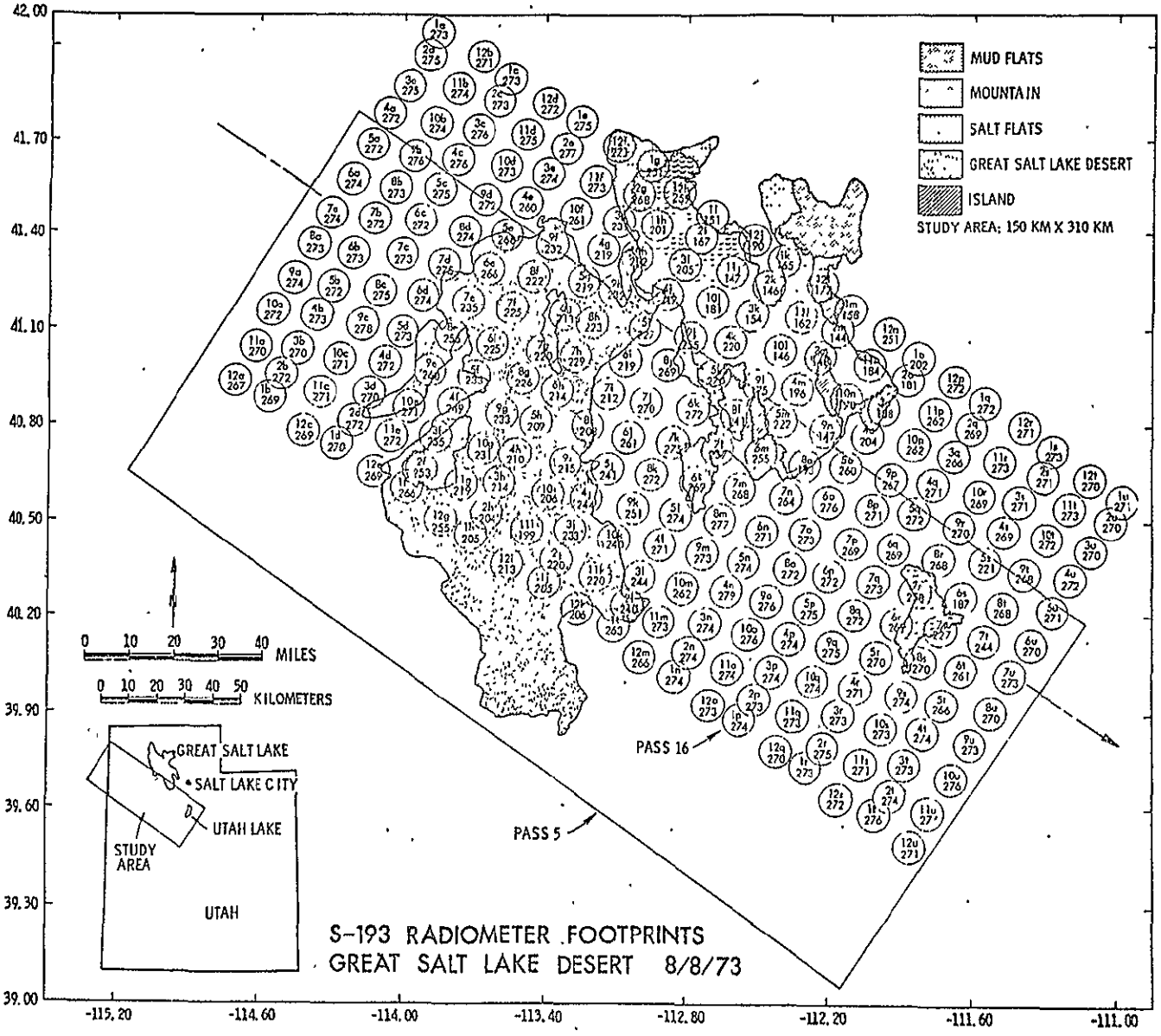

Figure 8. S-193 radiometer footprints, Pass 16, 8/8/73.

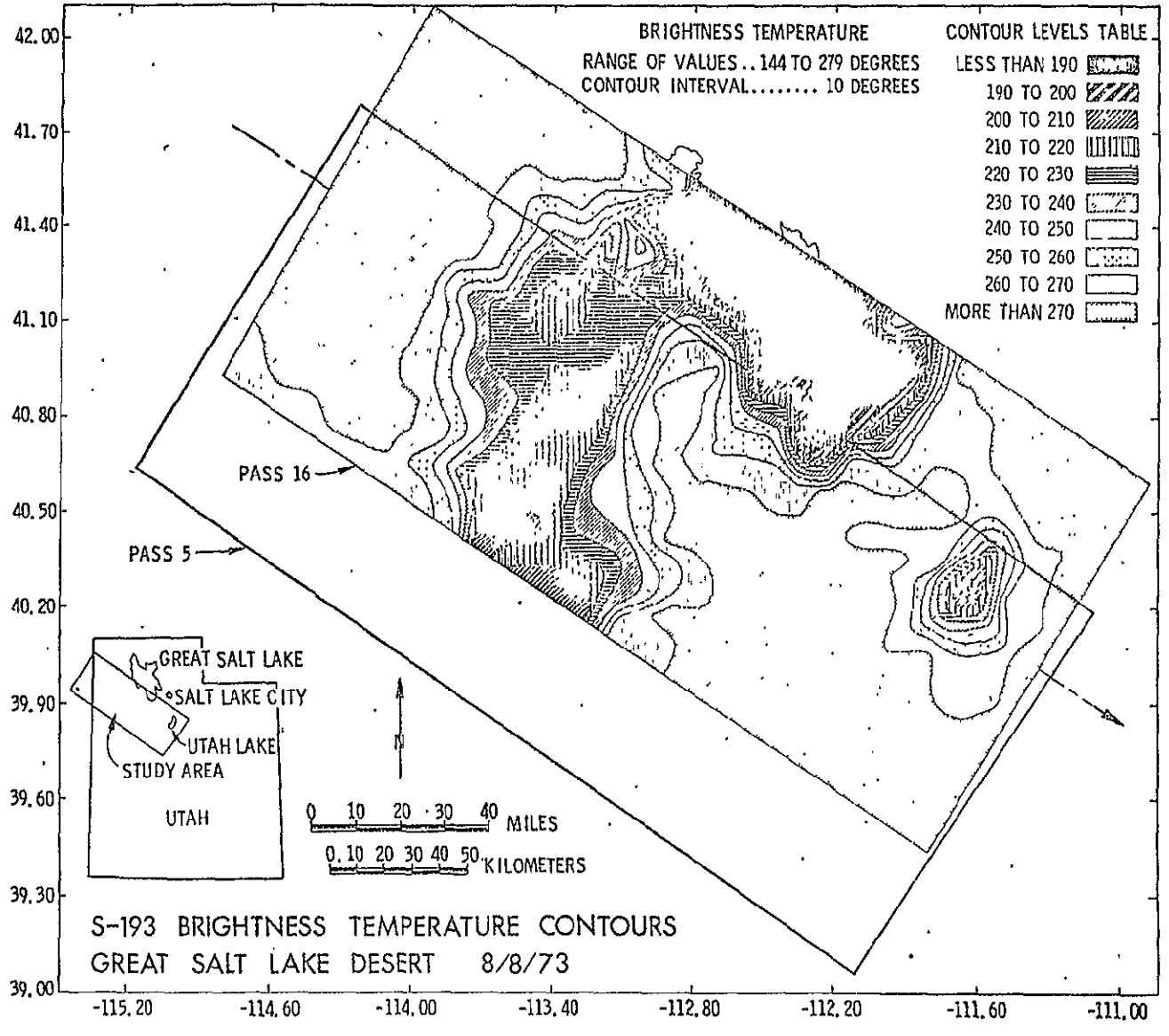

Figure 9. S-193 brightness temperature contours based on the data of Figure 8.

3.2 S-194 Observations

Simultaneous with the S-193 measurements discussed in the previous section, passive L-band (1.4 GHz) data were acquired during the same passes over Utah. The radiometer was nadir-looking having a circular footprint approximately 117 km in diameter. Ground distance covered between consecutive measurement points shown in Figure 10 is approximately 7km, producing about 94 per cent overlap. The measured data are plotted in Figure 11 as a function of distance from the center of a reference footprint. This plot represents a convolution of the ground brightness temperature (T_{BS}) spatial variation with the antenna power pattern as the latter is swept across the test site along the subsatellite track. Before crossing the desert boundary on the western side, the S-194 radiometer recorded a constant brightness temperature of 260°K for footprints 1 through 9. Between footprints 9 and 26, whose centers are separated by approximately 115 km, the brightness temperature dropped to a low of 202°K, after which it remained unchanged over the next 20 km and then it increased to a value of 252°K over the eastern section of the test site. With a 94 per cent overlap between successive footprints, the fast rate of change of the brightness temperature as the antenna beam swept across each of the two boundaries of the desert, signifies a much faster rate of change of the ground brightness temperature (T_{BS}) spatial distribution in the direction of the satellite track. The combination of S-193 and S-194 observations suggests that the lowest T_{BS} value of the desert center at 1.4 GHz must be much lower than 202°K.

Following the same basic procedure as described above, data recorded on Pass 16 (August 8, 1973) are shown in Figures 12 and 13. Figure 13 shows a plot similar in shape to the plot shown in Figure 11 although having a slightly wider range of T_B; west of the desert $T_B \approx 270°K$, east of the desert $T_B \approx 260°K$ and over the desert the lowest T_B recorded was 195°K. The difference between the brightness temperatures corresponding to footprints on the western and eastern sections of the test site (10°K) is comparable with the difference observed for Pass 5 (8°K), yet the absolute value is higher by about 10°K. Since the reported air temperature for Pass 16 is only 2°K higher than that of Pass 5, the 10°K increase in absolute value must be, for the most part, attributable to differences in the topography due to the ground separation of the two passes. The low of 195°K is attributed to partial contributions by the Great Salt Lake.

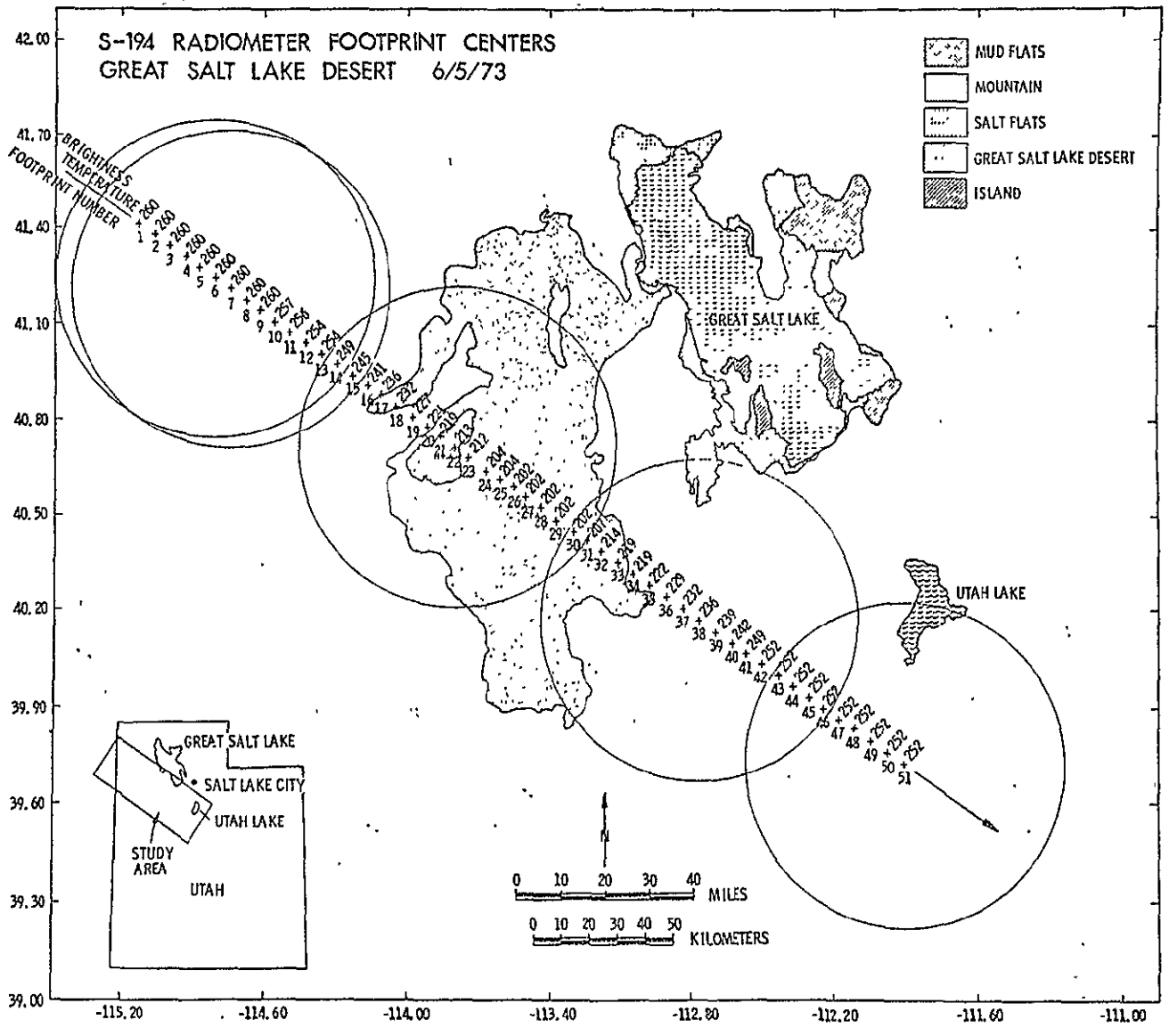

Figure 10. S-194 radiometer footprint centers, Pass 5, 6/5/73. Only footprints 6, 7, 22, 38 and 51 are shown.

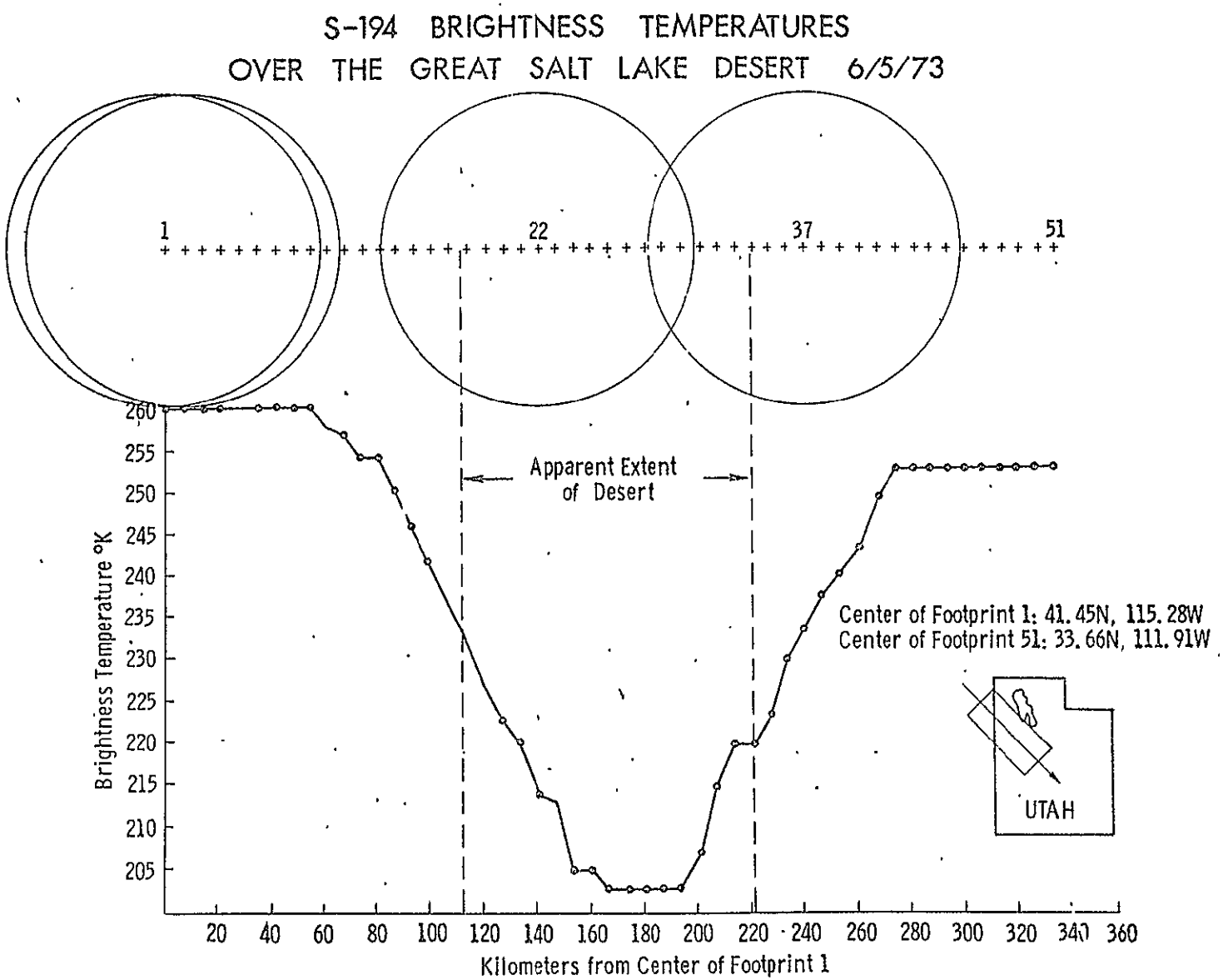

Figure 11. S-194 brightness temperature as a function of distance from the center of footprint 1 on Figure 8.

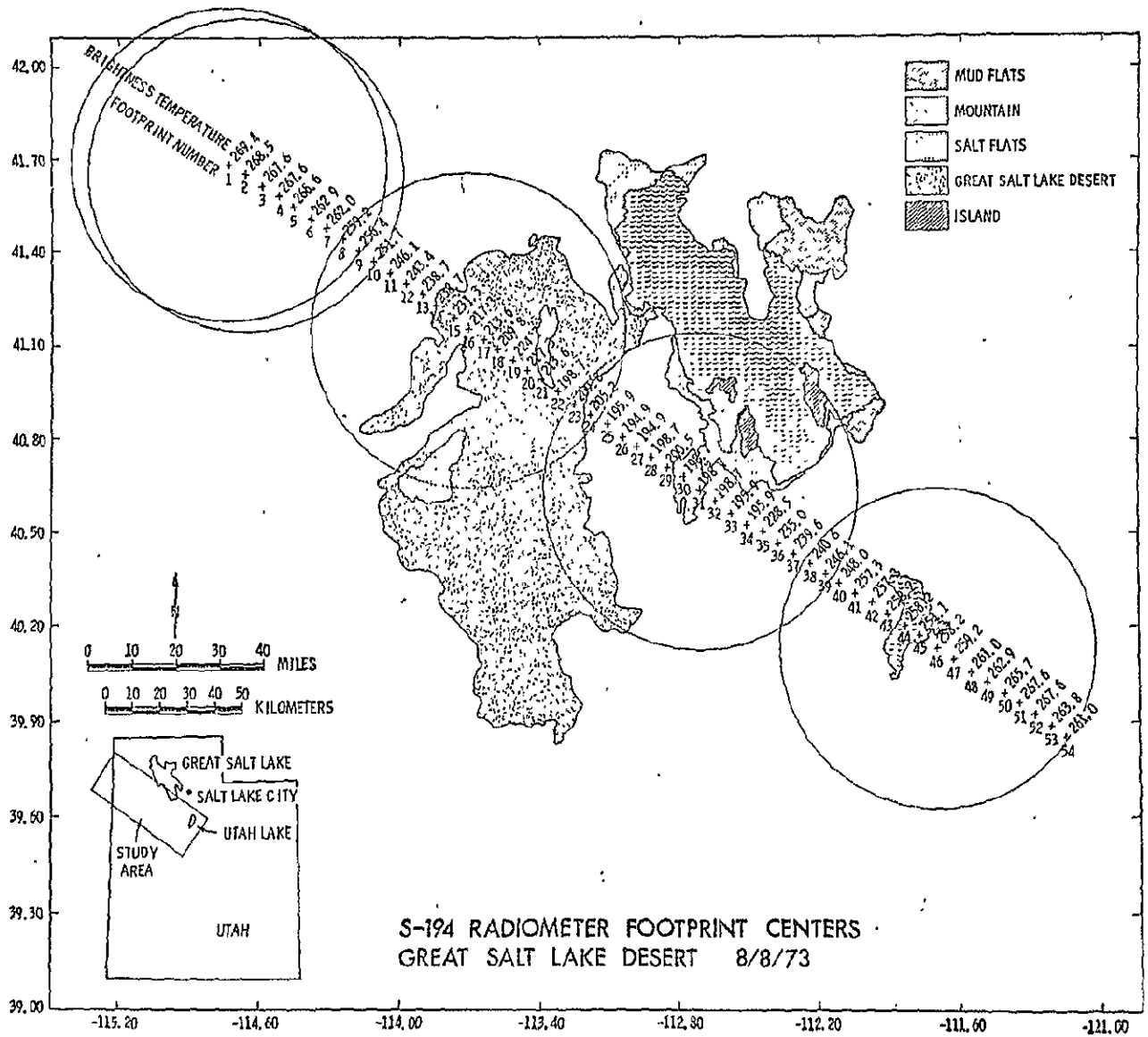

Figure 12. S-194 radiometer footprint centers, Pass 16, 8/8/73. Only footprints 1, 18, 37 and 54 are shown.

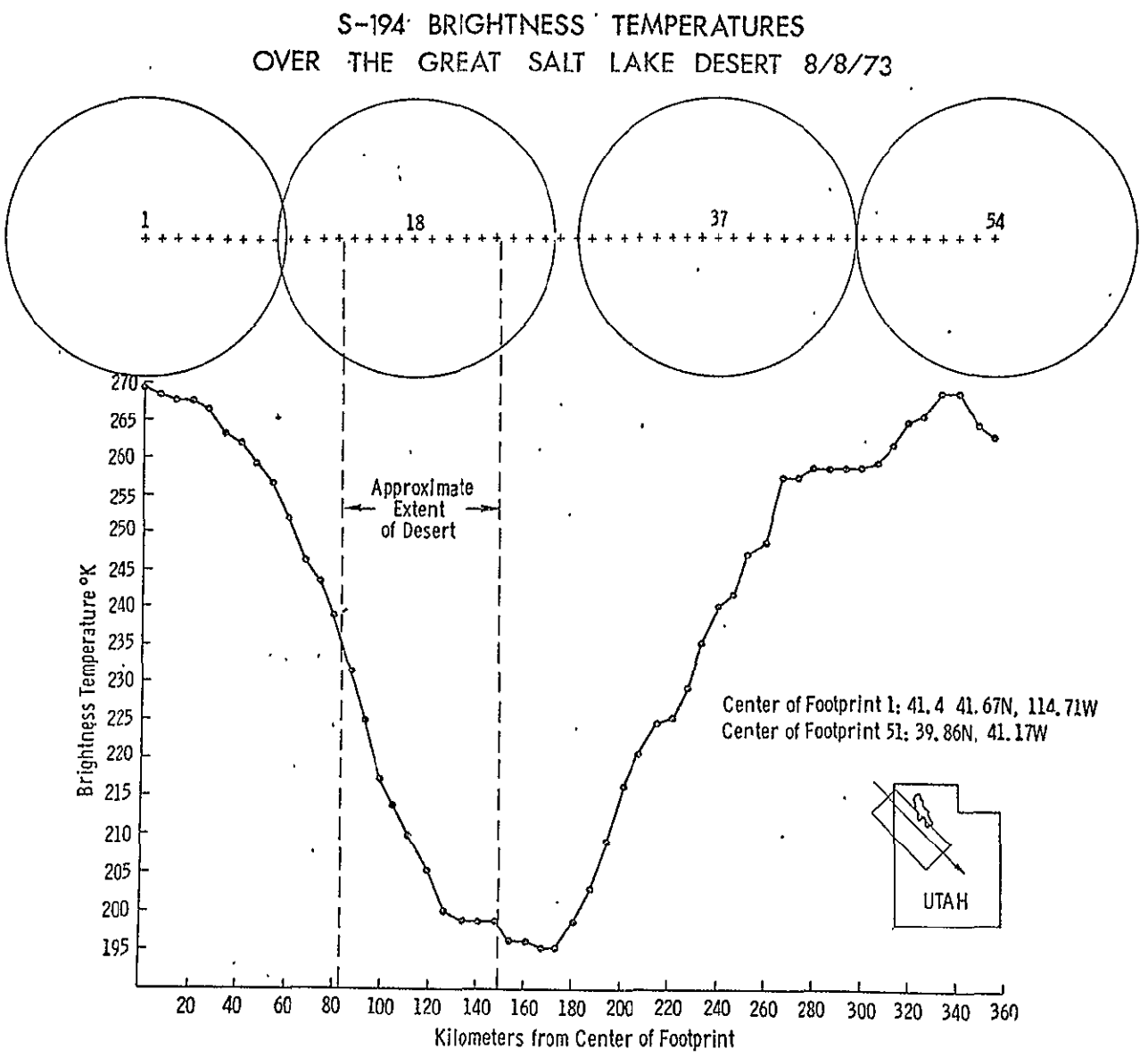

Figure 13. S-194 brightness temperature as a function of distance from the center of footprint 1 on Figure 12.

In support of Pass 16, aircraft data was acquired by NASA using the L-band portion of the Multi Frequency Microwave Radiometer (MFMR) on August 10, 1973, two days after the test site was traversed by Skylab. The course flown was a straight line from 41.275°N, 113.899°W to 40.843°N, 112.992°W, which crosses the desert along a line close to the subsatellite track of Pass 16 [NASA, 1974].

Figure 14 is a Skylab photographic image of the northern part of the Great Salt Lake Desert on which the course flown by MFMR is indicated. Also shown is a plot of the brightness temperature recorded by the MFMR instrument which indicates T_B values ranging between 285°K and 303°K over the mountains on the two ends of the pass and over the New Foundland mountains approximately half-way in between. In comparison, the brightness temperature of the desert portions of the pass are generally lower by 150°K or more. The lowest recorded T_B value was 93°K.

3.3 Nimbus 5 ESMR Observations

The Nimbus 5 satellite launched on December 11, 1972 carries an Electrically Scanning Microwave Radiometer (ESMR).

The ESMR consists of the following major components: [Wilheit, 1972]

a) A phased array microwave antenna consisting of 103 waveguide elements each having its associated electrical phase shifter. The aperture area is 83.3 cm x 85.5 cm. The polarization is linear, parallel to the spacecraft velocity vector.

b) A beam steering computer which determines the coil current for each of the phase shifters for each beam position.

c) A microwave receiver with a center frequency of 19.35 GHz and an IF bandpass of from 5 to 125 MHz; thus it is sensitive to radiation from 19.225 to 19.475 GHz, except for a 10 MHz gap in the center of the band.

The unit is arranged to scan perpendicular to the spacecraft velocity vector from 50° to the left to 50° to the right of nadir (in 78 steps) every four seconds. The beam width is 1.4° x 1.4° near nadir and degrades to 2.2° crosstrack x 1.4° downtrack at the 50° extremes. For a nominal orbit of 1100 km altitude, the resolution is 25 km x 25 km near nadir degrading to 160 km crosstrack x 45 km downtrack at the ends of the scan. The satellite orbit is polar with noon and midnight equator crossings.

MFMR BRIGHTNESS TEMPERATURE VARIATION
ACROSS THE GREAT SALT LAKE DESERT, UTAH 8/10/73

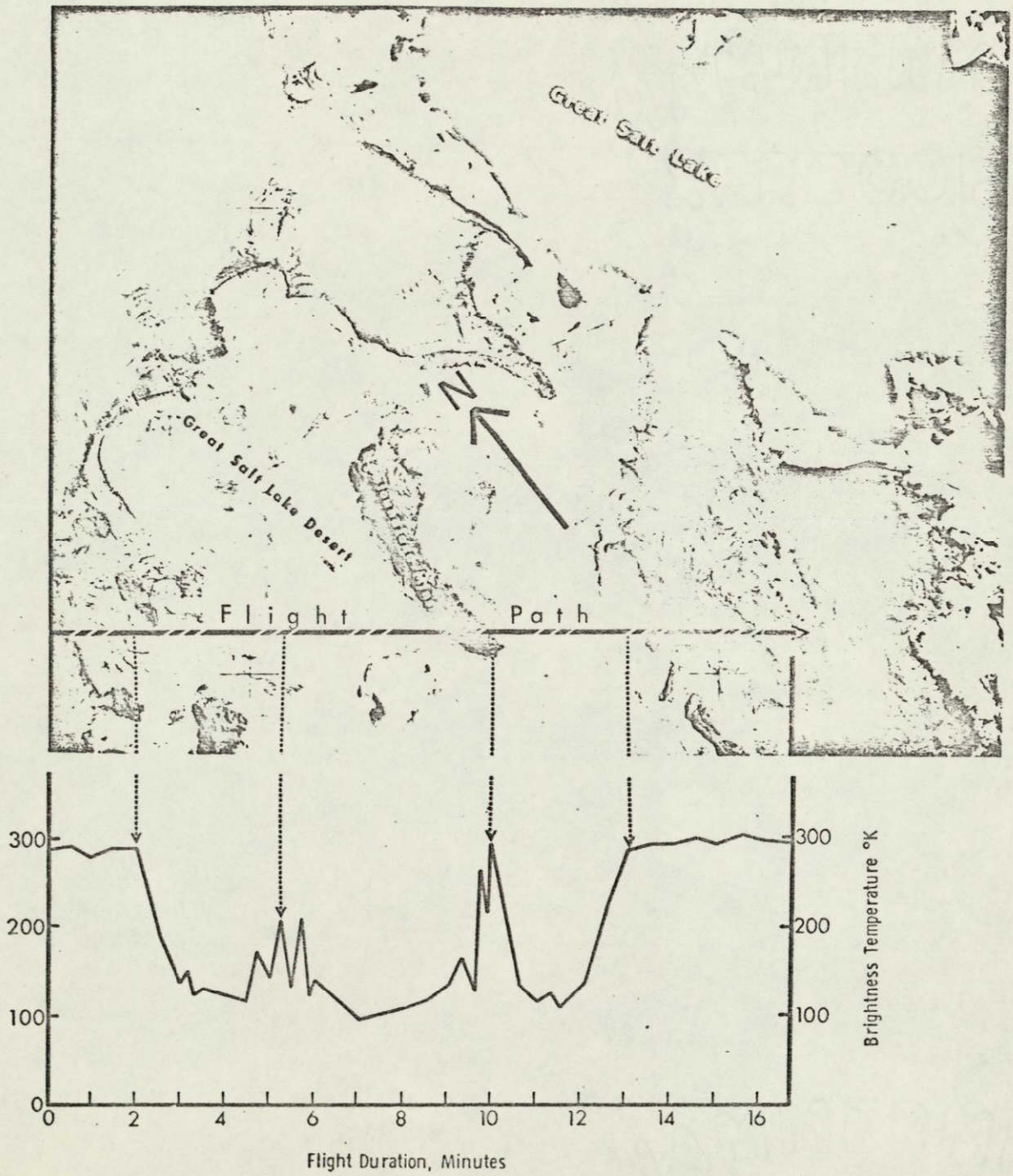

Figure 14. Skylab photographic image of the Northern portion of the Great Salt Lake Desert on which MFMR coverage on August 10, 1973 is indicated.

There is an empirical correction applied to the data for the off nadir beam positions, this correction is designed to eliminate the angular variation of brightness temperature over the ocean. To minimize the effect of this correction and the degradation of resolution, the analysis in this paper was primarily restricted to data from nadir angles of 30° or less.

A contour map of the ESMR brightness temperatures for the Great Salt Lake area is shown in Figure 15 with the outlines of the lake and desert indicated for reference. The brightness temperatures over the lake are not as low as those observed over the ocean (less than 140°K), because the width of the lake is comparable to the resolution of the instrument. Thus it is unlikely that the minimum over the desert is as low as it could be. The minimum T_B observation over the desert is about 70°K less than the surrounding areas, which were up to 280°K. On the following night, the minimum over the Great Salt Lake Desert was about the same while the observed brightness temperature over the surrounding desert dropped to below 260°K. Similar maps were produced for the area on a several per month basis from June, 1973 to December, 1974. The minimum brightness temperature observed over the desert is plotted as a function of time for that period (Figure 16). For comparison the brightness temperature of a spot (40°45'N x 114°45'W) 60 km west of Wendover is also plotted to indicate the type of seasonal variation that might be expected for the usual terrain outside the desert area. In general the brightness temperature for this location varies rather smoothly from a maximum of 280°K in July and August down to a minimum of 240°K for January and February and appears to repeat from one year to the next. The minimum brightness temperature over the Great Salt Lake Desert followed a similar sort of seasonal variation with its maximum occurring in July and August. However, the minima were in November in response to the fall rains during both years. There is a significant difference in the level of the brightness temperature for the summers of 1973 and 1974. The minimum temperatures observed over the Great Salt Lake Desert in the summer of 1974 were 20°-30°K higher than those observed during the summer of 1973. The rainfall during the summer of 1974 was only 50 per cent of normal while in 1973 it was slightly above normal. The average monthly rainfall for eight stations surrounding the basin is shown as bar graphs on the bottom of this figure and clearly indicates this difference in rainfall for the two summers. The response to the heavier fall rains of November, 1973 and October, 1974 is indicated and in particular the lowest brightness temperature was observed on 18 November 1973 when more than 1 cm of rain was recorded at the

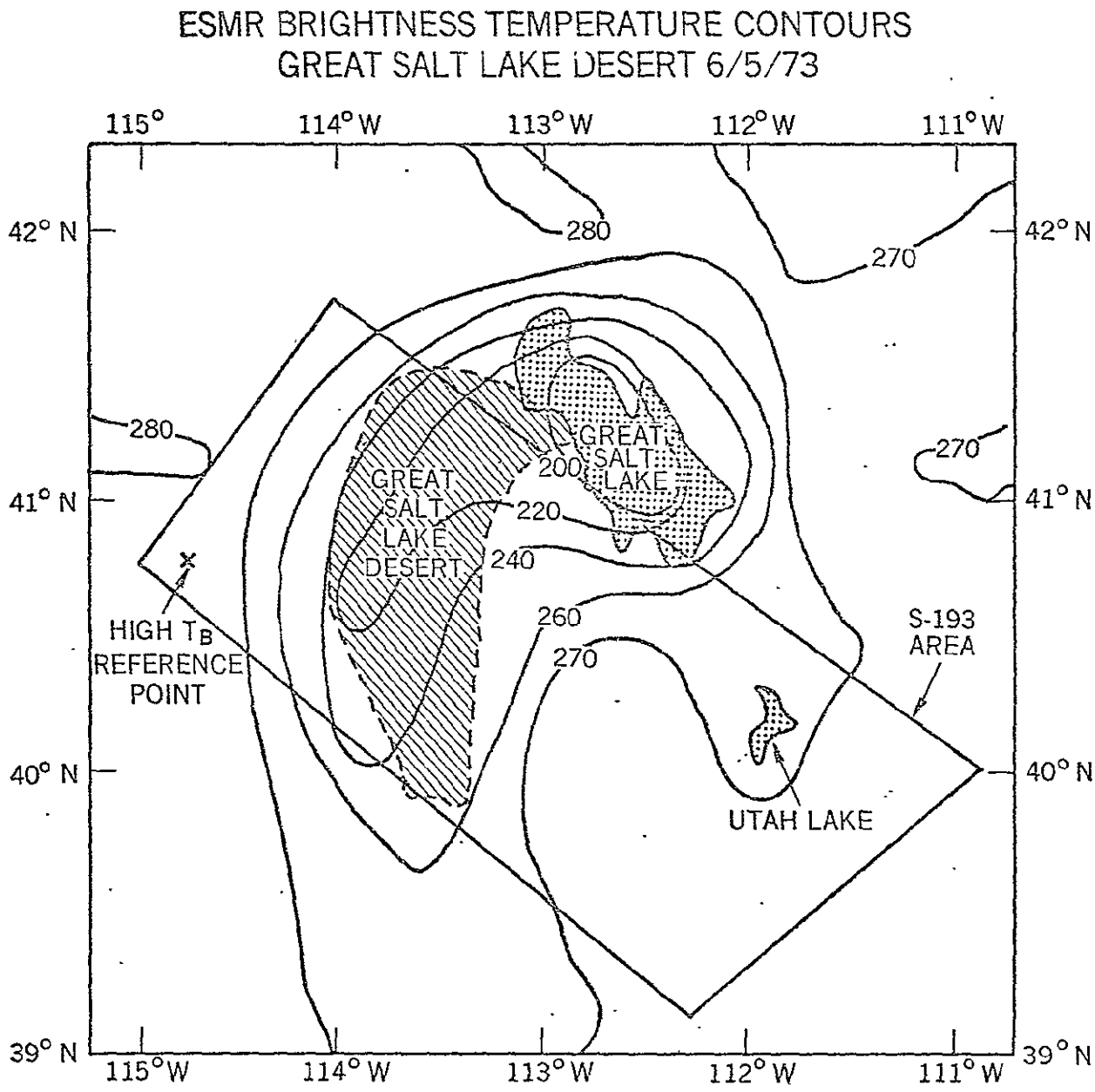

Figure 15. ESMR brightness temperature contours, 6/5/73.

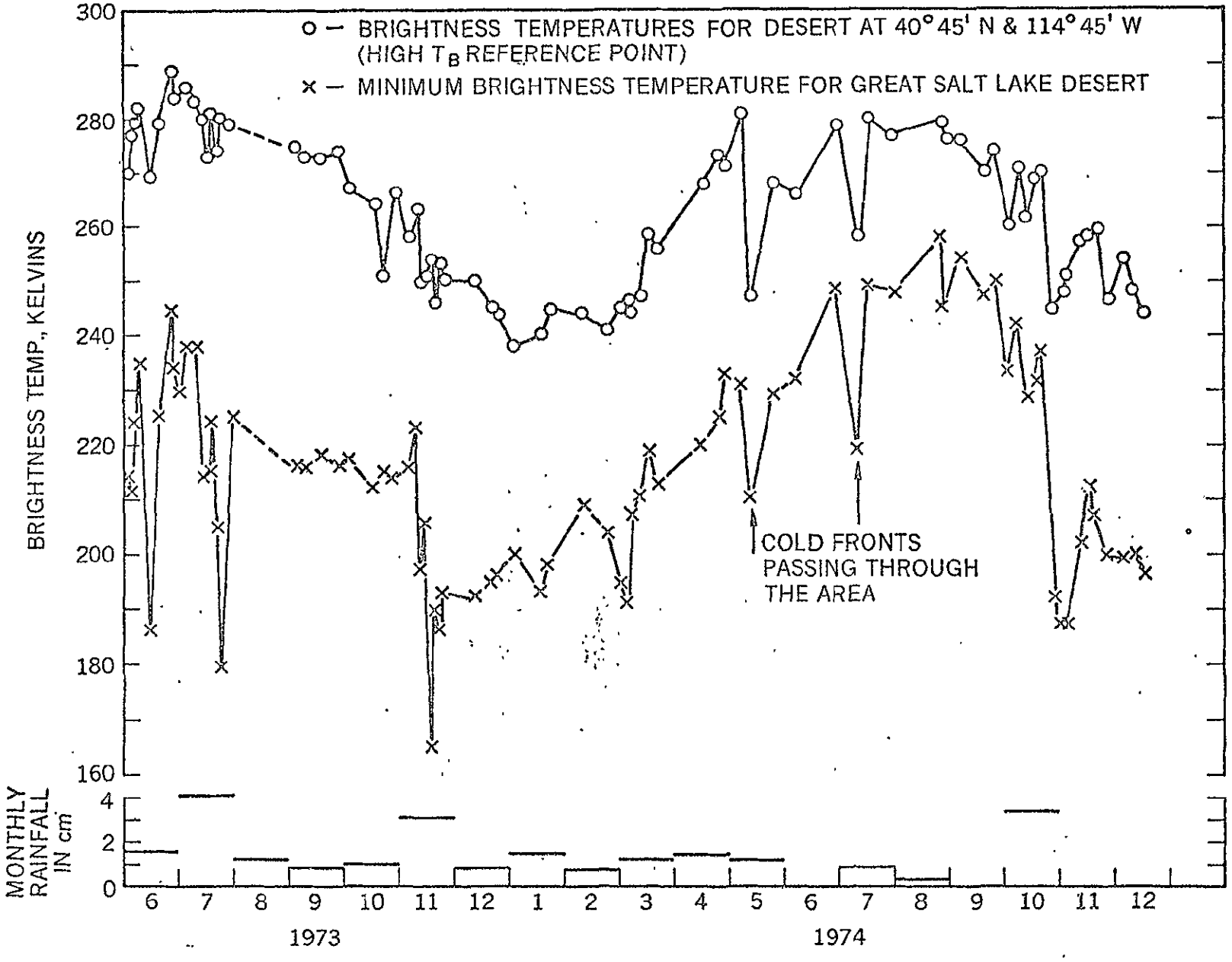

Figure 16. Temporal variations of the minimum recorded ESMR brightness temperature over the Great Salt Lake Desert (x) compared with the ESMR brightness temperature (o) of the reference point outside the desert (indicated in Figure 11).

eight stations. It appears that the radiometer may be responding to a combination of surface water resulting from the rain and a rise in the level of the water table.

There are several other areas of the world which have similar geological features; e.g. the salt deserts of Bolivia: the Salar de Coipasa and Salar de Uyuni. Figure 17 is a ESMR brightness temperature contour map of this area for 6 June 1973. Again the salt deserts have a much lower brightness temperature than the surrounding areas. These salt deserts are at the southern and lower end (altitude = 3660 m) of the drainage system of the great central plateau or Altiplano region of Bolivia. Thus the topography of these deserts is similar to that represented in Figure 2 with high mountains (5000-6000 m) on the east and west sides of the plateau. Because of the size of Salar de Uyuni (100 x 120 km) it is possible to have ESMR resolution elements looking only at the Salar. The lowest brightness temperature observed during this pass over the de Uyuni was 165°K. This is comparable to the lowest value observed over the Great Salt Lake Desert after a rain and is comparable to the value calculated for a saline soil. It is unlikely, however, that the low value over the de Uyuni was after a rain since the station at Oruro (200 km north of the de Uyuni) reported no rain for June, 1973. Thus in this case, the radiometer is most likely responding to subsurface water.

4.0 CONCLUDING REMARKS

Comparison of the microwave data acquired by Skylab, Nimbus and MFMR with the available information on the hydrology of the Great Salt Lake Desert suggests the following conclusions:

a) Subsurface water exhibits a strong influence on the measured scattering coefficient and brightness temperature, particularly over the central part of the desert where the water table is the closest to the surface. Although this influence is clearly discernible at 13.9 GHz and 19.35 GHz, it is most pronounced at 1.4 GHz; over the desert the minimum recorded brightness temperature by the L-band channel of the airborne MFMR radiometer was 93°K in comparison to 285°K-303°K over the mountains.

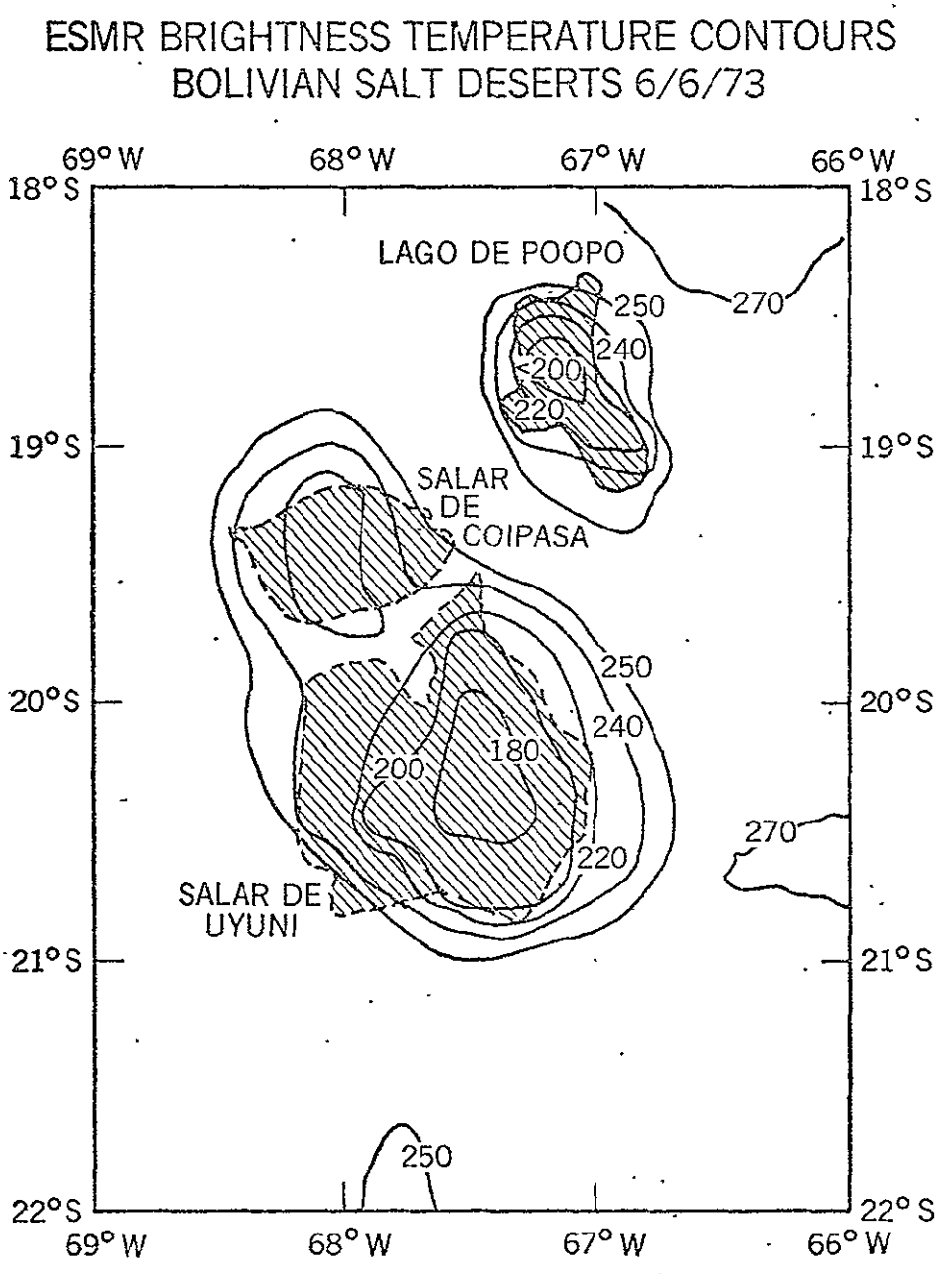

Figure 17. ESMR brightness temperature contours of the Bolivian salt deserts, 6/6/73.

b) According to the calculated emissivity of saline soil (with 150 °/oo) at 1.4 GHz (Table 1), it is not surprising that the 93°K brightness temperature recorded by MFMR is lower than the brightness temperature of water at the same frequency and ground temperature. For T_g = 296°K, $T_{BS} = \epsilon_{ss} T_g = 80.65^{\circ}K$. The presence of the surface layer above the brine increases T_{BS} to a higher temperature.

c) The configurations of the brightness temperature contours of the S-193 radiometer and the Nimbus 5 Electrically Scanning Microwave Radiometer are in agreement with the reported variation of the depth of the water table below the surface between the central part of the desert and the desert margins.

REFERENCES

Bagley, J. M., R. W. Jeppson, and C. H. Milligan, 1964, Water yields in Utah, Utah Agr. Expt. Sta. Spec. Rept. 18, Utah State Univ., Logan, Utah, p. 55.

Busby, M. W., 1966, Annual runoff in the conterminous United States, U. S. Geological Survey Hydrol. Inv. Atlas HA-212, 1 sheet. U. S. Geol. Survey, Room 8102 Federal Bldg., 125 South State Street, Salt Lake City, Utah, 94138.

Eagleman, J. and F. T. Ulaby, 1974, Remote sensing of soil moisture by Skylab radiometer and scatterometer sensors, Advances in the Astronomical Sciences, vol. 31, the American Astronomical Society, Tarzana, California, August.

Eardley, A. J., 1962, Gypsum dunes and evaporite history of the Great Salt Lake Desert, Utah Geol. and Mineralog. Survey Spec. Studies 2, p. 22. Utah Geological and Mineralogical Survey, 103 Utah Geol. Survey Bldg., Univ. of Utah, Salt Lake City, Utah.

Hoekstra, P. and A. Delaney, "Dielectric Properties of Soils at UHF and Microwave Frequencies," Journal of Geophysical Research, vol. 79, no. 11, pp. 1699-1708, April, 1974.

King, D. D., 1970, Passive detection, Chapter 39 of Radar Handbook, Edited by M. I. Skolnik, Mc-Graw Hill, New York, p. 39-9.

Moore, R. K., 1975, Microwave remote sensors, Chapter 9, vol. 1 of the Manual of Remote Sensing, Edited by F. Janza, American Society of Photogrammetry, Falls Church, Virginia.

NASA, 1974, Skylab program: Earth resources experiment package, sensor performance report, vol. 6 (S194), MSC-05528, Lyndon B. Johnson Space Center, Houston, Texas, September, pp. 1-1 to 9-45.

Newton, R. W., S. L. Lee, J. W. Rouse, Jr. and J. F. Paris, 1974, On the feasibility of remote monitoring of soil moisture with microwave sensors, Proc. Ninth Intl. Symp. on Remote Sensing of Environment, Environmental Research Institute of Michigan, Ann Arbor, Michigan, April, pp. 725-738.

Nolan, T. B., 1928, Potash brines in the Great Salt Lake Desert, Utah in: Loughlin, G. F. and G. R. Mansfield Contributions to Economic Geology, Part I--Metals and Nonmetals Except Fuels, U. S. Geological Survey Bulletin 795, p. 41. U. S. Geol. Survey, Room 8102 Federal Bldg., 125 South State Street, Salt Lake City, Utah, 84138.

Schmugge, T., P. Gloersen, T. Wilheit, and F. Geiger, 1974, Remote sensing of soil moisture with microwave radiometers, Journal of Geophysical Research, vol. 79, no. 2, pp. 317-323.

Sobti, A., 1973, A simulation study of the S-193 RADSCAT in orbit, RSL Technical Report 190-2, University of Kansas Center for Research, Inc., Remote Sensing Laboratory, Lawrence, Kansas, May, pp. 1-140.

Stephens, J. C., 1974, Hydrologic reconnaissance of the Northern Great Salt Lake Desert and summary hydrologic reconnaissance of Northwestern Utah, U. S. Geological Survey Tech. Publ. No. 42, Utah Dept. of Natural Resources, 442 State Capitol, Salt Lake City, Utah, pp. 3-18.

Stogryn, A., 1971, Equations for calculating the dielectric constant of saline water , IEEE Trans. on Microwave Theory and Techniques, vol. MTT-19, no. 8, August, pp. 733-736.

Ulaby, F. T., 1974a, Radar measurement of soil moisture content, IEEE Trans. on Antennas and Propagation, vol. AP-22, no. 2, pp. 257-265.

Ulaby, F. T., J. Barr, A. Sobti and R. K. Moore, 1974b, Soil moisture detection by Skylab's microwave sensors, Proc. URSI Specialist Meeting on Microwave Scattering and Emission from the Earth, Institute of Applied Physics, University of Berne, Berne, Switzerland, pp. 205-208.

Ulaby, F. T., J. Cihlar and R. K. Moore, 1975a, Active microwave measurement of soil water content, Remote Sensing of Environment, vol. 3, pp. 185-203.

Wilheit, T., 1972, The electrically scanning microwave radiometer (ESMR) experiment, in: The Nimbus 5 User's Guide, NASA Goddard Space Flight Center, Greenbelt, Maryland, November, pp. 59-105.

APPENDIX E

PRELIMINARY RESULTS FROM SL-4 (WINTER) MEASUREMENTS

WITH THE SKYLAB S-193 RADIOMETER/SCATTEROMETER

APPENDIX E

PRELIMINARY RESULTS FROM SL-4 (WINTER) MEASUREMENTS WITH THE SKYLAB S-193 RADIOMETER/SCATTEROMETER

The flight occupancy of Skylab was during three periods between May, 1973, and February, 1974. The winter occupancy, mission SL-4, provided the first opportunity to measure significant amounts of snow-covered ground with the 13.9 GHz S-193 scatterometer. Unfortunately, a malfunction in the scan mechanism of the S-193 during September, 1973, resulted in degraded winter observations. During the partial repair of the scanning mechanism, the antenna feed structure was damaged, with a resultant large reduction in antenna gain and great increase in side-lobe level. The width of the main beam was increased somewhat and its shape altered. This problem made the radiometer data useless, since more energy was in the large main sidelobe than in the central beam; but the scatterometer could be used because of the smaller sidelobe response resulting from the product of receiving and transmitting gains. Because of these problems, however, the arrival of the SL4 data at The University of Kansas was delayed until March, 1975, and it arrived in a form requiring subsequent processing before it could be used by the investigators, who received it in June, 1975. Consequently, this brief note only gives an indication of the SL-4 data, and detailed analysis is reserved for a later report.

The damage to the scanning mechanism was repaired by the astronauts in an EVA, but it was only possible to repair the cross-track scanner. Consequently, all SL-4 measurements were made with Pitch 0°. On January 9, 1974, a further failure in the scanning mechanism occured, so that it could scan only to the right, but not to the left of the Skylab. Unfortunately, some of the best snow measurements had to be made with the system operating in this crippled condition. Most were made in a nominal Pitch 0, Roll 0 mode.

Scatterometer Calibration Corrections

Much effort was expended by a multi-institution team to modify the processing for the SL-4 data from the techniques used for SL-2 and SL-3. Necessarily this included some rather gross estimates, for the antenna pattern had to be reconstructed partly from a few measurements made on the ground by the University of Kansas after the failure and partly from inducing a similar failure in the backup antenna -- there was no assurance the induced failure was exactly the same as the failure in space. The

resulting corrections brought the scatterometer data into a relatively correct set of values, but further refinement in these values was accomplished on this project by a comparison of SL2/3 measurements with SL4 measurements from the same type of target area.

Since the scatter from the oceans is believed to be largely independent of season, except perhaps in areas where the temperature of the oceans approaches 0° C, the ocean seems to be the best candidate for comparing SL2/3 with SL4 observations. Estimates of the surface winds were provided for our Skylab oceanographic studies by personnel at City University of New York under Prof. W. J. Pierson, Jr. For a comparison between the missions to be valid, it must be made for the same wind speeds.

Because of uncertainties about the exact wind speeds at most individual points on the oceans, caused by the scarcity of ships equipped with adequate measuring instruments and making frequent enough observations, single measurements of wind speed and scattering coefficient were not compared. Rather, a scattergram was prepared relating measured scattering coefficient to wind speed estimates from ship reports. Since many observations were made at wind speeds near 18 knots, the values of scattering coefficient that best fit the scattering vs. wind-speed relations at 18 knots were determined for SL2/3 data and separately for SL-4 data. These determinations were made at 17° and 33° angles of incidence, and the differences between the two observations used to correct the SL-4 scattering measurements. These observations are reported in Table E-1, and the difference between SL-4 observations and SL2/3 observations is plotted in Figure E-1 for the VV and HH polarizations as a function of angle.

TABLE E - 1

COMPARISON OF SL2/3 AND SL4 RESPONSE OVER OCEAN WITH 18 KNOT WINDS

Polarization	Angle ($^{\circ}$)	SL2/3 σ° in dB	SL4 σ° in dB	SL4 - SL2/3 σ° in dB
VV	17	0.4	6.7	6.3
HH	17	0.4	5.1	4.7
VV	33	-9.6	-2.6	7.0
HH	33	-11.0	-5.6	5.4

C.2

Near vertical the situation was somewhat more complicated. The uncertain change in the pattern of the antenna, combined with the extreme sensitivity of the scattering coefficient to angle within a degree or so of vertical over ocean, make the use of vertical incidence data for determining corrections questionable. Unfortunately, the CTC mode, which would have provided ample points at angles out to 10° or so, was not used over the ocean during SL-4. Consequently, an effort was made to find a suitable land surface that had been observed on both winter and summer missions, that had very little vegetative cover during the summer and no snow in winter so its winter response should be similar to the summer response, and that was observed within a few degrees of vertical. This turned out to be more difficult than at first thought because the CTC pitch 0° summer passes were mostly in areas covered by snow in winter, or in areas of heavy summer vegetation.

Fortunately, suitable angles were found in two ITC passes over dry rangeland in the Texas panhandle during SL2, and a CTC pass was made over the same area during SL4. On day 156 (5 June 1973) an ITC HH-polarization pass went from Utah across parts of Colorado, New Mexico and Texas. On day 162 (11 June 1973) crossed Colorado, Oklahoma, and Texas. On day 11 (11 January 1974) during SL4 a CTC Pitch 0° VV-polarization pass was made over Texas, Oklahoma, Kansas and Missouri. All of these passes covered about the same area of rangeland in the Texas panhandle, and the values of scattering coefficient for the almost-common area were separated out. Mean values and standard deviations were calculated for these data, and the SDs were small enough to warrant using the data for this comparison. Although both VV and HH passes were used for SL2, only a VV pass was available for SL4. During SL2/3, however, the calibration for VV and HH was the same, so that both of these could be used to cross-check the VV from SL-4; this is possible because for angles within 10° or so the only difference between VV and HH is the azimuth direction of the electric vector and this is not important over such a large area. The resulting difference was found to be about 5.6 dB at a nominal 2.3°. This is plotted on Figure 1 and shown to be consistent with the trend from the 17° and 33° oceanic data, so the corrections indicated in the figure have been applied to the SL-4 data. Actual values used for correction are shown in Table E-2.

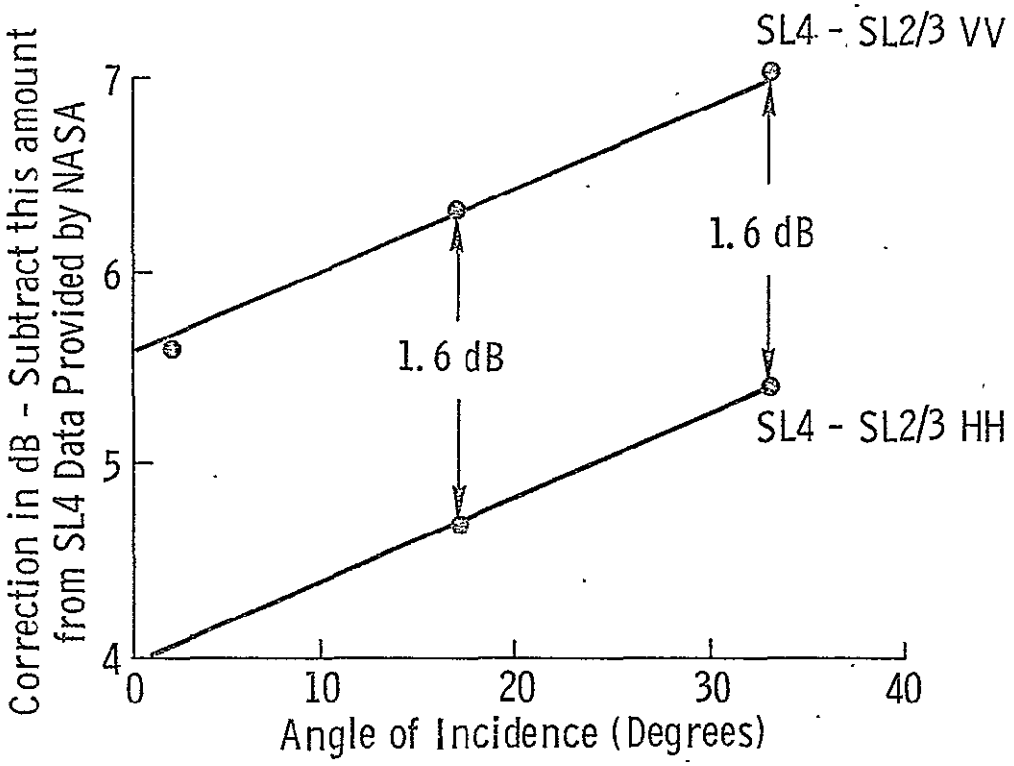

Figure E-1. Corrections To Be Made To SL4 Scatterometer Data. Points At 17° and 33° Based on 17-Knot Winds. Point At 2.3° Based on Texas Panhandle Rangeland.

TABLE E-2

Corrections Applied to SL-4 Scattering Coefficients

Angle	VV Correction	HH Correction
0 - 10°	- 5.8 dB	- 4.2 dB
10 - 20°	- 6.2 dB	- 4.6 dB

The few values for larger angles are obtained directly from the curve.

Some Preliminary SL-4 Results and Comparisons with SL2/3

SL-4 observations have been reduced and analysis and interpretation are underway. In this section, we present three examples of data plots that can be produced from the overland SL-4 data, along with some comparisons with SL2/3 data. No attempt should be made to generalize from these curves, for generalization will require much more study of the complete body of SL-4 scattering measurements and the related ground truth. In particular, conclusions should not be drawn on the basis of this limited sample as to the effect of snow. An attempt is being made to determine this effect in analysis of the complete data set, but it is not easy to do because of the difficulty in finding measurements made under conditions comparable except for the presence or absence of snow.

Figure E-2 shows examples of SL-4 returns from the same land-use category, Agriculture-Forest (mixture within a resolution cell). Quite clearly, the nature of the forests in the three cases will be different, although agricultural terrain in the winter should be relatively free of vegetation in all areas, with the possible exception of Louisiana-Mississippi. Perhaps this explains why the Pass 87 curve is above the others -- it represents scatter from standing crops and forests that have significant amounts of moisture in the branches and trunks -- and in some places the leaves may not have fallen. Most of the forest on the Texas-West Virginia pass is far enough north so that the deciduous trees will have shed their leaves and the trunks and branches will be relatively dry, and the same is probably true for the pass from the Texas panhandle to Iowa; actually the snow-covered part of this pass reported here is from southern Kansas to Iowa across part of northern Missouri. The lower value of scattering for this pass is too close to that for the non-snow pass on day 14 for the difference to be significant in terms of snow -- it could very well have been just this different without snow at all.

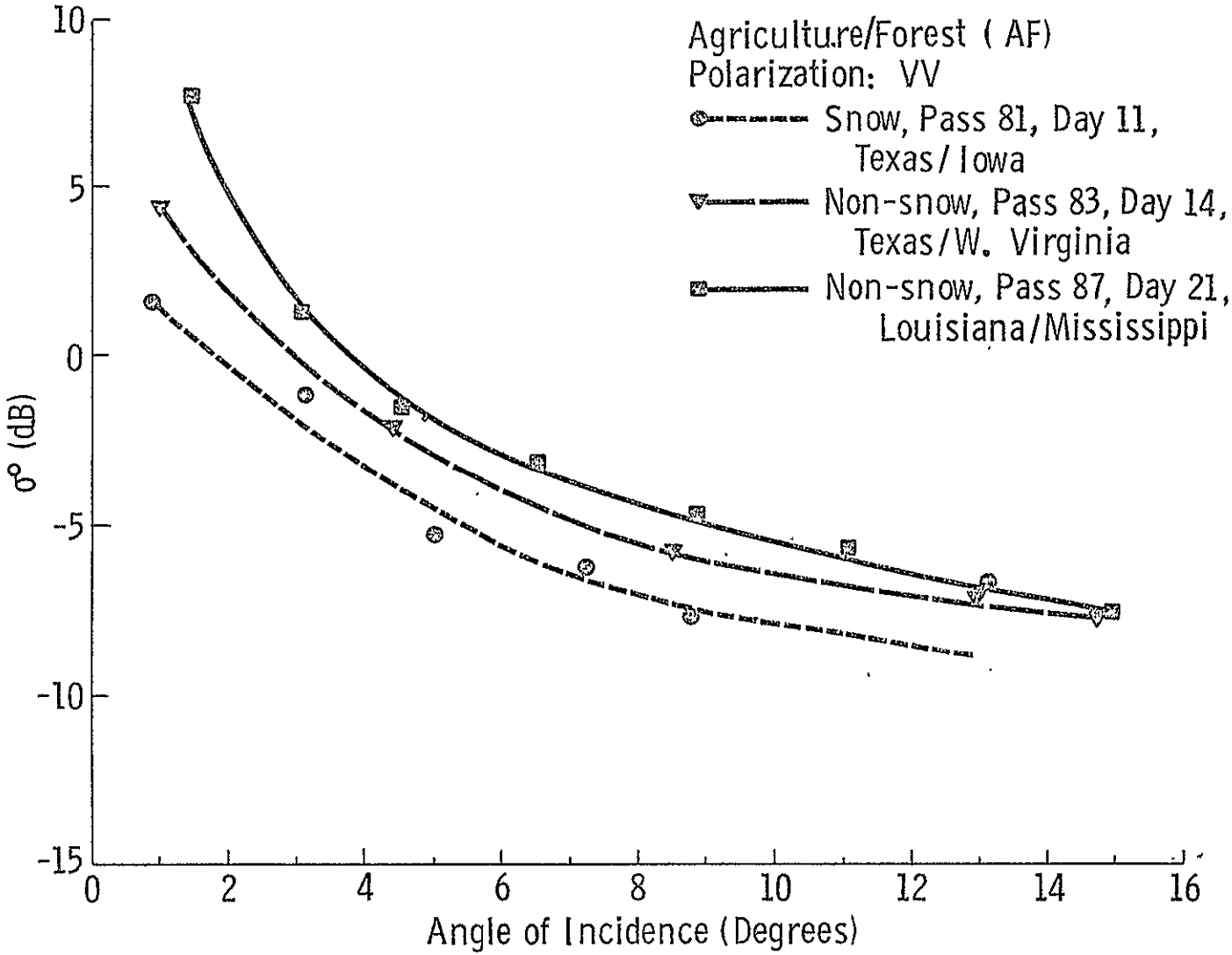

Figure E-2. Example of a Single-Category Set of Summer and Winter Measurements Including One Snow-Covered Area.

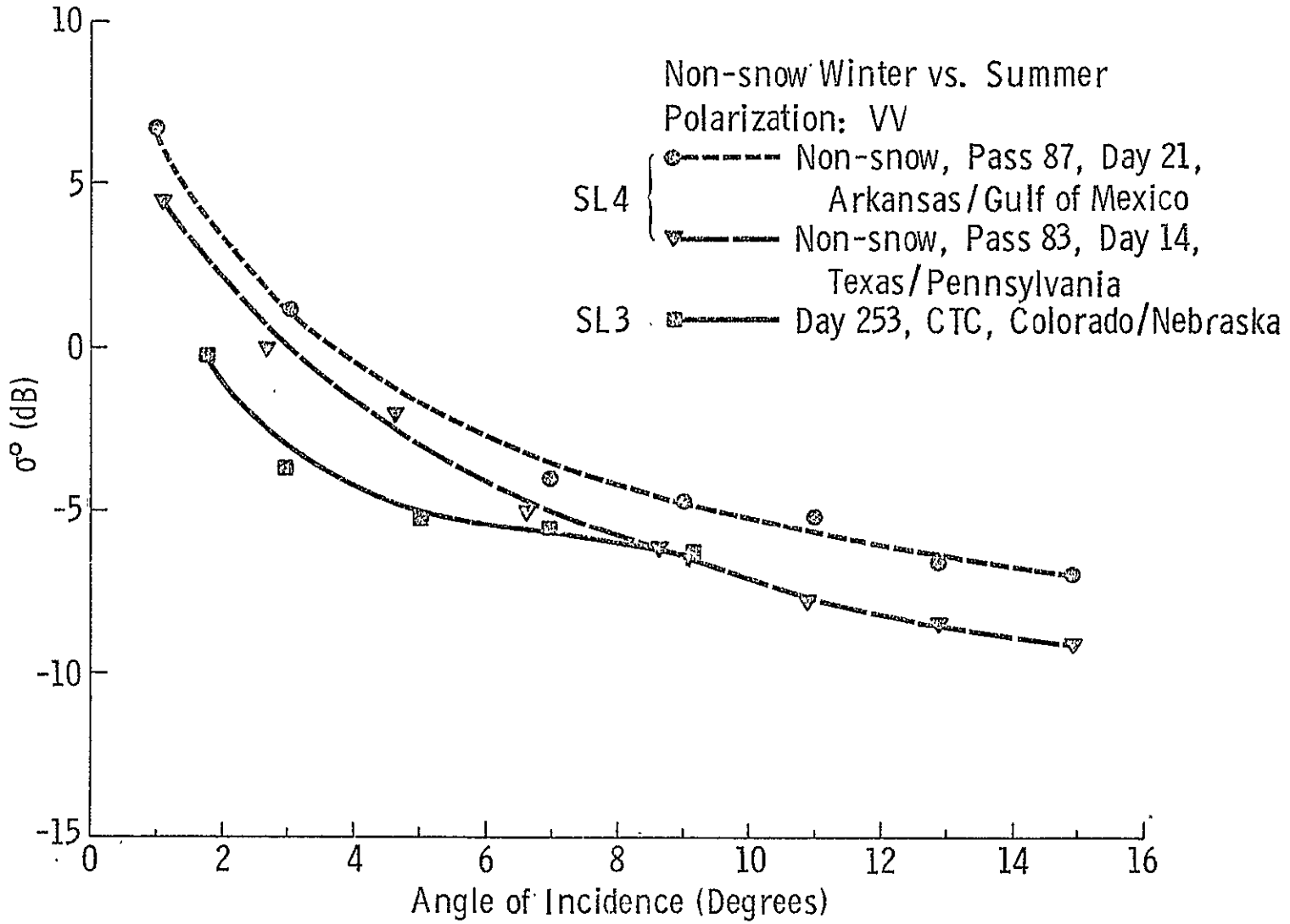

Figure E-3. Examples of Measurements Without Snow in Winter Compared with Summer Measurements in Different Areas.

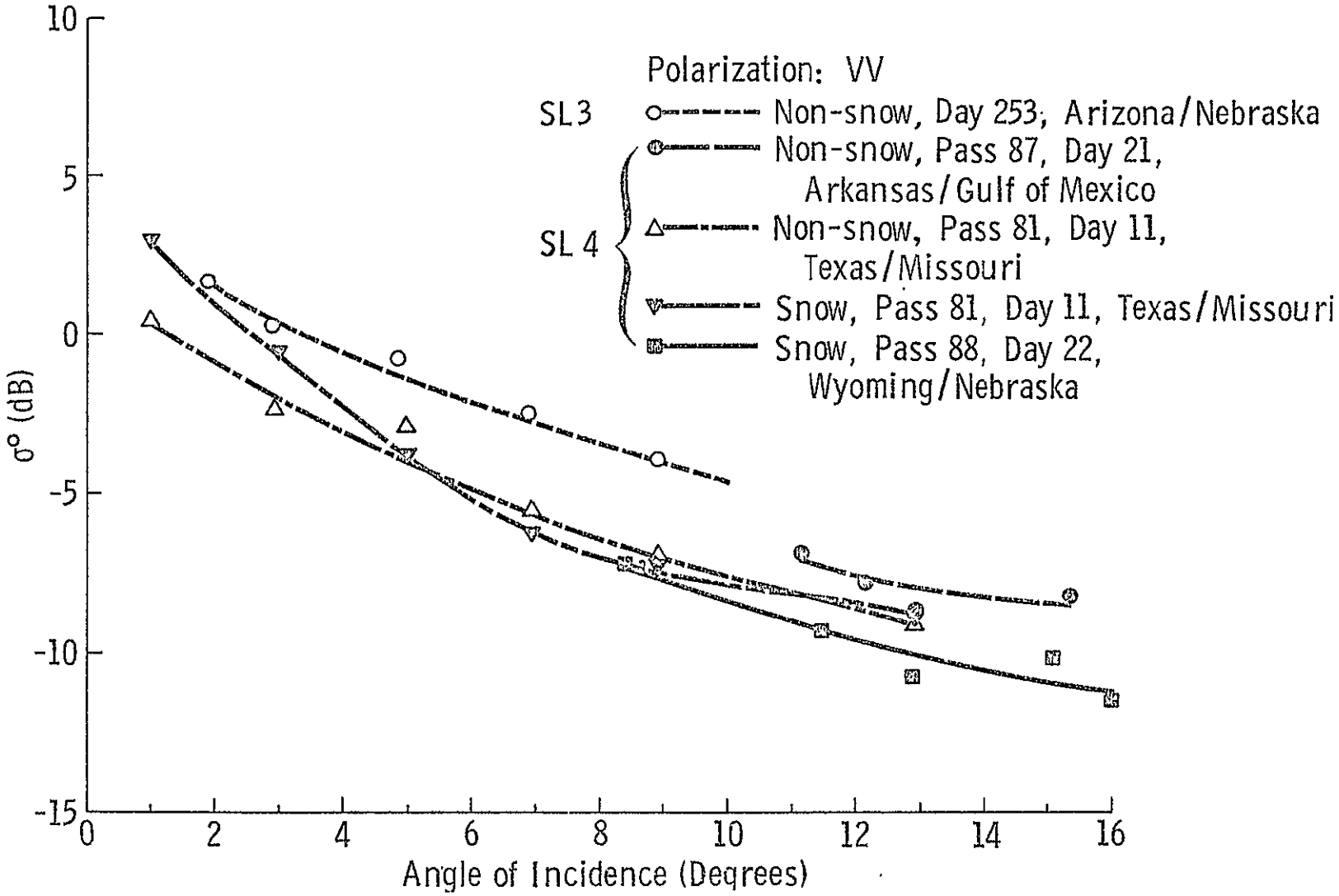

Figure E-4. Example Comparing Both Snow-Covered and Snow-Free Winter Measurements with Summer Measurements. The Wyoming/Nebraska and Arizona/Nebraska Measurements Include Similar Areas, But the Latter Also Includes Mountains.

Figure E-4 compares one summer pass with 2 snow and 2 non-snow pass sections from SL-4. Note that in this case the summer returns are all above the winter returns, which is the opposite of what happened in Figure E-3. The difference between snow and non-snow is too small to be significant.

The primary conclusion one can draw from such a presentation is that the SL4 data appear to be in general consistant with SL2/3 data after we make the corrections indicated earlier. Firmer conclusions must await more detailed analysis which is under way.

APPENDIX F

MICROWAVE SCATTERING MEASUREMENT

OVER BRAZIL AT 13.9 GHz

THE UNIVERSITY OF KANSAS SPACE TECHNOLOGY CENTER
Raymond Nichols Hall

2291 Irving Hill Drive—Campus West Lawrence, Kansas 66045

Telephone:

MICROWAVE SCATTERING MEASUREMENTS OVER BRAZIL AT 13.9 GHz

Remote Sensing Laboratory
RSL Technical Report 243-11

Arun Sobti
Evan C. Davison

September, 1975

Supported by:
NATIONAL AERONAUTICS AND SPACE ADMINISTRATION
Johnson Spacecraft Center
Houston, Texas 77058

Contract NAS 9-13331

APPENDIX F

MICROWAVE SCATTERING MEASUREMENTS OVER BRAZIL AT 13.9 GHz

by

Arun Sobti and Evan C. Davison

University of Kansas Center for Research, Inc.
Remote Sensing Laboratory
Lawrence, Kansas 66045

ABSTRACT

Certain correlations have been noted between microwave backscatter response at approximately 33° from SKYLAB's S-193 Scatterometer (operating at 13.9 GHz) and the configuration of ground targets in Brazil as discerned from coarse-scale maps. In spite of the limited nature of available ground truth, these correlations have been sufficient to permit the production of image-like displays which bear a marked resemblance to known terrain features in several instances. These terrain features have been identified by maps because S-190A and S-190B photographic imagery was almost useless (the areas being obscured by clouds). Among the features identified are large, nearly homogeneous portions of rainforest including one section of the Amazon basin and its attendant riverine formations.

Introduction

Backscattering coefficient measurements over Brazil using the scatterometer on the Skylab manned spacecraft were used to create image-like displays. These image-like displays show a distinct correlation between the backscatter response and the major terrain features as discerned from maps.

The scatterometer on Skylab, designated as S-193 was an interrupted-CW device with a mechanically scanning antenna that had an effective beamwidth of 1.45°. The scatterometer, operating at 13.9 GHz, shared the antenna and some of the rf hardware with a radiometer and an altimeter. The scan of the antenna was predesigned to one of four possible sequences which were chosen by astronaut control. Data from only one mode (cross track contiguous with a pitch offset of 29°) were used in preparing the images as reported here. At this angle the individual cells are ellipses with 13 x 15 km minor and major axes.

The large areas of homogeneous terrain found in South America (particularly the Brazilian region) made them attractive targets for producing the image-like display. The ability of the scatterometer to map, with a gross resolution, the surface could only be assessed by maps, because the spacecraft imagery obtained was rendered almost useless due to intervening clouds. The assessment of the ability of the Skylab scatterometer to respond to major terrain feature variations should be tempered by the fact that the regions in question have not been authoritatively and exhaustively mapped.

The images were created by interpolating the backscattering coefficient data ascribed to the middle point of any target to a finer grid. The interpolated values on the finer grid were quantized at 0.25dB to one bit and displayed on both a black-and-white video monitor and a color video monitor (through a density-to-hue converter). The IDECS*, a near real-time, analog/digital image processing device[1] was used to produce the images.

Selection of ground truth

More than 250 frames of imagery which were located over Brazil were received from NASA at the KU Remote Sensing Lab. All of these were derived from the Skylab 3 and Skylab 4 missions, with the immediate problem that no real time relationship could be established between imagery and scatterometer data. Further, examination of the imagery revealed that its utility was impaired by excessive cloud cover (some tracks were completely covered for hundreds of kilometers), as well as the exposure and filtering problems experienced periodically during the missions. Due to this combination of factors, it was decided

* IDECS stand for Image Discrimination Enhancement and Combination System.

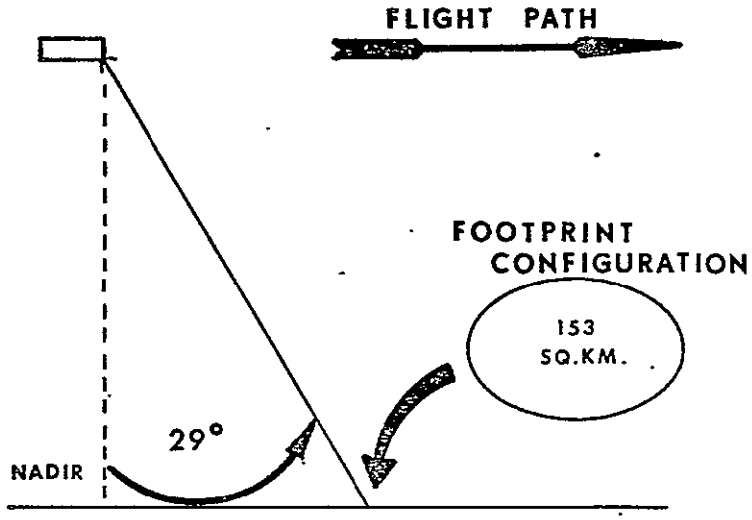

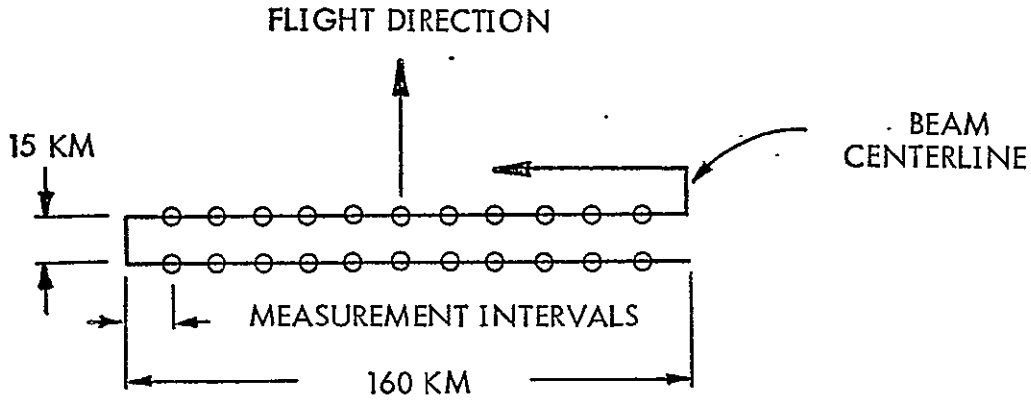

S-193 CROSS-TRACK-CONTIGUOUS
MODE SCHEMATIC

FIG. 1

GENERALIZED PATTERNS* OF NATURAL VEGETATION DISTRIBUTION IN BRAZIL IN RELATION TO S-193 PASSES

* NUMEROUS MINOR INTERIOR FORMATIONS AND NARROW COASTAL FORMATIONS HAVE BEEN OMITTED

FIG. 2

that this imagery should be relegated to a subordinate role in making determinations as to the nature of ground targets.

The potential ground truth base consisted of maps. As much of the territory examined was located in the interior, relatively little of it had been mapped at large scale. Furthermore, the limited time frame in which the study was to be completed made international inquiries, with possible weeks of turn-around time somewhat impractical. Hence, the decision was made to attempt correlations with the coarse scale vegetation and physiographic maps already available (often at 1:25,000,000 or smaller) supported occasionally by Operational Navigation Charts at 1:1,000,000 scale.

Selection of the data base

In the course of the Skylab 2 mission, several passes were made over Brazil using the S-193 Radiometer/Scatterometer in Cross-Track-Contiguous, Pitch 29°, mode. In this mode, the instrument takes twelve consecutive measurements as it scans from side-to-side, each resolution cell or footprint being approximately 153 square kilometers in area, with the indivicual scan tracks being separated by approximately 15 kilometers (Figure 1).

The first pass, Pass 7 (Day 161 - 10 June 1973), began off the northeast coast of Brazil, near the mouth of the Amazon (Figure 2), and terminated off the east coast near Salvador. The second, Pass 8 (day 162 - 11 June 1973) began in northeastern Columbia and terminated in southern Brazil, southwest of Brasilia. The third and final pass, Pass 11 (Day 165 - 14 June 1973) began on the border separating Brazil and Peru, bisecting the extreme western tip of the former and terminating in Bolivia. The extraordinary length of these passes enhanced their potential value.

Results of examination of the S-193 Scatterometer data

The data was visually examined to determine if trends existed which might be relevant to the goals of our study. It became apparent that large segments of the data in Pass 7 reflected such trends. In several instances, the scattering coefficients displayed remarkable consistency for numerous scans along the pass, giving way to abrupt changes on occasion, which suggested changes in surface configuration. In a similar fashion, Pass 8 exhibited large, nearly homogeneous segments of data with distinctive dips in the value of the scattering coefficient at both polarizations, and at several points along the pass. Pass 11, when examined, showed traits similar to the other two.

Quantification of the analysis was carried out by calculating the means, standard deviations and upper and lower bounds of the scattering coefficients of selected samples

from the data. These samples were taken from the center of several successive scans. The centroids of successive sample points, lying with areas identified as homogeneous by the Brazilian Forestry Atlas, were positioned approximately fifteen kilometers apart. As expected, these calculations revealed a high degree of homogeneity which supported the conclusions arrived at during visual examination and to a large extent, supported vegetation boundaries on which the sampling was based. Illustrating the trends mentioned here are the samples of the traces of backscatter from the center points of the scans (Figures 3a and 3b). It should be noted that the trends illustrated in these samples contrast to the data over North America, where much more variability was found.

Creation of the Images

The cross-track-contiguous, pitch 29°, mode provides 12 samples (almost equally spaced) in a cross-track dimension of 130 kilometers. The spacing between the points in the along-track direction is roughly 16 kilometers. The backscattering coefficient is ascribed to the middle point of the target; adjacent targets have some overlap. The long passes over Brazil were broken up into 48 scan segments for interpolation and subsequent display. The interpolation to a finer grid was performed by an inverse weighting of the distance from a target point with known backscattering coefficient. The interpolated values were then quantized into six-bit words providing 0.25 dB per bit from -12 dB to -4 dB. The range of the backscattering coefficient occasionally was below the lower threshold, and for such values the display was equivalent to the background. The ocean surface is usually below -12 dB at 33° and consequently appeared as the background tone. The calibration wedge was prepared by assigning values from 0 to 32 bits in one bit intervals. The files and the calibration wedge were displayed on a black-and-white, and on a color display through a density-to-hue converter which is part of the IDECS system. The display was produced under computer control.

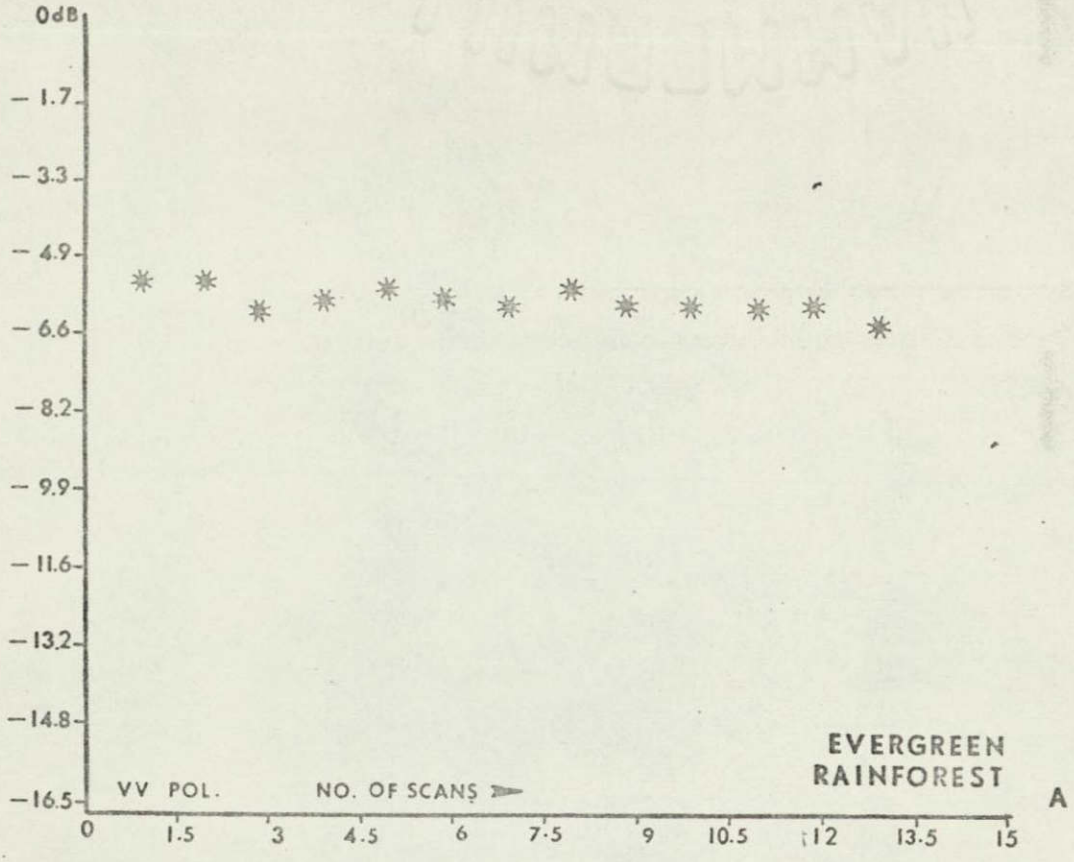

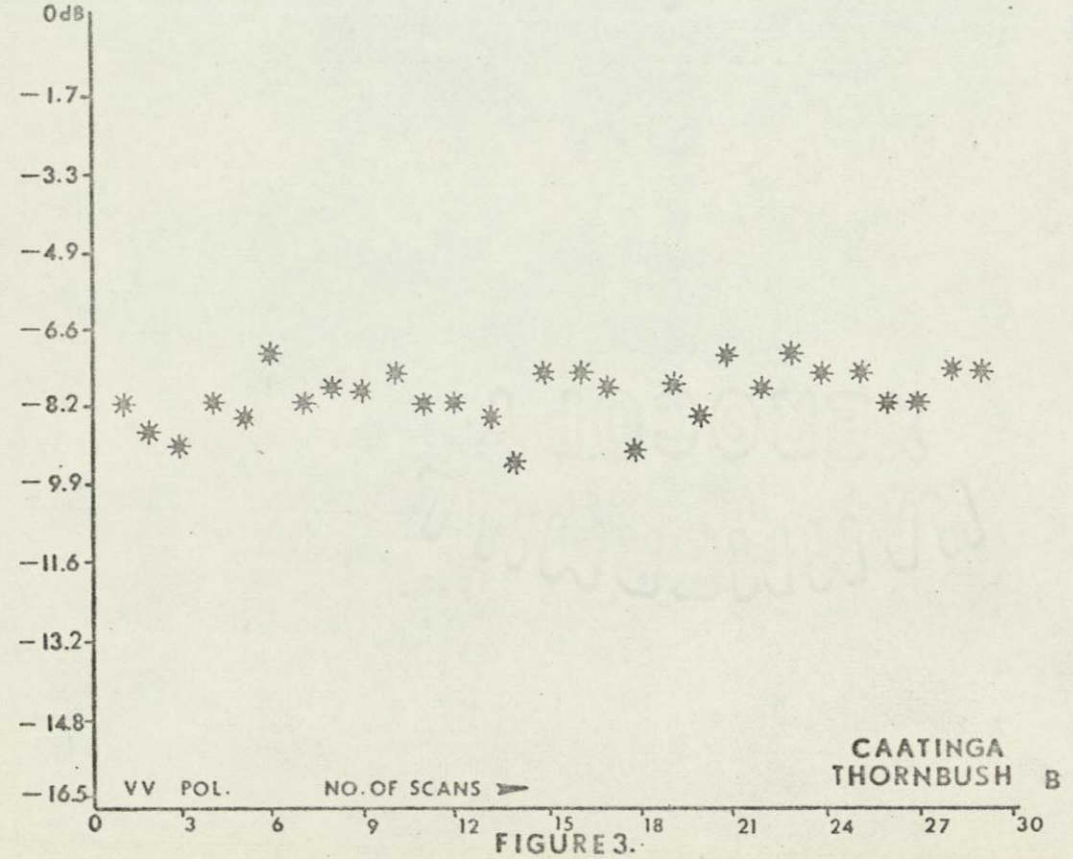

FIGURE 3.
SCATTERING COEFFICIENTS
VERSUS DISTANCE

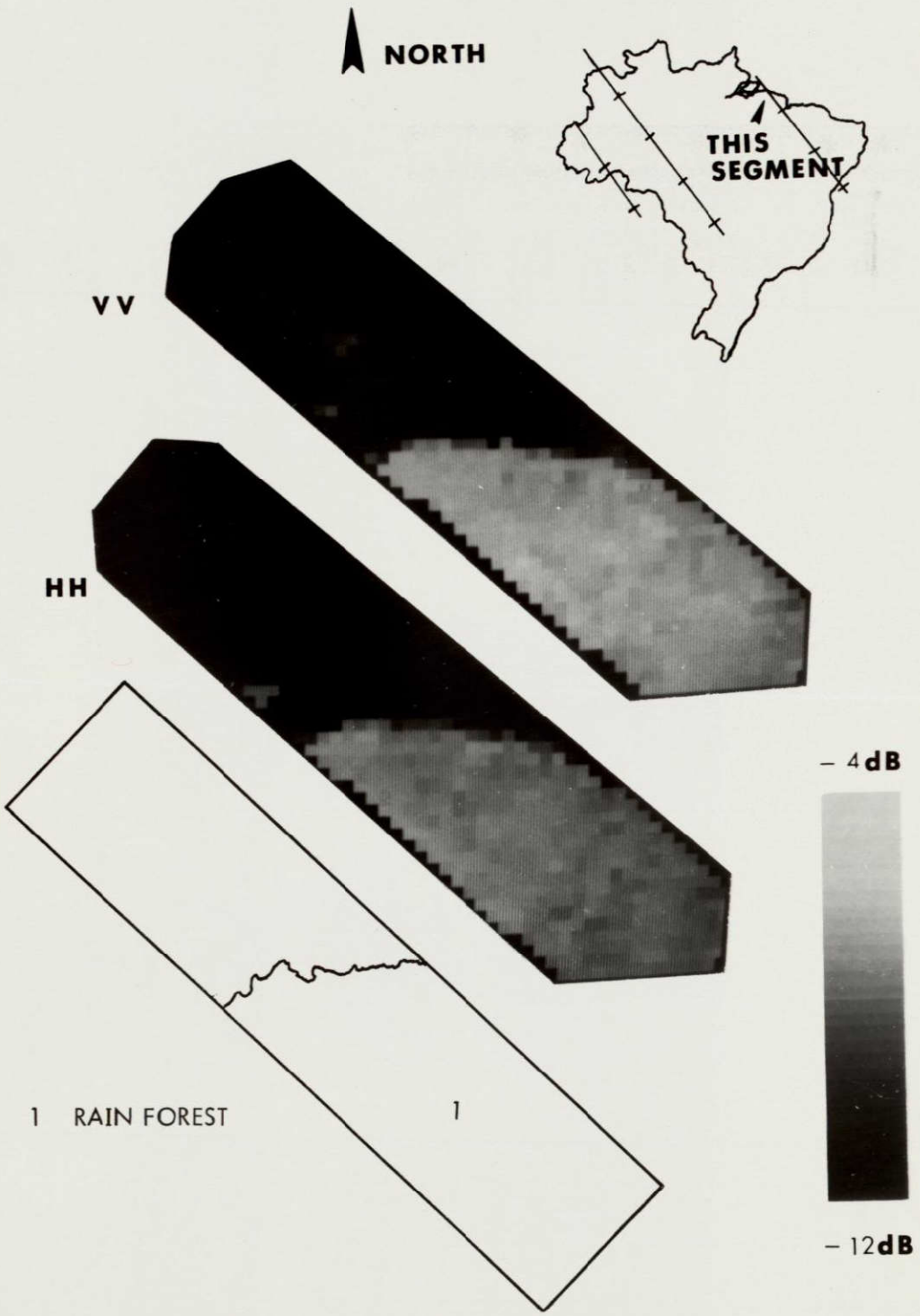

PSEUDO-IMAGES PRODUCED FROM BACKSCATTER RESPONSE WITH CROSS-TRACK CONTIGUOUS, PITCH 29^{0} MODE OF S-193 OPERATION ON DAY 161, PASS 7 SL-2 OVER BRAZIL

FIG. 4

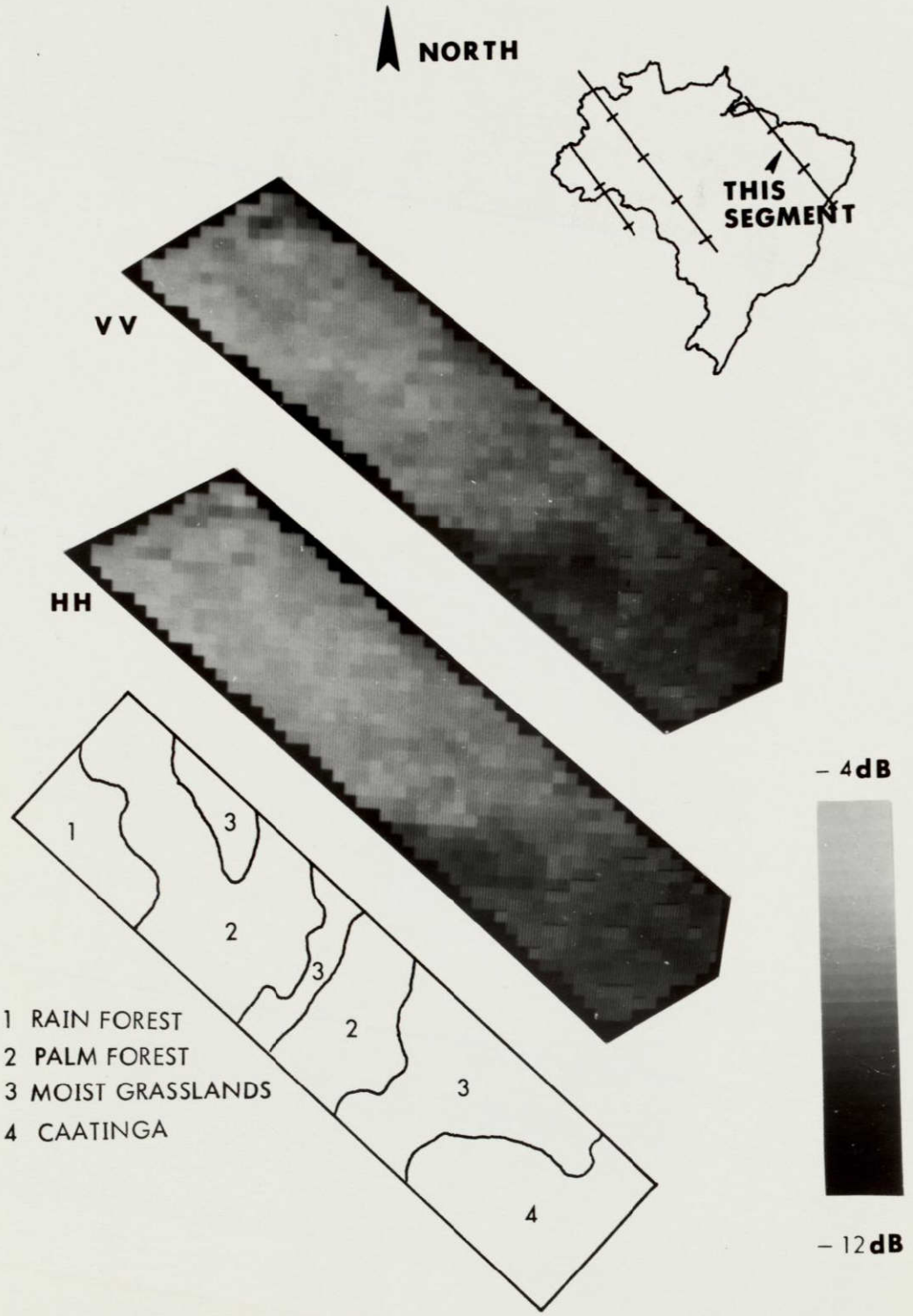

PSEUDO-IMAGES PRODUCED FROM BACKSCATTER RESPONSE WITH CROSS-TRACK CONTIGUOUS, PITCH 29° MODE OF S-193 OPERATION ON DAY 161, PASS 7 SL-2 OVER BRAZIL

FIG. 5

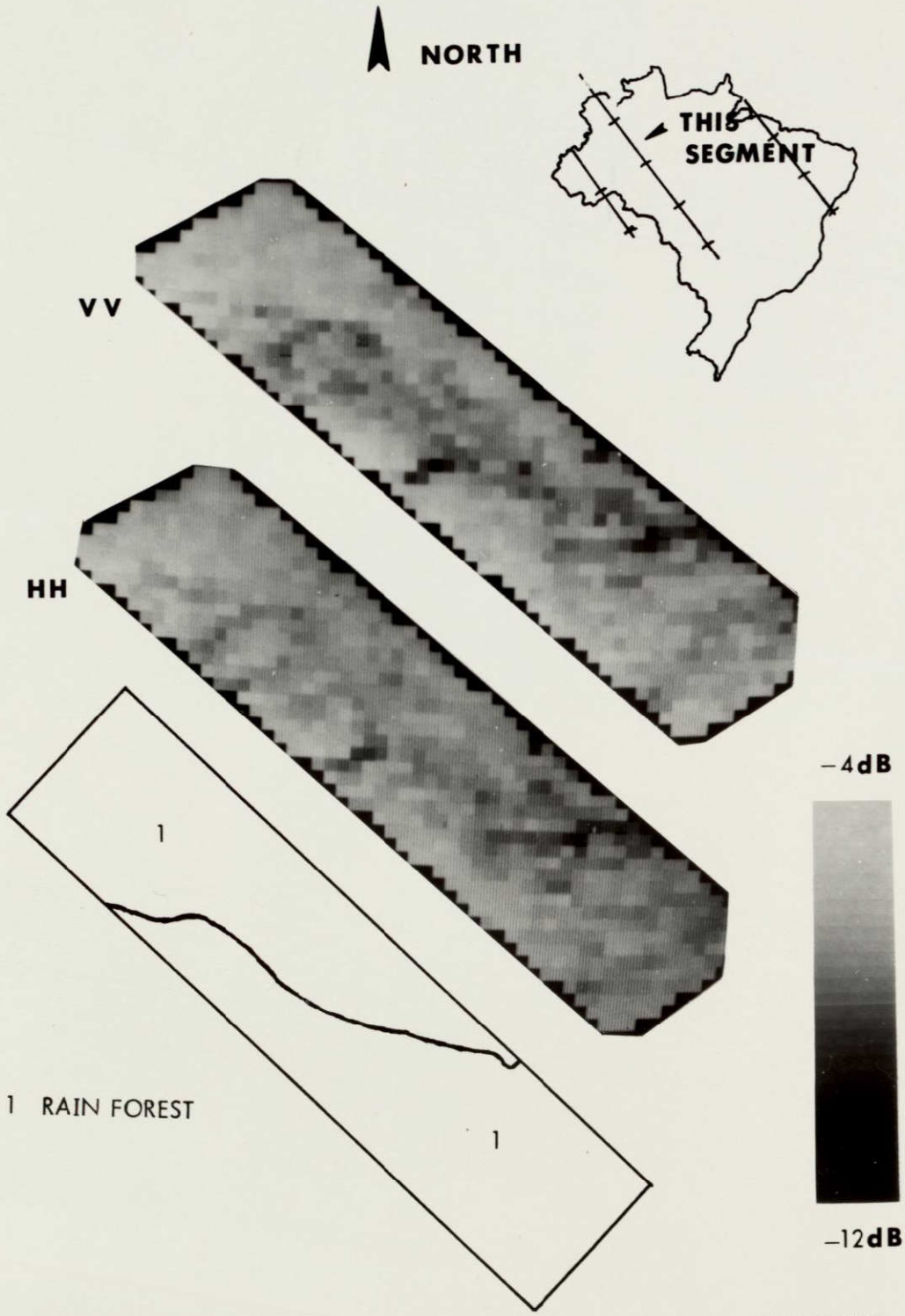

PSEUDO-IMAGES PRODUCED FROM BACKSCATTER RESPONSE WITH CROSS-TRACK CONTIGUOUS, PITCH 29 MODE OF S-193 OPERATION ON DAY 162, PASS 8, SL-2 OVER BRAZIL

FIG. 6

Correlations between the S-193 Passes and "Image-like" Displays, Pass 7, Day 161

This pass began over the ocean (off the Ilha de Marajo). Since the backscatter data were quantified so that scattering coefficients weaker than -12 dB register as black, the result is that the first portion of the pass segment is not visible in the image of segment 1 (Figure 4). When Figure 4 is compared to the map of generalized vegetation boundaries (Figure 1), it is clear that the general similarity of the predominant vegetation was recognized by the sensor. The second segment of the pass continues this general pattern in its initial portion, with the image (Figure 5) becoming abruptly irregular in the latter portion. At least one vegetation source (Hueck and Siebert, 1972) indicates this area as one containing grasslands with a high water table. This moisture variability may have been detected by the sensor, since correlations have been noted elsewhere between soil moisture and backscatter coefficients (Ulaby et al., 1974). The final full segment (of 48 scans) passed through a region generally considered to be dominated by Caatinga thornbush vegetation. A high degree of homogeneity was indicated, although a lower backscatter is indicated in the early part of the segment. This lower value probably represents an extension of the phenomena seen in the previous segment, or the relative openness of the vegetation as opposed to the more closed canopy of the forest areas. Near the coast, a belt of coastal forest and semi-dry woodland (transitioned between the former and the Caatinga) appeared in the image as a generally lighter area (stronger return). Little difference was found between polarizations.

Pass 8, Day 161

As in Figure 1, this pass began over Colombia, and passed into Brazil over the Rio Icana - Rio Uapés drainage system. The first forty-eight scan segments of the pass were over a nearly homogeneous region. The sensor has clearly detected this, as the image display for this region exhibited an almost monotonous continuity.

Not so monotonous is the second pass segment which centers over the Amazon Basin proper. Figure 6 shows the image display for this area and may represent the most positive correlation obtained within the experiment. The subject area lies almost directly to the west of Manaus. In this area, the Amazon undergoes a series of meanders, with numerous areas in which the forest opens briefly with lakes of various proportions being indicated at intervals. On some vegetation maps, the area directly adjacent to the river itself is indicated as a "swampy" rainforest. In any case, some function of the riverine system has clearly been "mapped" by the sensor. At two points in the image sharp dips in the backscatter value are noticeable; these areas are dominated by the aforementioned lake formations.

As in the case of the first segment, the third segment produced an extremely homogeneous image display. This was continued into the first half of the fourth and last full segment. This area corresponds to a region of rain forest intruded by savanna. The last half of the image corresponds to an area which is largely dominated by savanna. A lack of homogeneity is indicated in the image. Since navigation charts show abrupt changes of elevation in the area, the broken nature of terrain and attendant changes in vegetation could be expected to result in the variations of backscatter seen on the image.

Conclusion

It has been demonstrated that, even with the gross resolution of the Skylab scatterometer, image-like displays can be produced which clearly show the ability of the scatterometer to recognize variations in major terrain features in areas in Brazil where large homogeneous regions exist. The correlation between the back-scattering coefficient variations and major terrain type boundaries is high in many instances. In other instances, no significant terrain type variations can be found in the maps. This implies that the microwave "sees" things that are not necessarily represented as variations on a physiographic map, or, that the physiographic maps of the areas under study are somewhat outdated and/or erroneous -- a not surprising result in view of the difficulty of mapping this area by ground or photographic means. Unfortunately, the Project RADAM vegetation maps recently prepared in Brazil were unavailable for comparison.

REFERENCES

1. Brazilian National Forestry Atlas, 1966, Brazilian Ministry of Agriculture.
2. Hueck, Kurt and Paul Siebert, 1972, Vegetationskarte von Sudamerika Gustav Fischer Verlag, Stuttgart.
3. Longman, K. A. and J. Jenik, 1974, Tropical Forest and its Environment, Longman Group, Ltd., London.
4. Ulaby, F. T., John Barr, Arun Sobti and Richard K. Moore, 1974, "Soil Moisture Detection by SKYLAB's Microwave Sensors," University of Kansas Center for Research, Inc.
5. Walter, Heinrich, 1971, Ecology of Tropical and Subtropical Vegetation, Van Nostrand Reinhold Co., New York.

CRINC LABORATORIES

Chemical Engineering Low Temperature Laboratory

Remote Sensing Laboratory

Flight Research Laboratory

Chemical Engineering Heat Transfer Laboratory

Nuclear Engineering Laboratory

Environmental Health Engineering Laboratory

Information Processing Laboratory

Water Resources Institute

Technical Transfer Laboratory

Air Pollution Laboratory

Satellite Applications Laboratory

CRINC